Calculation and Measurement Methods for the Performance of Solar Collectors

Models of Flat Plate Collectors, Transparent Insulation and Efficiency Factors

Bengt Hellström

Division of Energy and Building Design
Department of Construction and Architecture
Lund University
Lund Institute of Technology, 2005
Report EBD-T--05/2

Lund University

Lund University, with eight faculties and a number of research centres and specialized institutes, is the largest establishment for research and higher education in Scandinavia. The main part of the University is situated in the small city of Lund which has about 101 000 inhabitants. A number of departments for research and education are, however, located in Malmö. Lund University was founded in 1666 and has today a total staff of 6 006 employees and 41 000 students attending 90 degree programmes and 1 000 subject courses offered by 88 departments.

Department of Construction and Architecture

The Department of Construction & Architecture is part of Lund Institute of Technology, the technical faculty of Lund University. The main mission of the Department of Construction & Architecture is to pursue research and education on topics related to the built environment. Some of the topics of interest are: restoration and maintenance of buildings, construction management, design processes, construction, energy efficiency, climatization and design of ventilation and heating systems, demolition, disposal and re-use of building materials.

These topics are treated from both a Swedish and an international perspective and collaboration between actors from mutidisciplinary fields of competence forms a particularly important aspect of research and education at the Department. The Department is divided into 5 sub-departments or divisions: Architectural Conservation & Restoration, Computer Aided Architectural Design, Construction Management, Energy & Building Design, and Housing Development & Management.

Division of Energy and Building Design

Reducing environmental effects of construction and facility management is a central aim of society. Minimising the energy use is an important aspect of this aim. The recently established division of Energy and Building Design belongs to the department of Construction and Architecture at the Lund Institute of Technology in Sweden. The division has a focus on research in the fields of energy use, passive and active solar design, daylight utilisation and shading of buildings. Effects and requirements of occupants on thermal and visual comfort are an essential part of this work. Energy and Building Design also develops guidelines and methods for the planning process.

Calculation and Measurement Methods for the Performance of Solar Collectors

Models of Flat Plate Collectors,
Transparent Insulation and Efficiency Factors

Bengt Hellström

Doctoral Dissertation

Key words

Calculation method, Collector model, Concentrating collector, Efficiency factor, Fin efficiency, Flat plate collector, Heat conductivity, Honeycomb, Measurement method, Performance, Solar collector, Solar transmittance, Test method, Transparent insulation.

The English language corrected by L. J. Gruber BSc(Eng) MICE MIStructE
Layout: Hans Follin, LTH, Lund
Cover photo: Flat plate solar collector with a FEP film between the absorber and the cover.

Printed by KFS AB, Lund 2005

Report No EBD-T--05/2
Calculation and Measurement Methods for the Performance of Solar Collectors. Models of Flat Plate Collectors, Transparent Insulation and Efficiency Factors.
Department of Construction and Architecture, Lund University, Division of Energy and Building Design, Lund

ISSN 1651-8136
ISBN 91-85147-06-0

Lund University, Lund Institute of Technology
Department of Construction and Architecture
Division of Energy and Building Design
P.O. Box 118
SE-221 00 LUND
Sweden

Telephone: +46 46 - 222 73 52
Telefax: +46 46 - 222 47 19
E-mail: ebd@ebd.lth.se
Home page: www.ebd.lth.se

Abstract

This thesis deals with models of flat plate collectors, transparent insulation and efficiency factors. An equation for the energy output from a glazed flat plate collector is derived by modelling the collector efficiency factor, F', as the sum of a constant and a temperature dependent part. An alternative way of testing a flat plate collector, based on this model, is suggested.

A complete set of algorithms for calculating the energy output for a flat plate collector with flat films or honeycombs between the cover and the absorber is presented. Algorithms for calculating the radiation heat exchange between the different sheets or layers in a honeycomb glazing are given. Formulas for calculating the absorbed solar energy in each layer are also given. The algorithms can be used in a computer program for determining the energy output, the efficiency and collector characteristic parameters.

Measurements of heat conductivity and total heat loss coefficients of glazings, performed for different transparent insulation materials, are presented and compared with calculations. Measurements of directional-hemispherical solar transmittance are also presented.

For a concentrating collector with an uneven irradiation on the absorber, the efficiency factor for the gain term of the energy output equation, here called the optical efficiency factor, F'_c, is different from F' and is a function of the irradiation distribution on the absorber. Formulas for calculating $F'_c(x)$ for the location x on a fin absorber with constant fin thickness are derived. The average optical efficiency factor, $F'_{c,a}$, can then be calculated from $F'_c(x)$ and the absorbed intensity distribution. Formulas for calculating the temperature distribution across the absorber for the case of uneven irradiation are also derived.

A method for accurate measurements of F' is presented and tested. The method uses accurate temperature measurements across the absorber plate, in the heat carrier fluid and in the ambient air for heat losses without irradiation. Two absorbers of different types were tested. For laminar flow, the measured values of F' for both absorbers were slightly higher than the calculated values, while in the transition region, the measured values were slightly lower.

Contents

List of symbols

α	absorptance (-), thermal diffusivity (m^2/s)
β	collector tilt angle (rad), thermal expansion coefficient (1/K)
δ	absorber fin thickness (m)
ΔT	$T_f - T_a$ (°C)
$\Delta T_f/\Delta\tau$	change of heat carrier fluid temperature per unit time (°C/s)
ΔT_g	temperature difference between boundary surfaces of an air gap (°C)
$\Delta T_S(x, x')$	contribution to $T(x) - T_b$ from the locally absorbed irradiance at $\Delta x'$ (°C)
$\Delta T_L(x, x')$	contribution to $T(x) - T_b$ from the heat losses due to $T_b - T_a$ (°C)
$\Delta x'$	finite part of the absorber fin at x', in the formula derivations assumed to approach zero (m)
ε	emittance (-)
η	collector efficiency (-)
η_0	collector efficiency for $\Delta T = 0$ °C (-)
θ	solar incidence or collector tilt angle (rad)
ν	momentum diffusivity (m^2/s)
ρ	reflectance (-)
σ	Stefan-Boltzmann constant (W/m^2K^4)
τ	transmittance (-)
$(\tau\alpha)$	effective transmittance-absorptance product (-)
A	effective absorptance (-), aspect ratio (-)
b	width of area on absorber in direct contact with the pipe (m)
d_i	pipe inner diameter (m)
C	effective heat capacity of the collector (J/m^2K)

E	effective emittance (-)
f	radiation exchange factor (-), fraction (-)
F	fin efficiency (-)
F_a	absorber average fin efficiency = $(2wF + b)/W = (1 - b/W)F + b/W$ (-)
$F_c(x)$	local fin efficiency for absorbed irradiation at the location x on the absorber (-)
F_e	fin efficiency of an outer part of a fin wing (-)
F'	collector efficiency factor (-)
F'_0	constant part of $F' = F'_0 + F'_1(T_p - T_a)$ (-)
F'_1	temperature dependent part of $F' = F'_0 + F'_1(T_p - T_a)$ (-)
$F'_c(x)$	local optical efficiency factor for absorbed irradiation at the location x on the absorber (-)
$F'_{c,a}$	absorber average optical efficiency factor (-)
F_R	heat removal factor (-)
$F_{R,c}$	heat removal factor for uneven irradiation (-)
g	total transmittance (-), acceleration due to gravity (m/s^2)
G	irradiance in the collector plane (W/m^2)
$G_c(x)$	irradiance at the location x on the absorber (W/m^2)
h_c	conduction/convection heat transfer coefficient (W/m^2)
h_i	heat transfer coefficient between the pipe inner wall and the heat carrier fluid (W/m^{2}K)
h_{rad}	radiation heat transfer coefficient (W/m^2)
k	heat conductivity (W/mK)
K	absorption coefficient (1/m), incidence angle modifier (-)
L	thickness, length (m)
m	$(U_L/(k\delta))^{0.5}$ (m^{-1})
n	refractive index (-)
Nu	Nusselt number, $Nu = h_c \cdot L/k$ (-)
q	thermal energy flow (W/m^2)
q_e	electrical power per measured surface (W/m^2)
q'	utilized thermal energy flow per length of the absorber (W/m)
$q'_e(x')$	thermal energy flow towards the fin edge from absorbed irradiation at x' (W/m)

$q'_p(x')$	thermal energy flow towards the pipe from absorbed irradiation at x' (W/m)
r	surface reflectance (-)
R	effective reflectance (-), distance (m), collector parameter (-)
Ra	Rayleigh number, $Ra = g\beta\Delta T_g L^3/(\nu\alpha)$ (-)
S	absorbed (evenly distributed) irradiance on the absorber (W/m^2)
$S_c(x')$	absorbed irradiance at the location x' on the absorber (W/m^2)
$S_{c,a}$	average value of the absorbed irradiance across the absorber (W/m^2)
t	surface transmittance (-)
t_w	wall thickness (m)
T	temperature (°C), effective transmittance (-)
$T(x)$	local temperature at the absorber location x (°C)
T_a	ambient temperature (°C)
T_b	fin base temperature (°C)
T_f	heat carrier fluid temperature (°C)
T_g	cover temperature (°C)
T_p	average absorber plate temperature (°C)
U_0	constant part of $U_L = U_0 + U_1\Delta T$ (W/m^2K)
U_1	temperature dependent part of $U_L = U_0 + U_1(T_p - T_a)$ (W/m^2K)
U_b	back and edge heat loss coefficient between the absorber and the ambient (W/m^2K)
$U_{b\text{-}f}$	heat transfer coefficient between the fin base and the heat carrier fluid (W/m^2K)
U_{fin}	heat transfer coefficient between the fin (average) and the fin base (W/m^2K)
U_{int}	heat transfer coefficient between the fin (average) and the heat carrier fluid (W/m^2K)
U_{sys}	heat transfer coefficient between the heat carrier fluid and the ambient (W/m^2K)
U_t	front or top heat loss coefficient between the absorber and the ambient (W/m^2K)
U_L	overall heat loss coefficient between the absorber and the ambient (W/m^2K)

w	$(W - b)/2$ (m)
W	absorber width (m)
x	location (m)
x'	location (m)

Subscript

a	air, ambient, average
b	beam, base, backward, back
c	cold, concentration, conduction, convection
conv	convection
d	diffuse
e	edge, effective, electrical
f	fluid, forward, front
g	ground, cover, gap
h	hot
hc	honeycomb
i	index number, inlet, inner, substitute index
j	index number
k	index number
m	mean
n	normal incidence
o	outlet, outer
p	plate, pipe
rad	radiation
t	top
w	wall
x	surface normal direction
y	surface normal direction
z	surface normal direction

Foreword

This thesis contains some different aspects of models, calculation and measurement methods for the performance of solar collectors. One objective has been to focus on aspects which I think are important for the theoretical understanding of solar collectors and which I believe are not always well known. Another objective has been to write a text which is comprehensible, but yet not shallow. Each chapter (2-6) is also aimed to be readable separately from the other chapters. For that reason, in a few cases, some background facts are given more than once in the thesis. Known facts and research results (with references) are in some cases included in the text. The intention has then been to give a full picture of the treated subject.

Lund, January 2005

Bengt Hellström

1 Introduction

Flat plate collectors usually have fin absorbers. For such collectors, the average temperature of the irradiated absorber will differ significantly from the temperature of the heat carrier fluid. This makes the collector more complex to model accurately than a collector with an overall wetted absorber. In the latter case there is also a slight difference between the absorber and the fluid temperature, but it is much smaller and the model could therefore, without major errors, be simplified. The higher absorber temperature of the irradiated fin absorber results in an extra heat loss, which is usually described through the concept of the collector efficiency factor, F'.

The energy output from a flat plate collector is often written (see for instance by Duffie and Beckman (1991)):

$$q = F'S - F'U_L\Delta T \tag{1.1}$$

where S is the absorbed irradiance, U_L is the heat loss coefficient from the absorber plate to the ambient and ΔT is the temperature difference between the heat carrier fluid and the ambient. The model, which originates from early work (e.g. Hottel and Whillier, 1958 and Bliss, 1959), does not (explicitly) take into account the temperature dependence of the collector efficiency factor.

In Chapter 2, a model is derived by dividing F' into a constant and a temperature dependent part, which results in an energy output equation with two "extra" terms, one proportional to ΔTS and one proportional to S^2. An equation similar to this one has earlier been given by Rockendorf et al. (1993, 1995). A test procedure, based on this model, is proposed. The test procedure includes heat loss measurements without irradiation and works stepwise, identifying, at most two parameters from each set of measurement periods. The differences between three collector models, of which one is eqn 1.1, one is used in a standard test method today (CEN 2001), and one is the basis for the proposed test procedure, are shown an explained.

Flat plate collectors usually have a low-emitting ("selective") absorber and an IR opaque cover with an air gap between the surfaces. As shown by eqn 1.1, the energy output from the collector consists of two major parts; a gain part, $F'S$, and a heat loss part, $F'U_L\Delta T$. The absorbed irradiance can also be written $S = (\tau\alpha)G$, where $(\tau\alpha)$ is the effective solar transmittance-absorptance product and G is the irradiance. In order to decrease the heat losses for flat plate collectors, so-called transparent insulation material (TIM) can be used. Transparent insulation materials are applied between the cover and the absorber to reduce heat losses, without significantly reducing the total solar transmittance of the glazing.

Much work has earlier been carried out on transparent insulation materials, both regarding calculations and measurements, see e.g. Hollands et al. (1978-1992) and Platzer (1988-1992). An extensive work was given by Platzer (1988a).

A classification of the transparent insulation materials, due to their structure, was done by Platzer (1988a). The classes are:

- Structures perpendicular to the absorber (honeycombs and slats)
- Structures parallel to the absorber (parallel films)
- Bubble structures (foam)
- Microporous structures (aerogel)

The concept of TIM is, however, often used in different ways. Absorber parallel films are not always referred to as TIM and sometimes the concept is used synonymously with honeycombs.

In this thesis only honeycombs and parallel films are treated. A complete set of algorithms for calculating the energy output for a flat plate collector with a transparent insulation glazing is given in Chapter 3. For the cases when the algorithms used in the calculations have been found in the literature, references are given. Reviews of the literature, valid for the different sections of the chapter, are also given.

For the radiation heat transport in a stack of parallel layers, out of which some can be transparent in the IR wavelength range, explicit formulas, based on ray tracing analysis, are given in Section 3.3. The method is more straightforward to use than the implicit net-radiation method, as given by e.g. Hollands and Wright (1983) and Edwards and Rhee (1984). The calculations can also more easily be made spectral and angular resolved using this method.

An approximate analytical method of calculating the coupled heat transport through a honeycomb structure was given by Platzer (1991). Hollands et al. (1984) presented a numerical method for this problem,

using a geometrical approximation. In Section 3.6, an alternative numerical method, based on view factors between the interacting surfaces, is given. The method, which divides the honeycomb into an arbitrary number of layers, is straightforward and easy to apply. The calculations can also easily be made spectral and angular resolved. A method to calculate the absorbed irradiation in each layer is also given in Section 3.8.

In Chapter 4, instruments for measurements of heat conductivity, overall heat loss coefficients and solar transmittance are described. Results of heat conductivity measurements on honeycombs are compared with calculations. Measurements of heat loss coefficients for glazings with an absorber parallel film between the cover and the absorber or with a honeycomb attached to the cover are also compared with calculations. Results of angle dependent measurements of solar transmittance of some TIM are also given.

Eqn 1.1 is valid for flat plate collectors, but for a concentrating collector with an uneven (non-uniform) irradiation on the absorber, the efficiency factor for the gain term, here called the optical efficiency factor, F'_c, is different from F' and a function of the irradiation distribution on the absorber. If the heat loss coefficient is assumed to be constant across the fin, the optical efficiency factor for absorbed irradiation at a certain distance from the edge of the absorber is independent of absorbed irradiation at other locations and can therefore be expressed as $F'_c(x)$, where x is the distance from the edge of the absorber. Close to the edge, $F'_c(x) < F'$ and close to the pipe, $F'_c(x) > F'$.

In Chapter 5, formulas for calculating $F'_c(x)$ for a fin absorber with constant fin thickness are derived. By weighting $F'_c(x)$ with the locally absorbed irradiance, $S_c(x)$, and integrating across the absorber, an absorber average optical efficiency factor, $F'_{c,a}$, is obtained. This value replaces F' in the gain term of the equation for thermal energy output (eqn 1.1). If, instead, the energy output equation is expressed as a function of the inlet temperature, $F'_{c,a}$ can be used for calculating a corresponding heat removal factor for uneven irradiation, $F_{R,c}$. Formulas for calculating the temperature distribution across the absorber for the case of uneven irradiation are also derived. The content of Chapter 5 is essentially the same as that of a published article (Hellström, 2004).

In chapter 6, an accurate method for measuring the collector efficiency factor, F', is presented. A review of other methods, described in the literature, is also given. The presented method is based on accurate temperature measurements across the absorber for heat losses without irradiation. The method is tested for two different absorbers, in the heat carrier fluid and in the ambient air. The resulting measured values are compared with results from calculations.

A list of publications with contributions from the author, which are referred to in the thesis, is here given in reversed chronological order:

Hellström, B. (2004) Derivation of efficiency factors for uneven irradiation on a fin absorber. *Solar Energy 77* (3), 261-267.

Adsten, M., Hellström, B., & Karlsson, B. (2004) Measurement of radiation distribution on the absorber in an asymmetric CPC collector. *Solar Energy 76* (1-3), 199-206.

Fischer, S., Heidemann, W., Müller-Steinhagen, H., Perers, B., Bergquist, P., & Hellström, B. (2004). Collector test method under quasi-dynamic conditions according to the European Standard EN 12975-2. *Solar Energy 76* (1-3), 117-123.

Hellström, B., & Håkansson, H. (2003). *Mätning av verkningsgradsfaktorn, F´*. (Measurements of the collector efficiency factor, *F´*). Final report of a research project. Internal Report EBD-R--04/4, ISBN 91-85147-03-6, Lund: EBD, LTH, Lund University. (In Swedish).

Adsten, M., Hellström, B., & Karlsson, B. (2002). Comparison of the optical efficiency of a wide and a narrow absorber fin in an asymmetrically truncated concentrating collector. *Proc. EuroSun 2002*, Bologna, Italy.

Adsten, M., Hellström, B., & Karlsson, B. (2001). Measurement of radiation distribution on the absorber in an asymmetric CPC collector. *Proc. ISES Solar World Congress*, Adelaide, Australia.

Hellström, B. (2001). *Parameter impact on temperature distribution and collector efficiency of a solar cell/collector hybrid in a CPC geometry*. Internal Report U01:22, Älvkarleby, Sweden: Vattenfall Utveckling AB.

Hellström, B., Adsten, M., Nostell, P., Wäckelgård, E., & Karlsson ,B. (2000). The impact of optical and thermal properties on the performance of flat plate solar collectors. *Proc. EuroSun 2000*, Copenhagen, Denmark.

Hellström, B., & Perers, B. (1998). Comparison of two standard collector test methods. *Proc. EuroSun 1998*, Portoroz, Slovenia.

Hellström, B. (1998). *Comparative evaluation of two solar collector test methods*. Internal Report UR 98:9, Älvkarleby, Sweden: Vattenfall Utveckling AB.

Hellström, B., Perers, B., & Karlsson, B. (1992). Comperative performance of TIM in collectors. *Proc. 5:th International Workshop on Transparent Insulation Technology*, Freiburg, Germany.

Hellström, B., & Karlsson, B. (1991). *Optimization of a honeycomb glazing*. Nordic Solar Energy R & D Meeting, Borlänge, Sweden.

Hellström, B., & Karlsson, B. (1991). Evaluation of a honeycomb glazing for high temperature solar collectors. *Proc. 4:th International Workshop on Transparent Insulation Technology*, Birmingham, England.

Hellström, B., Karlsson, B., & Svensson, L. (1990). Performance of collectors with flat films or honeycombs. *Proc. North Sun '90*, Reading, England.

Hellström, B., Bergkvist, M., Ribbing, C-G, & Karlsson, B. (1990). Solar transmittance and lambda values of transparent insulation. P*roc. Building Physics in the Nordic Countries*, Trondheim, Norway.

Hellström, B., Karlsson, R., & Karlsson, B. (1988). Convection dependent distribution of temperatures and heat losses in a flat plate collector model. *Proc. North Sun '88*, Borlänge, Sweden, 359-362.

Hellström, B. (1988a). *Inverkan av konvektion på temperaturfördelning och värmeförluster i solfångare*. (Influence of convection on temperature distribution and heat losses in solar collectors). Diploma work at the department of Heating and Ventilation, Royal Institute of Technology. Internal Report U(L) 1988/34, Älvkarleby, Sweden: Vattenfall Utveckling AB. (In Swedish).

2 Models of flat plate collectors

2.1 Introduction

Different models for the energy output from different types of solar collectors (unglazed, glazed flat plate and vacuum tube collectors) were reviewed by IEA, SH&C Task III (Harrison et al., 1993). A common way to write the energy output from a glazed flat plate collector, q, is as a linear function of expressions of operational and meteorological variables, x_i, such as the operating temperature, irradiance and the ambient temperature: $q = b_1x_1 + b_2x_2 + b_3x_3 \ldots$, where b_i are collector characteristic parameters.

Ever since the early theoretical work on flat plate collectors models (see e.g. Hottel and Whillier, 1958 and Bliss, 1959), the collector efficiency factor for a fin absorber flat plate collector, F', has been assumed to be (approximated as) a constant. In this chapter, a model for a glazed flat plate solar collector is theoretically derived by considering also the temperature dependence of the collector efficiency factor. The derived energy output equation is similar to an equation earlier given by Rockendorf et al. (1993, 1995). Compared with commonly used flat plate collector models, it has an extra term which is proportional to both G and ΔT.

The result could be used for an alternative way of testing a solar collector, using the model: $\eta = g_{sys} - U_{sys}\Delta T/G$. This model differs both from a model used in testing today: $\eta = \eta_0 - a\Delta T/G$ (CEN, 2001) and from a model often given in the literature: $\eta = F'(\tau\alpha) - F'U_L\,\Delta T/G$ (see for instance Duffie and Beckman, 1991). The differences between these equations are shown in the chapter where the symbols are also explained. The equations above are written in a compressed way, but will have more terms when expanded.

Much of the content of this chapter is a continuation and an extension of previous work by Rockendorf et al. (1993, 1995).

2.2 Derivation of a model for flat plate collectors

The steady state heat balance equation of the absorber can be written:

$$q = S - U_L(T_p - T_a) \tag{2.2.1}$$

where S is the irradiance absorbed by the absorber plate (including secondary heat from the irradiance absorbed by the cover), T_p is the average absorber plate temperature and T_a is the ambient temperature. The overall heat loss coefficient from the absorber to the ambient, U_L, is mainly a function of the temperature difference, $T_p - T_a$, but has also a dependence on the absolute temperature level. Different models for U_L were reviewed by IEA, SH&C Task III (Harrison et al., 1993). Although not providing the best fit, U_L is often (for reasons of simplicity) modelled as a linear function of $T_p - T_a$:

$$U_L = U_0 + U_1(T_p - T_a) \tag{2.2.2}$$

Since U_L does not fit the linear function well at low values of $T_p - T_a$, U_0 is generally not the limit value for U_L when $T_p - T_a$ approaches zero. U_0 and U_1 can be obtained from two values of U_L at different $T_p - T_a$ or from linear regression with several values of U_L at different $T_p - T_a$.

Since the absorber temperature is usually not known, it is better to base the model on the heat carrier fluid temperature. The heat balance equation for the fluid can then be written:

$$q = F'(S - U_L(T_f - T_a)) = F'S - F'U_L(T_f - T_a) \tag{2.2.3}$$

where F' is the collector efficiency factor (see, for instance, Duffie and Beckman, 1991) and T_f is the mean temperature of the heat carrier fluid. Substituting the expression of eqn 2.2.2 into eqn 2.2.3 results in:

$$q = F'S - F'U_0(T_f - T_a) - F'U_1(T_p - T_a)(T_f - T_a) \tag{2.2.4}$$

Combining eqn 2.2.1 and 2.2.3 gives:

$$(T_p - T_a) = F'(T_f - T_a) + (1 - F')S/U_L \tag{2.2.5}$$

Substituting this expression into eqn 2.2.4 then leads to:

$$q = F'S - F'U_0(T_f - T_a) - F'^2U_1(T_f - T_a)^2 - F'(1 - F')U_1(T_f - T_a)S/U_L \tag{2.2.6}$$

We now have an equation based on $T_f - T_a$. F' is, however, not a constant, but a function of U_L and thereby also of $T_p - T_a$. It can also be modelled as a linear function:

$$F' = F'_0 + F'_1(T_p - T_a) \tag{2.2.7}$$

where F'_0 is F' for $U_L = U_0$.

Rockendorf et al. (1993, 1995) suggested a simplified model for F', expressed as

$$F' = \frac{U_{int}}{U_{int} + U_L} \tag{2.2.8}$$

where $1/U_{int}$ is the sum of the internal heat resistance within the fin (average value) and between the fin base and the heat carrier fluid. This is described in more detail in Section 3.9. F'_0 can then be expressed:

$$F'_0 = \frac{U_{int}}{U_{int} + U_0} \tag{2.2.9}$$

U_{int} is a weak function of U_L, but can be approximated as a constant. It can be solved from eqns 2.2.8 or 2.2.9:

$$U_{int} = F'U_L/(1-F') = F_0'U_0/(1-F'_0) \tag{2.2.10}$$

F'_1 can then be obtained from eqns 2.2.7-10 by replacing U_L in Eq. 2.2.8 by the expression in Eq. 2.2.2:

$$F'_1 = -F'(1 - F'_0)U_1/U_0 \tag{2.2.11}$$

F' can then from eqns 2.2.7, 2.2.11, 2.2.5 and 2.2.10 be (implicitly) expressed as:

$$F' = F'_0 - F'^2(1 - F_0')U_1(T_f - T_a)/U_0 - F'^2(1 - F_0')^2U_1S/(F_0U_0^2) \tag{2.2.12}$$

The last two terms of eqn 2.2.12 are correction terms, which are much smaller than F'_0. Therefore, F' can be approximated by F'_0 in these terms. Also the last two terms of eqn 2.2.6 can be regarded as correction terms. The last term of eqn 2.2.6 can with help of eqn 2.2.10 be approximated as $-F'_0(1-F'_0)U_1(T_f-T_a)S/U_0$. Inserting the expression of eqn 2.2.12 into eqn 2.2.6 and simplifying by excluding the products of the correction terms gives the result:

$$q = F'_0 S - F'_0 U_0 (T_f - T_a) - F'^3_0 U_1 (T_f - T_a)^2 - 2F'^2_0 (1 - F'_0) U_1 (T_f - T_a) S/U_0 - F'_0 (1 - F_0')^2 U_1 S^2/U_0^2 \quad (2.2.13)$$

This equation differs from the equation given by Rockendorf et al. (1993, 1995) by a factor F'_0 in the last three terms. Their equation was derived using the concept of U_{int}, which was also part of the final equation. They did not express a temperature dependence of F', but defined F' as F'_0 in eqn 2.2.9.

S in eqn 2.2.13 can be expressed

$$S = (\tau\alpha)G = K(\tau\alpha)_n G = (\tau\alpha)_n (K_b G_b + K_d G_d + K_g G_g) \quad (2.2.14)$$

where $(\tau\alpha)$ is the total effective transmittance-absorptance product and G is the irradiance in the collector plane. The absorber heat gain part from the absorptance of the cover is also included in $(\tau\alpha)$. $(\tau\alpha)_n$ is $(\tau\alpha)$ for irradiation at normal incidence and K is the incidence angle modifier (IAM) for G. K_b, K_d and K_g are the incidence angle modifiers for the beam (G_b), the diffuse (G_d) and the ground reflected (G_g) irradiances in the collector plane, where $G_b + G_d + G_g = G$. Different models for K_b were reviewed by IEA, SH&C Task III (Harrison et al., 1993). A commonly used model is:

$$K_b(\theta) = 1 - b_0(1/\cos(\theta) - 1) \quad (2.2.15)$$

where b_0 is the collector characteristic parameter. Eqn 2.2.15 is sometimes used for all θ for which $K_b(\theta) \geq 0$. For larger θ then $K_b = 0$. In other cases, eqn 2.2.15 is used only for $\theta \leq 60°$, where $K_b(\theta)$ above this angle is obtained from $(1 - b_0)(90° - \theta)/30°$. G_g is often not measured separately, but included in G_d, which then also influences the value of K_d.

Inserting the expression of S into eqn 2.2.13 and substituting $T_f - T_a$ for the shorter expression ΔT gives:

$$q = F'_0(\tau\alpha)G - F'_0 U_0 \Delta T - F'^3_0 U_1 \Delta T^2 - 2F'^2_0 (1-F'_0)(\tau\alpha)(U_1/U_0)\Delta T G - F'_0 (1-F_0')^2 (\tau\alpha)^2 (U_1/U_0^2) G^2 \quad (2.2.16)$$

Eqn 2.2.16 can in a shorter way be expressed:

$$q = p_0 G - p_1 \Delta T - p_2 \Delta T^2 - p_3 \Delta T G - p_4 G^2 \quad (2.2.17)$$

where p_i are the corresponding parameters of eqn 2.2.16. The first three terms on the right hand side of eqn 2.2.16-17 give q as a function of G, ΔT and ΔT^2. The fourth and fifth terms, which are usually not considered in models for glazed flat plate collectors, show that q is a function also of ΔTG and G^2. For an example of a flat plate collector with F'_0 = 0.94, $(\tau\alpha)$ = 0.85, U_0 = 3.0 W/m^{2}K and U_1 = 0.015 W/m^{2}K^2, operating at ΔT = 40°C and G = 1000 W/m^2, the sizes of the different terms are 799, 113, 20, 18 and 4 W/m^2, respectively.

The last term in eqn 2.2.17 originates from the fact that F' in $F'(\tau\alpha)G$ decreases with increasing G, since the absorbed irradiance, $S = (\tau\alpha)G$, causes an increase of $T_p - T_a$, which increases U_L and thereby decreases F'. However, since this term is so small, it can without any severe loss in accuracy be included in the first term on the right hand side of the equation. This leads to:

$$q = \eta_0 G - p_1 \Delta T - p_2 \Delta T^2 - p_3 \Delta TG \qquad (2.2.18)$$

where $\eta_0 = p_0 - p_4 G$. In the above example, η_0 is 0.795. A lower irradiance level would (for the same incidence angle distribution) result in an η_0 which is, at most, 0.004 higher. The irradiance is, however, usually correlated to the incidence angle distribution. So, besides the term beeing very small, it is largely "absorbed" by the incidence angle dependence.

The last term in eqn 2.2.18 is proportional to both ΔT and G. If it is left out of the model as a separate term, its value will be included in the first or second term on the right hand side - or in both. By looking at the origin of this term, it can be seen that it is made up of two parts of about the same size. This is where the factor two in the corresponding term of eqn 2.2.16 comes from.

The first part of the term originates from the fact that $F'(\tau\alpha)G$ is not independent of ΔT, but decreases with increasing ΔT. This is because an increase in ΔT causes an increase in $T_p - T_a$, which increases U_L and thereby decreases F' and $F'(\tau\alpha)G$.

The origin of the second part of the term is that $F'U_L\Delta T$ is not independent of G, but increases with increasing G. This is because an increase in the absorbed irradiance, $S = (\tau\alpha)G$, causes an increase in $T_p - T_a$. This gives a decrease in F', but a relatively much larger increase in U_L and a total increase in $F'U_L\Delta T$ with increasing G.

In eqn 2.2.3, the first part of the term is included in $F'S$, while the second part is included in $F'U_L(T_f - T_a)$. Dividing by G and using the expressions $(\tau\alpha)G$ and ΔT instead of S and $T_f - T_a$, eqn 2.2.3 can be written:

$$\eta = F'(\tau\alpha) - F'U_L \Delta T/G \qquad (2.2.19)$$

In this equation, $F'(\tau\alpha)$ is not a constant, but decreases with increasing ΔT. U_L is the heat loss coefficient at the average absorber temperature, determined both by G and ΔT. Two other equations, one where the last term of eqn 2.2.18 is included in the first (gain) term and one where it is included in the second (heat loss) term, are treated in the next section.

2.3 Implications for test models

Two methods for testing glazed liquid flat plate collectors are described in a European standard, EN 12975 (CEN, 2001); one where the test is performed under steady state conditions and one where the so-called quasi-dynamic method is used. The latter is described extensively by Perers (1998). The two methods are compared by e.g. Hellström and Perers (1998a,b) and Fischer et al. (2004). Here, only a brief description of the two test methods is given. The focus is instead on the collector models of the methods.

For tests under steady state conditions, the efficiency of the collector is measured at or close to normal incidence for G $\geq$ 700 W/m^2 at four different values of $\Delta T = T_f - T_a$, out of which ΔT = 0°C is one. The mean heat carrier temperature, T_f, is obtained as $T_f = (T_i + T_o)/2$, where T_i and T_o are the (measured) inlet and outlet temperatures of the collector. If the heat carrier fluid is water, the highest mean temperature is required to be at least 80°C. If the ambient temperature is around 20°C, the other ΔT should then be approximately 20, 40 and 60°C. The angle dependence is determined by measuring the efficiency at 50° incidence angle for ΔT = 0°C. A calculation procedure for the effective thermal capacity of the collector is also given.

The collector specific parameters are obtained by fitting the parameters of eqn 2.3.1 to measured data (at normal incidence irradiation):

$$\eta = \eta_0 - a_1 \Delta T / G - a_2 \Delta T^2 / G \qquad (2.3.1)$$

If the theoretically derived eqn 2.2.18 is divided by G it becomes:

$$\eta = \eta_0 - p_1 \Delta T / G - p_2 \Delta T^2 / G - p_3 \Delta T \qquad (2.3.2)$$

Since the last term of eqn 2.3.2 does not correspond to any term in eqn 2.3.1, its value must instead be included in one (or several) of the other terms. The test measurements are performed with approximately constant G, but with varying ΔT. This implies that the extra term of eqn 2.3.2 is included in the second term on the right hand side of eqn 2.3.1.

The solar gain term of eqn 2.3.1, η_0, is then, in contrast to that of eqn 2.2.19, a constant. The obtained parameters can be identified as: $a_1 = p_1 + p_3 G$ and $a_2 = p_2$. η_0 is the efficiency measured at $\Delta T = 0$°C. The incidence angle modifier at 50° incidence angle for the beam irradiation is obtained as $K(50°) = \eta_0(50°)/\eta_0(0°)$.

For tests under quasi dynamic conditions, the energy output rate of the collector is measured at all angles of incidence for which G ≥ 300 W/m^2 and four different values of ΔT: 0, 20, 40 and 60°C. The model used for this test is:

$$q = \eta_{0,n} G_b - \eta_{0,n} b_0 (1/\cos(\theta)-1) G_b + \eta_{0,d} G_d - c_1 \Delta T - c_2 \Delta T^2 - c_5 \Delta T_f / \Delta \tau \qquad (2.3.3)$$

where $\eta_{0,n}$ is η_0 for beam irradiance at normal incidence and $\eta_{0,d}$ is η_0 for diffuse irradiance. The last term is the stored energy per unit time for the collector, where c_5 is the effective heat capacity and $\Delta T_f / \Delta \tau$ is the change in mean fluid temperature per unit time. The parameters $\eta_{0,n}$, b_0, $\eta_{0,d}$, c_1, c_2 and c_5 are obtained from multiple linear regression analysis, performed on the measured collector output for the expressions of operational and climatic data in eqn 2.3.3.

The six terms on the right hand side of the equation are mandatory according to the standard. Three more terms, giving the dependencies on the wind speed and the effective sky temperature, are recommended only if the ratio between the obtained parameter value and the standard deviation from the linear regression is at least 2. For unglazed collectors all these terms are mandatory.

Compared with the theoretically derived eqn 2.2.18, the term $-p_3 \Delta T G$ does not have a corresponding term in eqn 2.3.3. In contrast to the steady state test, both G and ΔT will be varied in the quasi dynamic test, which has the result that the term can not be directly included in ("absorbed" by) another term in eqn 2.3.3.

In eqn 2.2.19, the corresponding value of the extra term of eqn 2.2.18, $-p_3 \Delta T$, is partly included in the gain term, $F'(\tau\alpha)$, and partly in the loss term, $-F' U_L \Delta T / G$. In eqn 2.3.1, the extra term is included only in the heat loss term, $-a_1 \Delta T / G$. A third possibility is to include the extra term in the solar gain term. Since the solar gain term is then consistent with the common definition of the total energy transmittance, g, of the system it is here denoted g_{sys}. The heat loss coefficient of the corresponding heat loss term then also becomes consistent with the common definition of a heat loss coefficient, which is without the influence of irradiation. The total heat loss coefficient for the system between the heat carrier fluid

and the ambient will here be denoted U_{sys}. To clarify the differences, eqn 2.3.1 can be written in the same form as eqn 2.2.19, together with it and the new equation:

$$\eta = \eta_0 - a\Delta T/G \quad (2.3.4)$$

$$\eta = F'(\tau\alpha) - F'U_L\,\Delta T/G \quad (2.2.19)$$

$$\eta = g_{sys} - U_{sys}\Delta T/G \quad (2.3.5)$$

where $a = a_1 + a_2\Delta T$.

The differences between the three equations are illustrated in Fig. 2.1 and 2.2. The efficiencies and heat loss coefficients of the diagrams are calculated for a "standard" flat plate collector with a fin absorber for different ΔT, using a procedure described in Chapter 3. A single glazed collector with a 5 cm airgap is assumed to be irradiated with 1000 W/m^2 beam irradiance at normal incidence. The absorber emittance, $\varepsilon_p = 0.1$, the edge and back side losses, $U_b = 1 + 0.0025(T_p - T_a)$ W/m^{2}K, $U_{int} =$ 46 W/m^{2}K and the ambient temperature, $T_a = 20$ °C.

In Fig. 2.1, the differences between η_0, $F'(\tau\alpha)$ and g_{sys} are shown as functions of ΔT. η_0 is a constant, while the other two decrease with ΔT. This is because the "extra" term of eqn 2.3.2, $-p_3\Delta T$, is partly or fully included in the last two parameters. In $F'(\tau\alpha)$ about half of the term is included and in g_{sys} the whole term. For $\Delta T = 0$, the three parameters are the same. A linear fit for $g_{sys} = g_{sys,0} - g_{sys,1}\Delta T$, made from $\Delta T = 20$°C and 50°C, is included in the diagram. The calculated efficiency, η, is also shown as a function of ΔT.

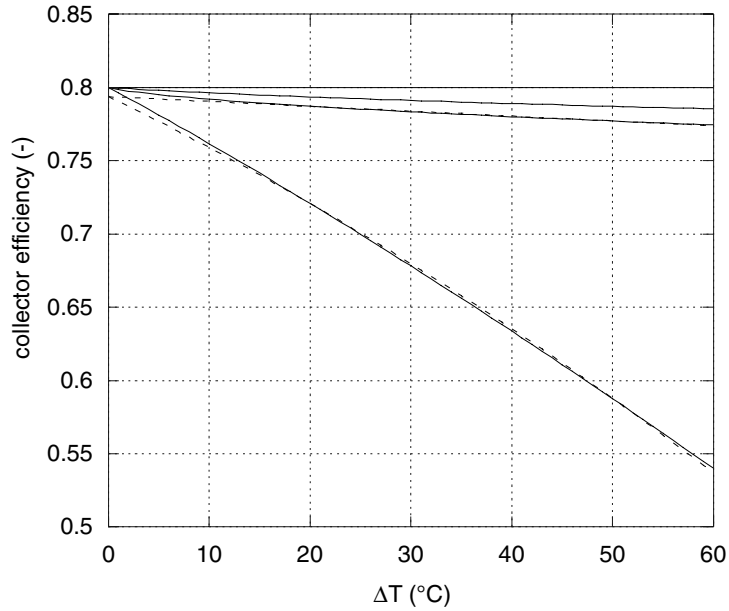

Fig. 2.1 *Upper lines, from the top: η_0, $F'(\tau\alpha)$ and g_{sys} + a linear fit: $g_{sys} = g_{sys,0} - g_{sys,1}\Delta T$ (dotted line). Lower lines: η calculated for a "standard" collector and η from fitted parameters: $\eta = g_{sys,0} - g_{sys,1}\Delta T - U_{sys,0}\Delta T/G - U_{sys,1}\Delta T^2/G$ (dotted line). The collector was assumed to be irradiated with 1000 W/m^2 beam irradiance at normal incidence.*

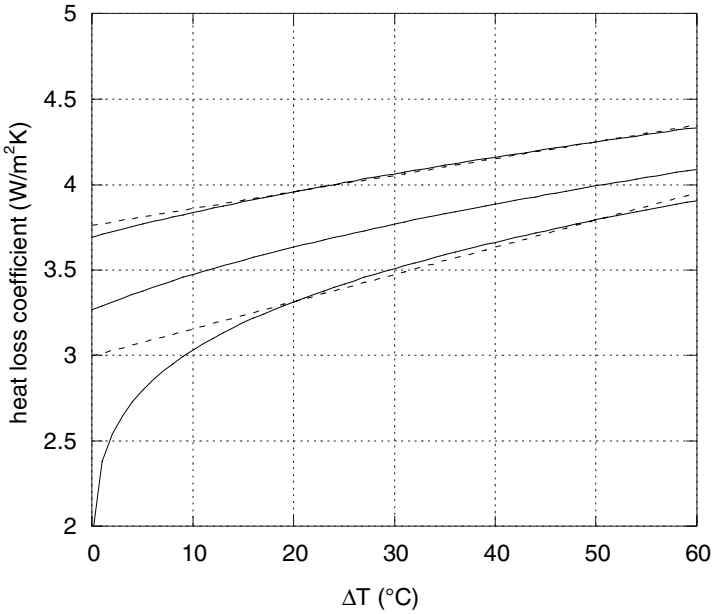

Fig. 2.2 *From the top: CEN test heat loss coefficient with a linear fit: $a = a_1 + a_2\Delta T$ (dotted line), $F'U_L$ and finally U_{sys} with a linear fit: $U_{sys} = U_{sys,0} - U_{sys,1}\Delta T$ (dotted line), all calculated for a "standard" collector.*

The differences between η_0, $F'(\tau\alpha)$ or g_{sys} and the efficiency, η, give the heat loss parts of the equations, which are then also different for the three equations. In Fig. 2.2, the heat loss coefficients of the equations are shown. The corresponding "extra" term, p_3G, is then partly and fully included in $F'U_L$ and a, respectively. Linear fits, made from values at ΔT = 20°C and 50°C, are given for $a = a_1 + a_2\Delta T$ and $U_{sys} = U_{sys,0} + U_{sys,1}\Delta T$. $F'U_L$ is the heat loss coefficient obtained under irradiation, while U_{sys} is obtained without irradiation. The coefficient a is even larger than $F'U_L$, since the decrease of $F'(\tau\alpha)$ with increasing ΔT is also included in $a\Delta T/G$.

In Fig. 2.1 the resulting efficiency, calculated from the fits of g_{sys} and U_{sys} is also shown. This resulting linear efficiency equation is then:

$$\eta = g_{sys,0} - g_{sys,1}\Delta T - U_{sys,0}\Delta T/G - U_{sys,1}\Delta T^2/G \qquad (2.3.6)$$

In this equation the "extra term", $-p_3\Delta T$, of the theoretically derived eqn 2.2.18 is included as a separate term.

2.4 Suggestion for an alternative test procedure

A suggestion for an alternative test procedure, where all the terms of the theoretically derived eqn 2.2.18 are represented, is given here. It is mainly aimed as a basis for further discussions. The used model is eqn 2.3.6 multiplied by G, expressed with an angle dependence and with the addition of a heat capacity term:

$$q = g_{sys,0,n}K(1\text{-}R\Delta T)G - U_{sys,0}\Delta T - U_{sys,1}\Delta T^2 - C\Delta T_f/\Delta\tau \qquad (2.4.1)$$

where $R = g_{sys,1}/g_{sys,0}$, $K = (K_bG_b + K_dG_d)/G$ and C is the effective heat capacity of the collector.

The suggested test procedure works stepwise. A maximum of two parameters are determined from each set of data, which minimizes errors due to cross-dependecies of parameters. The collector is measured both with and without irradiation for two different ΔT, for example, ΔT = 20°C and ΔT = 50°C. No measurements are made for ΔT = 0°C. The number of measurements periods needed is the same as for the CEN steady state test method.

Firstly, the approximate value of C (equal to parameter c_5 of eqn 2.3.3) can be calculated according to a formula given by the CEN standard for the steady state test method. $C\Delta T_f/\Delta\tau$ is only a correction term and has only small influence on the result when used for predicting the energy output from the collector. The test should also be made with only small variations in T_f and it is therefore not critical to obtain an exact value of C for use in the measurement evaluation. By adding this term to the measured energy output: $q_1 = q + C\Delta T_f/\Delta\tau$, the next step in the parameter identification process can be made for $q_1 = g_{sys,0,n}K(1\text{-}R\Delta T)G - U_{sys,0}\Delta T - U_{sys,1}\Delta T^2$.

The two heat loss coefficients, $U_{sys,0}$ and $U_{sys,1}$ can be obtained from the two measurement periods without irradiation, where $q_1 = - U_{sys,0}\Delta T - U_{sys,1}\Delta T^2$. After they are determined, the heat loss terms are added to the collector output: $q_2 = q_1 + U_{sys,0}\Delta T + U_{sys,1}\Delta T^2 = g_{sys,0,n}K(1\text{-}R\Delta T)G$, which is then used in the next step.

From measured data with high irradiation at or close to normal incidence, assuming K is constant, R can be solved from the two measurement periods with the equation: $X_0 - X_1\Delta T = q_2/G$, where R is obtained as X_1/X_0. q_2 is then divided by $(1\text{-}R\Delta T)$ and the new equation can be written: $q_3 = g_{sys,0,n}KG$.

If the incidence angle dependence is expressed with the b_0 function (see eqn 2.2.15), the equation will become: $q_3 = g_{sys,0,n}((1-b_0(1/\cos(\theta)-1))G_b + K_dG_d)$. Since there is a strong correlation between K_d and b_0, K_d could be replaced by a function of b_0. A correlation which is approximately valid for flat plate collectors is $K_d = 1 - 0.8b_0$. We then have: $q_3 = g_{sys,0,n}G - g_{sys,0,n}b_0((1/\cos(\theta)-1)G_b + 0.8G_d)$. If the test is made indoors with a solar simulator, the diffuse irradiation can be neglected and the equation is: $q_3 = g_{sys,0,n}(1 - b_0(1/\cos(\theta)-1))G$.

By using data close to normal incidence and at a higher incidence angle, for instance at around 60°, the value of b_0 and $g_{sys,0,n}$ can be determined by a linear regression analysis for q_3. It is of course possible to use data also for other angles of incidence in the regression analysis. This would probably increase the validity of the b_0 parameter but also decrease the repeatability, since the b_0 function does not perfectly fit the angle dependence of the beam irradiation (see e.g. Helgesson and Karlsson 2001). Different sets of incidence angles for different seasons and locations could therefore then result in different values of b_0.

All parameters of eqn 2.4.1 are thereby identified.

2.5 Accuracy aspects of the suggested test model

One thing that has not been considered in this model (eqn 2.2.18) is that F', in reality, is also a function of the heat carrier fluid temperature, since the heat transfer coefficient between the pipe wall and the fluid, h_i, is determined by temperature dependent flow conditions. This is, of course, especially the case if the flow rate is at or close to the transition region between laminar and turbulent flow, which however, according to CEN, should be avoided in a collector test. This effect will however, on the whole, be "absorbed" by the temperature dependence of F' in the model, see eqn 2.2.7, and will therefore mainly influence the size of the three "correction" (last) terms on the right hand side of eqn 2.2.13.

Since the ambient temperature for outdoor testing is lower at night time (for clear weather conditions) than in the daytime, the lower values of T_f and T_a for the same ΔT could result in a slightly lower U_{sys}. The difference is however in most cases negligible. The parameter $(\tau\alpha)$ is a weak function of both ΔT and G, but is here treated as a constant. The error due to this is however also negligible.

The influence from wind and sky radiation is not considered in the model. For this and other reasons, best accuracy and repeatability would probably be achieved with indoor testing, with a controlled "wind" and "sky temperature" influence. For energy simulation, it is possible to make theoretically based corrections for the influence of these climatic variables.

2.6 Discussion

Some advantages of the suggested test method are:

- The used model fits that theoretically derived. A dependence on ΔTG is included as a separate term, which gives a better agreement between model and reality.
- In contrast to the CEN test models, this model uses the values of g and U_L for the collector, which are physically well defined concepts that are used also for windows and buildings.
- In the CEN quasi-dynamic test method, the 6 parameters are determined from all periods of data. In the steady state test method 3 parameters are determined from 4 periods of measurements. In the proposed method, at most 2 parameters are determined from 2 periods of data. Although the model has one extra term, the two heat loss terms are identified from separate measurements without irradiation, which gives one parameter less to identify with irradiation. This gives fewer "degrees of freedom" for the parameter identification process, which minimizes errors due cross-dependecies of the parameters. It should therefore be possible to obtain both good accuracy and good repeatability.

A disadvantage of the suggested test method is that the model gives a discrepancy for efficiencies close to $\Delta T = 0$. This is because the linear model of U_L does not describe well the actual value of U_L close to $\Delta T = 0$, where U_L increases rapidly with ΔT. However, since collectors are not often operated at such low values of ΔT, the problem is mainly theoretical. It could also be seen from Fig. 2.2 that the size of $U_{sys,1}$ is larger than a_2, which makes the fit line in Fig. 2.1 slightly more curved than the efficiency. The error from this is however small.

2.7 Conclusions

- If the temperature dependence of the collector efficiency factor is taken into account in the energy output equation for a flat plate collector, a dependence of the product of the irradiation and the temperature difference, ΔTG, is also obtained. This extra term, proportional to ΔTG, is usually not part of the energy output equation. If the term is not explicitly expressed in the equation, its value will instead be implicitly included in other terms of the equation. It is shown that for the theoretical equation $q = F'S - F'U_L\Delta T$, the extra term is about equally included in the gain and the loss terms. For the equation often used in tests today, $q = \eta_0 - a\Delta T$, the extra term is mainly included in the loss term. For the equation $q = g_{sys} - U_{sys}\Delta T$, which uses the conventional definitions of g and U, the term is included in the gain term.

- The equation $q = g_{sys} - U_{sys}\Delta T$ is suggested as the basis for an alternative way to test solar collectors, using measurements without irradiation to determine the heat loss coefficients. The test method works stepwise, identifying at most two parameters from each set of measurement periods, which reduces errors due to cross-dependences between parameters. This could result in both good accuracy and good repeatability, although the model has an extra term compared with the CEN standard test models.

3 Calculation of collector parameters and energy output

3.1 Introduction

The energy output from a flat plate solar collector can be calculated by setting up energy balance equations for each layer of the collector and solving the equation system for the temperatures. The term "layer" here denotes a sheet modelled with a uniform temperature, such as the cover, the absorber or any intermediate parallel sheet such as a polymer film. The temperatures of the heat carrier fluid and the ambient are part of the boundary conditions. For a honeycomb between the cover and the absorber, a finite difference solution, in which the honeycomb is divided into a number of layers, is applied.

In order to calculate the heat exchange between the different layers, coefficient correlations for the convection heat transfer between two plane, parallel and adjacent layers, are used. Some of these correlations, available in the literature, are here compared. For the IR radiation exchange, a general formula to calculate the IR radiation exchange factor between any two layers in a stack of parallel layers is given. For honeycombs, a technique to calculate the IR exchange factors between different layers of the honeycomb is presented. Also formulas for calculating the solar absorption in the different layers are given.

The temperatures of the layers are determined by a process of iteration between calculating the heat transfer coefficients (starting with guessed temperatures) and solving the equation system for the layer temperatures. The collector output can then be calculated from the layer temperatures.

The algorithms are suitable for computer programming. Collector specific parameters (see Section 2.2) can be calculated by running the program with different boundary conditions.

3.2 Optical properties of plane layers

The angular dependent and spectral optical properties of plane sheets are used in the calculation procedures given in Chapter 3. Therefore, formulas for calculating the incidence angle dependent properties for the two polarization components from (measured) normal reflectance and transmittance values are given here. For a homogeneous, smooth and dielectric material (such as uncoated plastic or glass panes) surrounded by air, the following expressions (as adapted from Källblad, 1998) derived from the Fresnel equations and Snell's law, can be used. The surface reflectance for the *s*- and *p*-polarized components of the light, r_s and r_p, and the bulk transmittance of the sheet, t, for the incidence angle, θ, can be calculated from:

$$r_s = \left(\frac{\cos(\theta) - (n^2 - \sin^2(\theta))^{0.5}}{\cos(\theta) + (n^2 - \sin^2(\theta))^{0.5}} \right)^2 \tag{3.2.1}$$

$$r_p = \left(\frac{n^2\cos(\theta) - (n^2 - \sin^2(\theta))^{0.5}}{n^2\cos(\theta) + (n^2 - \sin^2(\theta))^{0.5}} \right)^2 \tag{3.2.2}$$

$$t = e^{-KLn/(n^2 - \sin^2(\theta))^{0.5}} \tag{3.2.3}$$

where n is the refractive index, K is the absorption coefficient and L is the thickness of the sheet. The values can then be used for calculating the angle dependent transmittance (τ), reflectance (ρ) and absorptance (α) of the sheet for the two polarization components, *s* and *p*, of the light, here replaced by index *i*:

$$\tau_i = t\,(1 - r_i)^2 / (1 - t^2 r_i^2) \tag{3.2.4}$$

$$\rho_i = r_i + t^2 r_i\,(1 - r_i)^2 / (1 - t^2 r_i^2) = r_i\,(1 + t\,\tau_i) \tag{3.2.5}$$

$$\alpha_i = 1 - \rho_i - \tau_i = (1 - t)(1 - r_i) / (1 - t\,r_i) \tag{3.2.6}$$

The corresponding properties for unpolarized light are then:

$$\tau = (\tau_s + \tau_p) / 2 \tag{3.2.7}$$

$$\rho = (\rho_s + \rho_p) / 2 \tag{3.2.8}$$

$$\alpha = (\alpha_s + \alpha_p) / 2 = 1 - \rho - \tau \tag{3.2.9}$$

The refractive index, n, and the product of the absorption coefficient, K, and the layer thickness, L, used in the equations above, can be obtained from (measured) values at normal incidence of the transmittance (τ_n) and the reflectance (ρ_n) through:

$$n = \frac{1 + r_n^{0.5}}{1 - r_n^{0.5}} \tag{3.2.10}$$

$$KL = \ln\left(\frac{\tau_n \cdot r_n}{\rho_n - r_n}\right) \tag{3.2.11}$$

where

$$r_n = \frac{\tau_n^2 - \rho_n^2 + 2\rho_n + 1 - ((\tau_n^2 - \rho_n^2 + 2\rho_n + 1)^2 + 4\rho_n^2 - 8\rho_n)^{0.5}}{4 - 2\rho_n} \tag{3.2.12}$$

r_n is here the surface reflectance at normal incidence. Eqns 3.2.10-12 can be derived from eqns 3.2.1-5 for $\theta = 0°$. All properties in the eqns 3.2.1-12 are functions of wavelength.

3.3 Radiation heat exchange in a glazing with absorber-parallel layers

Several studies in the literature treat the problem of calculating the radiation heat losses through a stack of parallel layers. There are in general two ways of solving this type of problem; the so-called net-radiation method (sometimes also called the radiosity method) and the ray-tracing method (see Siegel and Howell, 2002).

In the net-radiation method an equation system is set up for the radiosities leaving the surfaces in both directions in each gap. By including the energy balance equations for each layer and solving the equation system, the temperatures of the layers and the total heat transfer can be calculated. Used in a straightforward way, the method works only with integrated IR-properties of the layers, which means that the calculations can not be made angular resolved or spectral. The net-radiation method was used by Hollands and Wright (1983). They solved the radiosity balance equations together with the energy balance equations and iterated with calculations of the (temperature dependent) gap convection heat

transfer coefficients. By calculating with and without solar irradiation they obtained values of ($\tau\alpha$) and U_t (see Duffie and Beckman, 1991) for a collector.

In order to make the calculations angle resolved and/or spectral using the net-radiation method, the radiation exchange factors between all layers of the stack have to be calculated. This can be done by setting the blackbody radiosity to one for a specific layer and to zero for all the other layers and then solving the system of radiosity equations. The equation system has to be solved for each emission angle, polarization and/or wavelength. The radiation exchange factors between this layer and the others can then be obtained by angular and spectral integration. Such a solution was used by Edwards and Rhee (1984).

In this chapter explicit formulas for calculating the radiation heat transfer coefficients between any two layers in a stack are given. The formulas have been derived from ray tracing analysis. An explicit solution has the advantage that the calculations can easily be made spectral and/or angular and polarization resolved. It is also convenient for computer programming.

The formulas are derived for a stack of layers numbered from 0 to n, where layers 0 and n are the opaque boundaries (the ambient and the absorber). All the other layers may be semitransparent to IR radiation. The height and width of the layers are assumed to be large compared with the distance between them, so edge effects are not considered.

The term front side denotes the side facing the ambient (the outside). Radiation in the forward direction is assumed to impinge on the front side of the layer.

A so-called effective reflectance, R, is calculated for the different layers. The effective reflectance of layer i is here defined as the reflectance of the stack of layer i and all layers behind it.

The effective reflectance for the radiation incident in the forward direction on layer i can be calculated recursively with the following formula:

$$R_{f,i} = \rho_{f,i} + \tau_i^2 R_{f,i+1}/(1 - R_{f,i+1}\,\rho_{b,i}) \tag{3.3.1}$$

where

$$R_{f,n} = \rho_{f,n} \tag{3.3.2}$$

For radiation incident in the backward direction the effective reflectance is:

$$R_{b,i} = \rho_{b,i} + \tau_i^2 R_{b,i-1}/(1 - R_{b,i-1}\,\rho_{f,i}) \tag{3.3.3}$$

where

$$R_{b,0} = \rho_{b,0} \tag{3.3.4}$$

Since layer 0 corresponds to the ambient, $\rho_{b,0}$ and $R_{b,0}$ are zero.

An effective transmittance of layer i (for $0 < i < n$) can for both directions be defined as

$$T_{f,i} = \tau_i / (1 - R_{f,i+1}\, \rho_{b,i}) \tag{3.3.5}$$

$$T_{b,i} = \tau_i / (1 - R_{b,i-1}\, \rho_{f,i}) \tag{3.3.6}$$

Indices f and b denotes that the incident radiation impinges on the front and the back side of the layer, respectively.

The effective emittance of both sides of layer i (for $0 < i < n$) is here defined by

$$E_{f,i} = \varepsilon_{f,i} + \varepsilon_{b,i}\, \tau_i\, R_{f,i+1} / (1 - R_{f,i+1}\, \rho_{b,i}) \tag{3.3.7}$$

$$E_{b,i} = \varepsilon_{b,i} + \varepsilon_{f,i}\, \tau_i\, R_{b,i-1} / (1 - R_{b,i-1}\, \rho_{f,i}) \tag{3.3.8}$$

For $i = 0$ (the ambient), $E_{b,0} = \varepsilon_{b,0} = 1$, and for $i = n$ (the absorber), $E_{f,n} = \varepsilon_{f,n} = \varepsilon_{abs}$. For E, indices f and b denote that the totally emitted radiation leaves the front and the backside of the layer, respectively.

The net radiation heat transfer from layer i to layer j, where $i < j$ is then:

$$q_{rad,\, ij} = f_{ij}\sigma(T_i^4 - T_j^4) \tag{3.3.9}$$

where

$$f_{ij} = E_{b,i}E_{f,j} / (1 - R_{f,i+1}R_{b,i}) \cdot [T_{f,i+1}\, T_{f,i+2} \ldots T_{f,j-1}] \tag{3.3.10}$$

For adjacent layers, when $j = i+1$, the value within the square brackets equals one. An equivalent formula is:

$$f_{ij} = E_{b,i}E_{f,j} / (1 - R_{f,j}R_{b,j-1}) \cdot [T_{b,i+1}\, T_{b,i+2} \ldots T_{b,j-1}] \tag{3.3.11}$$

The radiation heat transfer coefficient between layer i and j can then be written:

$$h_{rad,ij} = q_{rad,ij} / (T_i - T_j) = f_{ij}\, \sigma\, (T_i^2 + T_j^2)(T_i + T_j) \tag{3.3.12}$$

3.4 Convection/conduction heat losses in a glazing with absorber-parallel layers

There are numerous studies in the literature on the natural convection heat transfer in the air gaps between two absorber-parallel layers, with the hot plate below the cold one. Correlations of the convection heat transfer coefficient, h_c, are usually given by the relationship, $Nu = f(Ra,\theta)$, where $Nu = h_c/(k/L)$, $Ra = g\beta\Delta T_g L^3/(\nu\alpha)$ and θ is the tilt angle. In some cases there is also a dependence on the aspect ratio (the ratio of the height (or width) of the plates to the distance between them). Most studies treat the case of heat transfer between two isothermal plates. Three such correlations by Hollands et al. (1976), Edwards et al. (1976) and Inaba (1984) are shown in Fig. 3.1 for the tilt angle 45° and the plate temperatures 75°C and 25°C (ΔT_g = 50°C and T_m = 50°C). The correlations are only shown in the range of *Ra* for which they are recommended by the authors.

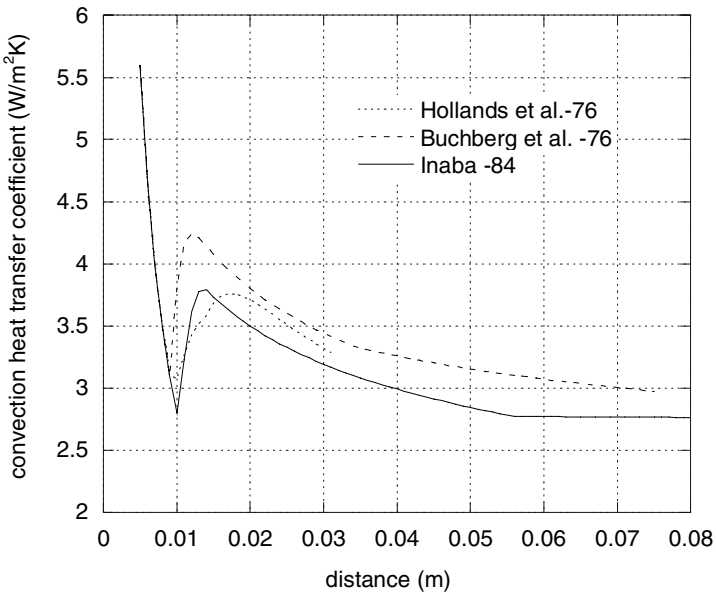

Fig. 3.1 *Convection heat transfer coefficient as a function of the distance between two 45° tilted, isothermal plates at 75°C and 25°C, with the hot plate below the cold one, calculated from correlations by Hollands et al. (1976), Buchberg et al. (1976) and Inaba (1984).*

A solar collector, however, does not in general have isothermal surfaces. If the heat carrier inlet is at the bottom and the outlet at the top of the collector, there will be a vertical temperature gradient in the collector, whose size depends (among other things) on the volume flow rate and the tilt angle. A lower flow rate will give a higher temperature gradient. The absorber will in such a case be more like isoflux (having a constant heat flux) than isothermal.

Schinkel and Hoogendoorn (1983) showed with measurements that the convection heat transfer coefficient is much larger at the bottom of the collector than at the top, a factor 2.5 higher for an isothermal absorber with A = 13.8, $Ra = 8.3 \cdot 10^4$ and $\theta = 60°$. Hellström et al. (1988a,b) obtained from measurements a factor of approximately 4.4 for an isothermal absorber and 2.4 for an isoflux absorber in a collector model with the absorber height/width of 1.14/1.50 m, A = 11.4, $Ra = 1.5 \cdot 10^6$ and $\theta = 45°$.

This has consequences for the heat losses of the collector. If the vertical temperature gradient and the local variation of the overall heat loss coefficient are taken into account, the heat losses (as given in eqn 2.1) can be written:

$$F'U_L(T_f - T_a) = \int_0^1 F'(x)U_L(x)(T_f(x) - T_a)dx \qquad (3.4.1)$$

where x is the relative height of the absorber. It can be seen from eqn 3.4.1 that $F'U_L$ is a mean value of $F'(x)U_L(x)$, weighted against $\Delta T(x) = T_f(x) - T_a$. If $U_L(x)$ were the same for both an isoflux and an isothermal absorber, eqn 3.4.1 would result in a lower U_L for the isoflux than for the isothermal absorber at the same mean temperature, since the high $U_L(x)$ at the bottom of the collector would be weighted against a low $\Delta T(x)$. For a reversed flow direction (with the inlet at the top), the weighting would be the opposite and result in a higher U_L. Measurements (and calculations) by Schinkel and Hoogendoorn (1983) indicate however that $h_c(x)$ (and thereby $U_L(x)$), for most values of x, is higher for an isoflux than for an isothermal absorber, which makes the prediction of the influence of the flow type on U_L more complex. (The influence of the radiation heat transfer coefficient on $U_L(x)$ is small provided that a low-emitting absorber is used).

The average convection heat loss coefficient, h_c, can be calculated from:

$$h_c = \frac{\int_0^1 h_c(x)(T_p(x) - T_g)dx}{\int_0^1 (T_p(x) - T_g)dx} \qquad (3.4.2)$$

where T_p and T_g are the the temperatures of the absorber plate and the cover, respectively. Hellström et al. (1988a,b) obtained from measurements in a collector model with a h_c 5% higher for the isoflux than for the isothermal absorber with the same mean temperature. Schinkel and Hoogendoorn (1983) obtained a higher difference (11%) for θ = 40°, but then calculated h_c as the (unweighted) average value of $h_c(x)$ along the absorber.

Yiqin et al. (1991) derived a correlation valid for air gaps between two surfaces, out of which only one is isothermal. A collector with a plastic film between an isothermal absorber and an isothermal cover will have two such air gaps. This correlation gives a higher h_c than the corresponding correlation for isothermal surfaces by Hollands et al. (1976). It does not however take into account that the absorber and (to a lesser extent) the cover are non-isothermal.

Most correlations given in the literature are obtained for idealized conditions. A real collector with fin absorbers has, apart from a vertical temperature gradient, also temperature gradients across the fins. Furthermore, the absorber is usually not perfectly flat. A study that experimentally investigated the convection heat transfer for a real collector under typical operating conditions was performed by Bartelsen et al. (1993). They obtained convection heat transfer coefficients that were significantly higher than if given by correlations of isothermal boundaries. For a case comparable with Fig. 3.1 (with $T_m = \Delta T_g$ = 50.9°C instead of 50°C), they received values of h_c = 4.5 W/m^{2}K at 0.02 m distance, descending asymptotically to h_c = 4.0 W/m^{2}K at 0.08 m. Furthermore, they did not obtain the dip in the curve at small distances (as shown in Fig. 3.1). Although there are uncertainties in the measurements (as the authors underline), the results indicate that there might be a need for further investigations in this area.

Since the results of the mentioned studies indicate that the convection heat transfer coefficient is somewhat higher for an air gap in a real collector than between plane, isothermal boundaries, the correlation by Buchberg et al. (1976) could be used as a compromise for calculations of solar collector air gaps, since it gives the highest values of the three correlations in Fig. 3.1. The correlation is written:

$$Nu = 1 \text{ for } Ra\cos(\theta) < 1708 \tag{3.4.3}$$

$$Nu = 1 + 1.446(1\text{-}1708/(Ra\cos(\theta))) \text{ for } 1708 < Ra\cos(\theta) < 5900 \tag{3.4.4}$$

$$Nu = 0.229(Ra\cos(\theta))^{0.252} \text{ for } 5900 < Ra\cos(\theta) < 92300 \tag{3.4.5}$$

$$Nu = 0.157(Ra\cos(\theta))^{0.285} \text{ for } 92300 < Ra\cos(\theta) < 10^6 \qquad (3.4.6)$$

The convection heat transfer coefficient, $h_{c,ij}$, between the two layers i and j, can then be calculated from

$$h_{c,ij} = Nu \cdot k / L \qquad (3.4.7)$$

where k is the heat conductivity of the medium (air) and L is the distance between the layers i and j.

3.5 Solar absorption in a glazing with absorber-parallel layers

When the total solar absorptance of a layer i is calculated, it can be treated as a radiation exchange between layer 0 (the ambient) and layer i with solar (instead of IR) radiation. Therefore, eqn 3.3.10 can be used by substituting index i for 0 and j for i, and also replacing $E_{b,i}$ by $A_{b,0} = 1$ and $E_{f,j}$ by $A_{f,i}$, which is the effective absorptance of layer i for solar radiation. We also have that $R_{b,0} = 0$. (The absorptance of the ambient is one and the reflectance is zero). The total solar absorptance, A_i, of layer i is then

$$A_i = A_{f,i} \cdot [T_{f,1} T_{f,2} \ldots T_{f,i-1}] \qquad (3.5.1)$$

where for $1 \leq i \leq n$-1:

$$A_{f,i} = \alpha_{f,i} + \alpha_{b,i} T_{f,i} R_{f,i+1} \qquad (3.5.2)$$

and

$$T_{f,i} = \tau_i / (1 - R_{f,i+1} \rho_{b,i}) \qquad (3.5.3)$$

The effective reflectance $R_{,f,i}$ is obtained from the recursive formula:

$$R_{f,i} = \rho_{f,i} + \tau_i^2 R_{f,i+1} / (1 - R_{f,i+1} \rho_{b,i}) \qquad (3.5.4)$$

where

$$R_{f,n} = \rho_{f,n} \qquad (3.5.5)$$

For $i = 1$ (the cover), the value within the square brackets of eqn 3.5.1 equals one. For $i = n$ (the absorber), $A_{f,n} = \alpha_{f,n} = \alpha_{abs}$.

The above calculation algorithm is the same as was given by Edwards (1977). The optical properties of the layers in eqns 3.5.1-5 have the same meaning as in Section 3.3, except that they are valid in the solar wavelength range instead of the IR range.

Eqns 3.5.1-5 are valid for either beam or diffuse irradiation, using corresponding angle dependent and diffuse optical properties. If some layer(s) would partly diffuse the beam irradiation, a special algorithm is needed. If prim (x') and bis (x'') denote diffusing and diffuse, respectively, the formulas corresponding to eqn 3.5.1-5 are:

$$A_i' = A_{f,i}'' [(T_{f,1}' T_{f,2}'' \ldots . T_{f,i-1}'') + (T_{f,1} T_{f,2}' \ldots . T_{f,i-1}'') + \ldots + (T_{f,1} T_{f,2} \ldots . T_{f,i-1}')] + \alpha_{b,i}''(T_{f,1} T_{f,2} \ldots . T_{f,i-1})(\tau_i' R_{f,i+1}'' + T_{f,i} (R_{f,i+1}' + R_{f,i+1} R_{f,i+1}'' \rho_{b,i}'))/(1 - R_{f,i+1}'' \rho_{b,i}'') \quad (3.5.6)$$

$$T_{f,i}' = (\tau_i' + T_{f,i} (R_{f,i+1}' \rho_{b,i}'' + R_{f,i+1} \rho_{b,i}'))/(1 - R_{f,i+1}'' \rho_{b,i}'') \quad (3.5.7)$$

$$R_{f,i}' = \rho_{f,i}' + T_{f,i} \tau_i' R_{f,i+1} + \tau_i''(\tau_i' R_{f,i+1}'' + T_{f,i} (R_{f,i+1}' + R_{f,i+1} R_{f,i+1}'' \rho_{b,i}'))/(1 - R_{f,i+1}'' \rho_{b,i}'') \quad (3.5.8)$$

$$R_{f,n}' = \rho_{f,n}' \quad (3.5.9)$$

For $i = 1$ (the cover), the value within the square brackets in eqn 3.5.6 equals zero. For $i = n$ (the absorber), $\alpha_{b,i}'' = 0$ and $A_{f,i}'' = \alpha_{f,n}'' = \alpha_{abs}''$.

A_i' is the total solar absorptance of layer i for diffused beam irradiation. The total absorptance for beam irradiation is then $A_i + A_i'$, while the total absorptance for diffuse irradiation is A_i''. The latter is obtained by using diffuse properties in eqns 3.5.1-5.

3.6 Radiation heat exchange in a honeycomb glazing

Both analytical and numerical solutions to the problem of heat transport through a honeycomb are given in the literature. In order to get accurate results, the heat transport by radiation and conduction has to be treated as a coupled mechanism, although a decoupled calculation is assumed to give acceptable results for the case of black end surfaces, see e.g. Hollands at al. (1984) and Platzer (1992a,b).

Hollands et al. (1984) modelled a hexagonal honeycomb as an opaque wall cylinder with an effective IR reflectance, $\rho_{eff} = \rho + \tau$. The opaque wall model gives an equivalent solution of the radiation transport due to the symmetry of the honeycomb structure. The cylindrical form is (of course) an approximation. They divided the cylinder into a number of "rings" of wall elements, between which the view (configuration) factors for both specular and diffuse wall reflection can be obtained from analytical expressions (see e.g. Siegel and Howell, 1994). A numerical solution of the system of radiosity and energy balance equations for the elements gave results which agreed well (within 5%) with reported measurements, performed with a guarded hot-plate apparatus. Suehrcke et al. (2004) used the same numerical method for a square cell honeycomb and included also an air gap in the calculations. Their measurements with a guarded hot-plate apparatus agreed well with their calculated results.

Hollands et al. (1984) presented also an approximate analytical solution, which was faster to use but did not agree quite as well (within 10%) with the measurements as the numerical model. The analytical solution generally underpredicted the heat transfer compared with the numerical solution, especially for honeycombs of high aspect ratio (honeycomb thickness to cell width). The analytical model was later extended to include an air gap between the honeycomb and one of the boundary plates (Hollands and Iyankaran, 1992a). An air gap (1 cm wide) between the absorber and the honeycomb had earlier been suggested by Hollands et al. (1984), in order to decouple the radiation and conduction modes and thereby better utilize the low emittance of a selective absorber.

Edwards and Tobin (1967) derived an approximate analytical solution for the radiation heat transport through a long rectangular passage with adiabatic, gray, opaque walls and black end surfaces. The solution is a function of the diffuse-diffuse IR transmittance and its integral for half/whole of the honeycomb thickness and was later extended to gray end surfaces by Platzer (1992a).

To obtain a solution for the coupled radiation/conduction heat transfer, Platzer (1992a) used the resulting radiation heat transport for black end surfaces to calculate an effective optical thickness of the honeycomb with an approximate formula for radiation heat transport through a gas layer between black end surfaces. This effective optical thickness was then used for an analytical solution of the coupled radiation/conduction heat transport of an absorbing/emitting gas between black boundaries, using the so-called exponential kernel approximation (see e.g. Sparrow and Cess, 1966) and a fourth-power temperature linearization.

Such a solution had earlier been provided by Marcus (1983), who, however, calculated the effective optical thickness from the transmittance in the same way as for a gas, which, according to Platzer, leads to an underestimation of the radiation transport. This calculation was based on an approximation of the honeycomb transmittance as an exponential function, which was earlier proposed by Tien and Yuen (1975), a similar approximation that also Hollands et al. (1984) made.

Platzer (1992a) included an air gap (with possible convection) between the honeycomb and the absorber in the calculations, using an iterative method. He reported good agreement between calculations and measurements, which were performed with a guarded hot-plate apparatus.

Platzer (1992b) also showed that the effective optical thickness of the honeycomb could be obtained from measurements of the total heat transport for a honeycomb between black end surfaces by subtracting the conduction part, assuming the heat transfer modes (radiation and conduction) to be uncoupled. An effective extinction coefficient for the honeycomb could then be determined as a function of the honeycomb thickness from measurements of honeycombs with different thickness. The inverse of this effective extinction coefficient was modelled by Platzer as the sum of a constant and a thickness dependent part.

In this chapter, a numerical solution to the problem is given. The symmetry of the honeycomb structure is used for simplifying the optical properties, but in contrast to the solution given by Hollands et al (1984), the IR reflectance is assumed to be included in (added to) the IR transmittance, giving $\tau_{eff} = \tau + \rho$ and $\rho_{eff} = 0$. The honeycomb is divided into a number of absorber-parallel layers and the heat transfer coefficients between the different layers, including the absorber and the cover (and the ambient), are determined. The temperatures of the layers can then be calculated in the same way as for a glazing with absorber-parallel sheets (see Section 3.10).

This procedure for calculating the radiation heat transfer coefficients between any two layers is to calculate the radiation exchange factors from the walls of a honeycomb cell in layer i to all the cell walls in layer j, which are within a certain (horizontal) distance. The distance is chosen so large that increasing it does not affect the result (within a given limit). Outside this distance, the radiosity originating from the cell of layer i is negligible, since (almost) all radiation has been absorbed by the closer walls. This means that a higher absorptance of the honeycomb wall will require a shorter distance and vice versa. Due to the symmetry of the honeycomb structure, it is enough to consider radiation from only one cell.

A line between the midpoints of two interacting surfaces gives the approximate direction and distance between the surfaces for the view factor and transmittance calculations, used for calculating the radiation exchange. (For adjacent surfaces a better accuracy can be obtained by dividing the surfaces into parts). Since the angles between the radiation direction and the honeycomb walls are unchanged after both specular reflection and transmittance, the reflected radiation can be treated as transmitted. The reflectance of the honeycomb wall can therefore be included in (added to) the transmittance. (Shifts in position due to the honeycomb wall thickness are neglected). The view factor for the transmitted radiation only is the same as for the radiation reflected on one or several walls along the way (although the radiation then is finally absorbed by a different wall in layer j).

In order to account for reflections at the boundary surfaces, i. e. at the absorber and the cover, the number of layers which are calculated for should exceed the number of layers of the honeycomb to account for reflections at the boundary surfaces. These reflections are assumed to be specular, which only prolongs the pathway between the interacting cells (and reduces the intensity). The number of multiple reflections which are taken into account is optional, but in practice, if for instance a glass pane is used as cover, taking two absorber/cover reflections into account would give an accuracy that is good enough. This is partly due to the low IR reflectance of most cover materials (such as glass or plastics). For a high IR reflectance of both the absorber and the cover, the required number of boundary surface reflections taken into account would probably need to be higher.

A schematic sketch of a honeycomb with a coordinate system is given in Fig. 3.2. The boundary surfaces (the absorber and the cover) and the division of the honeycomb into layers in the z-direction are not shown in the figure.

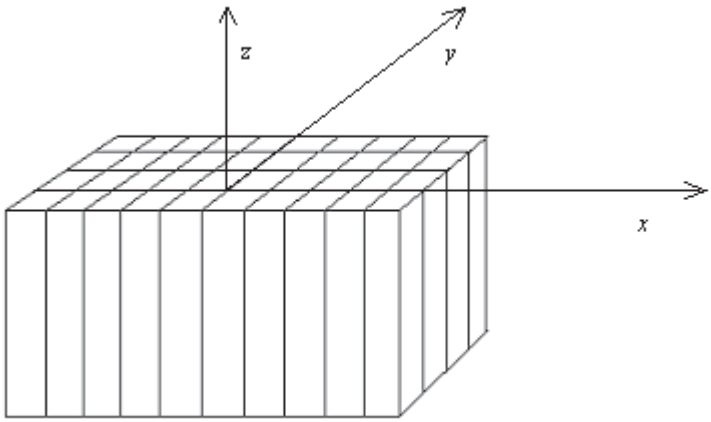

Fig. 3.2 *Schematic sketch of a honeycomb. The layer division in the z-direction and the boundary surfaces are not shown.*

The sum of the radiation exchange factors between a wall surface in the *x*-direction in layer *i* and the wall surfaces in the *y*-direction in layer *j*, f_{xy}, can be calculated as:

$$f_{xy} = 4\, A_x / A_z \sum_{m=0}^{M} \sum_{n=0}^{N} \varepsilon_x\, \varepsilon_y\, \tau_x^m \tau_y^n\, \nu_{xy} \qquad (3.6.1)$$

where A_i is the cell area facing in the *i* direction. If *dx*, *dy* and *dz* are the dimensions of the cell, $A_x = dydz$, $A_y = dxdz$ and $A_z = dxdy$. The factor 4 is due to the summation being made for both positive and negative *x*- and *y*-directions (= 4 combinations). *m* and *n* are the number of wall transmissions in the *x* and *y* directions, where *M* and *N* are the (chosen) maximum numbers. $(M+1)dx$ and $(N+1)dy$ are thereby the maximum distances in the *x*- and the *y*-directions, respectively. f_{xy} is normalized to the layer plane by the factor A_x/A_z. ε_x, ε_y, τ_x and τ_y are the angle dependent emittances and transmittances for the *x*- and the *y*-facing walls. ν_{xy} is the view factor from the cell wall in layer *i* to the cell wall in layer *j*. It can be approximately calculated as:

$$\nu_{xy} = A_y / (\pi R^2) \cdot \Delta x / R \cdot \Delta y / R \qquad (3.6.2)$$

where *R* is the distance between the centre points of the two wall surfaces:

$$R = ((\Delta x)^2 + (\Delta y)^2 + (\Delta z)^2)^{0.5} \qquad (3.6.3)$$

For this case (with radiation between one x- and one y-directed honeycomb wall), $\Delta x = (m+0.5)dx$, $\Delta y = (n+0.5)dy$ and $\Delta z = kdz$, where k is the number of layers separating the walls: $k = j - i$. $\Delta x/R$ and $\Delta y/R$ in eqn 3.6.2 are the cosines of the incidence angles of the x- and the y-facing walls.

The incidence angles can be calculated from the cosines. The angular dependent properties of the honeycomb film can be calculated from the known (measured) values at normal incidence using the Fresnel relations (see Section 3.2). To account for the effects of polarization from the passage through the honeycomb walls, the intensity of the p- or s- polarized radiation would have to be transformed for each change of (x-/y-) direction of the interacting wall, which was shown by Edwards and Tobin, 1967. They also showed that the effect of polarization for a (square celled) honeycomb structure is small (in contrast to the slat structure), which means that the effect could be neglected without a severe loss in accuracy.

Substituting the expression from eqn 3.6.2 into eqn 3.6.1 gives:

$$f_{xy} = 4 \sum_{m=0}^{M} \sum_{n=0}^{N} \varepsilon_x \varepsilon_y \tau_x^m \tau_y^n \Delta x \Delta y A_x A_y / (A_z \pi R^4) \qquad (3.6.4)$$

where $A_x = dydz$, $A_y = dxdz$ and $A_z = dxdy$.

In analogy, the sum of the radiation exchange factors between a wall facing in the y-direction in layer i and a wall surface in the x-direction in layer j can then be calculated as:

$$f_{yx} = 4 \sum_{m=0}^{M} \sum_{n=0}^{N} \varepsilon_x \varepsilon_y \tau_x^m \tau_y^n \Delta x \Delta y A_x A_y / (A_z \pi R^4) = f_{xy} \qquad (3.6.5)$$

If both walls are facing in the x-direction, the corresponding formula is:

$$f_{xx} = 4 \sum_{m=0}^{M} \sum_{n=1}^{N} \varepsilon_x^2 \tau_x^m \tau_y^n (\Delta x)^2 A_x^2 / (A_z \pi R^4) + 2 \sum_{m=0}^{M} \sum_{n=0}^{0} \varepsilon_x^2 \tau_x^m (\Delta x)^2 A_x^2 / (A_z \pi R^4) \qquad (3.6.6)$$

where (for this case) $\Delta x = (m+1)dx$, $\Delta y = ndy$ and $\Delta z = kdz$. R is calculated with eqn 3.6.3.

The reason that a factor 2 instead of 4 is used for $n = 0$ is that, since $\Delta y = 0$, the summation is made only for the positive and the negative x-direction. f_{xx} is normalized to the layer plane by the factor A_x/A_z.

In analogy, if both the walls (in layer 1 and 2) are facing the *y*-direction, the corresponding formula is:

$$f_{yy} = 4\sum_{m=1}^{M}\sum_{n=0}^{N} \varepsilon_y{}^2\, \tau_x{}^m \tau_y{}^n\, (\Delta y)^2 A_y{}^2/(A_z \pi R^4) + 2\sum_{m=0}^{0}\sum_{n=0}^{N} \varepsilon_y{}^2\, \tau_y{}^n\, (\Delta y)^2 A_y{}^2/(A_z \pi R^4) \qquad (3.6.7)$$

where (for this case) $\Delta x = mdx$, $\Delta y = (n+1)dy$ and $\Delta z = kdz$. R is obtained from eqn 3.6.3.

In the same way, the sum of the radiation exchange factors between the cell surface of the absorber or the cover, facing in the z-direction, and the honeycomb wall surfaces in the *x*-direction, f_{zx}, is obtained from:

$$f_{zx} = 4\sum_{m=0}^{M}\sum_{n=1}^{N} \varepsilon_x \varepsilon_z\, \tau_x{}^m \tau_y{}^n\, \Delta x \Delta z\, A_x/(\pi R^4) + 2\sum_{m=0}^{M}\sum_{n=0}^{0} \varepsilon_x \varepsilon_z\, \tau_x{}^m\, \Delta x \Delta z\, A_x/(\pi R^4) \qquad (3.6.8)$$

where (for this case) $\Delta x = (m+0.5)dx$, $\Delta y = ndy$ and $\Delta z = (k\text{-}0.5)dz$. R is then calculated with eqn 3.6.3. $\mathring{a}_z$ is the emittance of the absorber or the back side of the cover.

By analogy, the sum of the radiation exchange factors between a cell surface in the *z*-direction and the surfaces in the *y*-direction, f_{zy}, is:

$$f_{zy} = 4\sum_{m=1}^{M}\sum_{n=0}^{N} \varepsilon_y \varepsilon_z\, \tau_x{}^m \tau_y{}^n\, \Delta y \Delta z\, A_y/(\pi R^4) + 2\sum_{m=0}^{0}\sum_{n=0}^{N} \varepsilon_y \varepsilon_z\, \tau_y{}^n\, \Delta y \Delta z\, A_y/(\pi R^4) \qquad (3.6.9)$$

where (for this case) $\Delta x = mdx$, $\Delta y = (n+0.5)dy$ and $\Delta z = (k\text{-}0.5)dz$. R is obtained from eqn 3.6.3. The relations $f_{yz} = f_{zy}$ and $f_{xz} = f_{zx}$ are also valid.

Finally, the sum of the radiation exchange factors between a cell surface in the absorber and cell surfaces in the cover, f_{zz}, can be calculated from:

$$f_{zz} = 4\sum_{m=1}^{M}\sum_{n=1}^{N} \varepsilon_{z1}\varepsilon_{z2}\,\tau_x^{\,m}\tau_y^{\,n}\,\Delta z^2 A_z/(\pi R^4) + 2\sum_{m=1}^{M}\sum_{n=0}^{0} \varepsilon_{z1}\varepsilon_{z2}\,\tau_x^{\,m}\,\Delta z^2 A_z/(\pi R^4) + 2\sum_{m=0}^{0}\sum_{n=1}^{N} \varepsilon_{z1}\varepsilon_{z2}\,\tau_y^{\,n}\,\Delta z^2 A_z/(\pi R^4) + \sum_{m=0}^{0}\sum_{n=0}^{0} \varepsilon_{z1}\varepsilon_{z2}\,\Delta z^2 A_z/(\pi R^4) \qquad (3.6.10)$$

where (for this case) $\Delta x = mdx$, $\Delta y = ndy$ and $\Delta z = (k\text{-}1)dz$. R is obtained from eqn 3.6.3. ε_{z1} and ε_{z2} are the emittances for the cover (the backside) and the absorber.

If the radiation reflected by the cover and the absorber is disregarded, the radiation exchange factor between two layers within the honeycomb is:

$$f_s(\Delta z) = f_{xy}(\Delta z) + f_{yx}(\Delta z) + f_{xx}(\Delta z) + f_{yy}(\Delta z) \qquad (3.6.11)$$

If the number of reflections on the end surfaces is limited to two, one on the cover (layer 1) and one on the absorber (layer n), the radiation exchange factor between layer i and j $(i < j)$ within the honeycomb is:

$$f_{ij} = f(\Delta z_1) + \rho_{f,n}\, f_s(\Delta z_2) + \rho_{b,1}\, f_s(\Delta z_3) + \rho_{f,n}\,\rho_{b,1}(\, f_s(\Delta z_4) + f_s(\Delta z_5)) \qquad (3.6.12)$$

where $\rho_{f,n}$ is the reflectance of the absorber and $\rho_{b,1}$ is the reflectance of the backside of the cover and

$$\Delta z_1 = (j - i)dz$$
$$\Delta z_2 = (j - i + 2(n - 0.5 - j))dz$$
$$\Delta z_3 = (j - i + 2(i - 1.5))dz$$
$$\Delta z_4 = (2(n - 2) - (j - i))dz$$
$$\Delta z_5 = (2(n - 2) + j - i)dz$$

where layer n is the absorber and layer 1 is the cover.

The radiation exchange factor between layer i within the honeycomb $(1 < i < n)$ and layer n (the absorber) is:

$$f_{in} = f_{zs}(\Delta z_6) + \rho_{b,1}\, f_{zs}(\Delta z_7) + \rho_{b,1}\,\rho_{f,n}\, f_{zs}(\Delta z_8) \qquad (3.6.13)$$

where

$$f_{zs}(\Delta z) = f_{zx}(\Delta z) + f_{zy}(\Delta z) \tag{3.6.14}$$

and

$$\Delta z_6 = (n - 0.5 - i)dz$$
$$\Delta z_7 = (n - 0.5 - i + 2(i - 1.5))dz$$
$$\Delta z_8 = (n - 0.5 - i + 2(n - 2))dz$$

The radiation exchange factor between layer 1 (the cover) and layer j within the honeycomb ($1 < j < n$) is:

$$f_{1\,j} = f_{zs}(\Delta z_9) + \rho_{f,n} f_{zs}(\Delta z_{10}) + \rho_{f,n} \rho_{b,1} f_{zs}(\Delta z_{11}) \tag{3.6.15}$$

where

$$\Delta z_9 = (j - 1.5)dz$$
$$\Delta z_{10} = (j - 1.5 + 2(n - 0.5 - j))dz$$
$$\Delta z_{11} = (j - 1.5 + 2(n - 2))dz$$

Finally, the radiation exchange factor between layer 1 (the cover) and layer n (the absorber) can be calculated with:

$$f_{1n} = f_{zz}(z_{12}) + \rho_{f,n} \rho_{b,1} f_{zz}(z_{13}) \tag{3.6.16}$$

where

$$\Delta z_{12} = (n - 2)dz$$
$$\Delta z_{13} = 3(n - 2)dz$$

In case the cover is not opaque for IR radiation, there will also be a radiation exchange with the ambient. The radiation exchange factor between the ambient (layer 0) and any layer behind the cover, f_{0i}, can be obtained with the same formulas as for the exchange factors of the cover, f_{1j}, (eqn 3.6.15), but with the backside emittance of the cover, $\varepsilon_{b,1}$ (= ε_z or ε_{z1}), replaced by the IR transmittance, τ_1, in eqns 3.6.8-10. If the used transmittance and emittance values of the cover are not angular dependent, f_{0i} could also be calculated with the following formula:

$$f_{0i} = f_{1i} \cdot \tau_1 / \varepsilon_{b,1} \tag{3.6.17}$$

where $2 \leq i \leq n$.

The radiation exchange factor between the ambient and the cover, f_{01}, can be calculated by replacing $\varepsilon_{z1}\varepsilon_{z2}$ in the expression for f_{zz} in eqn 3.6.10 with $\varepsilon_{b,1}\rho_{f,n}\tau_1$:

$$f_{01} = \varepsilon_{f,1} + f_{zz}(\Delta z_{14}) \tag{3.6.18}$$

where

$$\Delta z_{14} = 2(n - 2)dz$$

The net radiation heat transfer from layer i to layer j, where $i < j$, is:

$$q_{rad,ij} = f_{ij}\sigma(T_i^4 - T_j^4) \tag{3.6.19}$$

The radiation heat transfer coefficient between layer i and j is then:

$$h_{rad,ij} = q_{rad,ij} / (T_i - T_j) = f_{ij}\,\sigma\,(T_i^2 + T_j^2)(T_i + T_j) \tag{3.6.20}$$

The calculation of the radiation heat transfer coefficients between layers has here been limited to include two end surface reflections, one at the absorber and one at the cover. In a computer program, it is of course possible to add contributions also from higher order multiple reflections and not stop until the added value is negligible (smaller than a given limit).

3.7 Conduction/convection heat losses in a honeycomb glazing

The honeycomb is usually attached to the cover (by for instance strings of silicon rubber), which prevents inter-cellular natural convection (air exchange between the cells) from taking place. If the honeycomb cells are also small enough, free convection within the honeycomb cells will also not take place. Cane et al. (1977) found a simple correlation for the convection heat transfer for a square-celled honeycomb between two isothermal plates (without an extra air gap), which fitted experimental data within ± 7.5% for $Ra/A^4 \leq 6000$ and $30° \leq \theta \leq 90°$. It was expressed as Nu = f(Ra,θ,A), where $Nu = h_c/(k/L)$, $Ra = g\beta\Delta T_g L^3/(\nu\alpha)$, θ is the tilt angle and A is the aspect ratio (the ratio of the distance between the plates, L, to the width of the honeycomb cell, d). The correlation gives Ra/A^4, proportional to $d^3/A = d^4/L$, as the critical parameter for a given tilt angle. The cell width, d, is therefore the most critical dimension for the onset of natural convection. For a 5 cm honeycomb with the tilt

angle 45° and the plate temperatures 75°C / 25°C (ΔT_g = 50°C and T_m = 50°C), the correlation gives that $Nu < 1.05$ for $d \leq 9.2$ mm, which means that h_c for this d is less than 5% higher than it would be with only conduction in the air.

The correlation is valid for a honeycombs between two plates without an air gap. The effect of small air gaps has also been investigated. Edwards et al. (1976) investigated the influence of small gaps and concluded that 1.5 mm air gaps at the top and/or bottom did not significantly influence the performance of the honeycomb. Hollands and Iynkaran (1985) recommended a 10 mm air gap between the honeycomb and a low-emitting absorber to decouple the radiation-conduction modes and found from measurements that the air gap did not significantly influence the onset point for convection.

Hollands et al. (1992b) also investigated a 40 mm thick FEP film honeycomb with a square cell width of 9.5 mm, mounted between two plates of 45° tilt and leaving a 9 mm air gap to the lower, low emitting plate. The result showed that the honeycomb was on the limit for onset of convection, which was to be expected also without the air gap due to the large cell size of the honeycomb. So the air gap can not in this case be said to have started or increased natural convection in the honeycomb.

Measurement results given in Chapter 4 show however that a large air gap between the honeycomb and the absorber, where convection occurs in the air layer, seems to reduce the heat resistance of large cell honeycombs (d = 8 mm), while honeycombs with small cells (d = 4 mm) are unaffected. A possible explanation for this could be that the convection in the air gap induces an air exchange also in (parts of) the honeycomb cells.

It will here be assumed that the honeycomb cells are small enough to prevent convection within the cells. The conduction heat transfer coefficient, $h_{c,ij}$, between two adjacent layers i and j of the honeycomb can then be calculated from conduction in the air and in the cell walls:

$$h_{c,ij} = ((1 - f_w)k_a + f_w k_w)/dz \tag{3.7.1}$$

where k_a and k_w are the conductivities of the air and the wall, dz is the layer thickness and f_w is the wall fraction of the honeycomb area. The latter can be calculated from:

$$f_w = t_w(dx+dy-t_w)/(dxdy) \tag{3.7.2}$$

where t_w is the (average) thickness of the cell walls and $dxdy$ is the rectangular cell area of the honeycomb.

An air gap between the absorber and the honeycomb is often used for minimizing the heat losses. As described in Section 3.4, natural convection will under certain circumstances occur in a gap. In contrast to gaps between parallel plane layers, the air gap of the honeycomb glazing does not have a plane surface on one side, so the convection correlations given in Section 3.4 are not automatically valid here. However, since most of the heat resistance of a honeycomb glazing is located within the honeycomb, the use of such a correlation can be expected to give only a minor error. The conduction/convection heat transfer coefficient, $h_{c,ij}$, at the absorber can then be calculated with the help of the convection heat transfer coefficient of the gap, $h_{conv,ij} = Nu \cdot k/L$, where Nu is calculated from eqns 3.4.3-6:

$$h_{c,ij} = ((((1 - f_w)k_a + f_w k_w)/(dz/2))^{-1} + h_{conv,ij}^{-1})^{-1} \quad (3.7.3)$$

where $i = n$-1 and $j = n$. In eqn 3.7.3 $dz/2$ is used instead of dz, since this is the distance between the layers at the boundaries. The corresponding formula for the layer at the cover is therefore:

$$h_{c,ij} = ((1 - f_w)k_a + f_w k_w)/(dz/2) \quad (3.7.4)$$

where $i = 1$ and $j = 2$.

3.8 Solar absorption in a honeycomb glazing

The subject of solar transmittance through a honeycomb glazing has been treated in the literature. Hollands et al. (1978) used the symmetry of a (square celled) honeycomb to simplify the geometry as an opaqe long passage with $\rho_{eff} = \rho + \tau$. Platzer (1992a) refined the model for a rectangular geometry.

The angles that determine the solar transmittance of a rectangular honeycomb are the projected solar incidence angles, θ_x and θ_y, (where θ is the incidence angle) in the y-z- and x-z- planes of the honeycomb (where x and y are the normal directions of the planes). Provided that the honeycomb is mounted with the cell walls perpendicular to the cover/absorber and parallel to the sides of a rectangular collector, they can for the general case be calculated from the collector tilt (β), the collector azimuth (γ), the solar azimuth (γ_s) and the solar altitude (α_s):

$$\theta_x = \arctan(\cos(\alpha_s)\sin(\gamma_s-\gamma)/(\cos(\beta)\sin(\alpha_s)+\sin(\beta)\cos(\alpha_s)\cos(\gamma_s-\gamma))) \quad (3.8.1)$$

$$\theta_y = \arctan((\cos(\beta)\cos(\alpha_s)\cos(\gamma_s-\gamma)-\sin(\beta)\sin(\alpha_s))/(\cos(\beta)\sin(\alpha_s) + \sin(\beta)\cos(\alpha_s)\cos(\gamma_s-\gamma))) \quad (3.8.2)$$

For a horizontal collector the equations are reduced to:

$$\theta_x = \arctan(\cot(\alpha_s)\sin(\gamma_s-\gamma)) \quad (3.8.3)$$

$$\theta_y = \arctan(\cot(\alpha_s)\cos(\gamma_s-\gamma)) \quad (3.8.4)$$

and for a vertical collector:

$$\theta_x = \gamma_s - \gamma \quad (3.8.5)$$

$$\theta_y = -\arctan(\tan(\alpha_s)/\cos(\gamma_s-\gamma)) \quad (3.8.6)$$

The formulas for the whole honeycomb, as given by Platzer (1992a) can not be directly applied for each layer since the uniformity of light is changed after the passage of the first honeycomb layer. Therefore, the light impinging on the edges of the honeycomb material must be treated separately from the light between the walls. For calculating the absorptance in each layer from the light impinging between the walls, the transmittance for i number of layers, $\tau_{i,a}$, is first calculated:

$$\tau_{i,a} = \tau_{i,x} \cdot \tau_{i,y} \quad (3.8.7)$$

where

$$\tau_{i,x} = (1-r_x)(\tau_x+\rho_x)^m + r_x(\tau_x+\rho_x)^{m+1} \quad (3.8.8)$$

$$m = \text{trunc}(idz/dx \cdot \tan(\text{abs}(\theta_x))) \quad (3.8.9)$$

$$r_x = idz/dx \cdot \tan(\text{abs}(\theta_x)) - m \quad (3.8.10)$$

and

$$\tau_{i,y} = (1-r_y)(\tau_y+\rho_y)^n + r_y(\tau_y+\rho_y)^{n+1} \quad (3.8.11)$$

$$n = \text{trunc}(idz/dy \cdot \tan(\text{abs}(\theta_y))) \quad (3.8.12)$$

$$r_y = idz/dy \cdot \tan(\text{abs}(\theta_y)) - n \quad (3.8.13)$$

The functions "trunc" and "abs" here denote "truncation to the nearest integer of" and "absolute value of". The obtained values can be used for calculating the absorptance in each layer through:

$$\alpha_{i,a} = \tau_{i\text{-}1,a} - \tau_{i,a} \tag{3.8.14}$$

where for the first honeycomb layer, i: $\tau_{i\text{-}1,a} = 1$ (the cover is included later). All reflections and transmissions are assumed to take place without scattering.

As shown by Hollands et al. (1978), the light impinging on the edge of the honeycomb walls will be internally reflected within the walls for all angles of incidence if the refractive index is larger than $2^{0.5}$ (which is the case for glass and most plastics). The absorptance of layer i for the light impinging on the wall edges of a honeycomb, divided into Z layers, can then be written:

$$\alpha_{i,w} = (1 - r_w)(t_{i\text{-}1,w} + r_w\, t_{Z\text{-}1,w}\ t_{Z\text{-}\,i+1,w})(1 - t_{1,w})/(1 - r_w^2\, t_{Z,w}^2) \tag{3.8.15}$$

where

$$t_{i,w} = e^{-idzKn/(n^2 - \sin^2(\theta))^{0.5}} \tag{3.8.16}$$

and r_w is the surface reflectance of the honeycomb wall edge, see eqn 3.2.1-2. The transmittance and the reflectance of the honeycomb walls (for the incidence angle θ) are then given by (compare eqns 3.2.4-5):

$$\tau_w = t_{Z,w}\,(1 - r_w)^2 / (1 - t_{Z,w}^2\, r_w^2) \tag{3.8.17}$$

$$\rho_w = r_w\,(1 + t_{Z,w}\,\tau_w) \tag{3.8.18}$$

The total transmittance and reflectance for the honeycomb and the total absorptance for the different layers for light impinging on the front side can then be obtained as weighted mean values:

$$\tau_{hc} = f_w\tau_w + (1\text{-}f_w)\tau_{Z,a} \tag{3.8.19}$$

$$\rho_{hc} = f_w\rho_w \tag{3.8.20}$$

$$\alpha_{i,hc} = f_w\alpha_{i,w} + (1\text{-}f_w)\alpha_{i,a} \tag{3.8.21}$$

where f_w is the wall area fraction, given by eqn 3.7.2.

If also the cover and the absorber are included in the calculations, the absorptance of the cover, the absorber and the honeycomb layers may be calculated with the same technique as for the absorber-parallel sheets in Section 3.5:

$$A_{abs} = T_{cov} T_{hc} \alpha_{abs} \tag{3.8.22}$$

$$A_{cov} = (1 + T_{cov} R_{hc}) \alpha_{cov} \tag{3.8.23}$$

$$A_{i,hc} = T_{cov} \alpha_{i,hc} + T_{hc} \rho_{abs} \alpha_{Z-i+1,hc} \tag{3.8.24}$$

where

$$T_{hc} = \tau_{hc} / (1 - \rho_{abs} \rho_{hc}) \tag{3.8.25}$$

$$T_{cov} = \tau_{cov} / (1 - R_{hc} \rho_{cov}) \tag{3.8.26}$$

$$R_{hc} = \rho_{hc} + \tau_{hc}^2 \rho_{abs} / (1 - \rho_{abs} \rho_{hc}) \tag{3.8.27}$$

With the same type of notation as used before we get: $A_1 = A_{cov}$, $A_n = A_{abs}$ and $A_{i+1} = A_{i,hc}$ for $1 \leq i \leq Z = n - 2$.

3.9 Collector efficiency factor and internal heat resistance

The collector efficiency factor, F', is a strong function of the heat loss coefficient, U_L, between the absorber and the ambient. It can be expressed as the ratio between the system heat loss coefficient between the heat carrier fluid and the ambient, U_{sys}, and U_L:

$$F' = \frac{U_{sys}}{U_L} = \frac{\dfrac{1}{U_L}}{\dfrac{1}{U_{sys}}} \tag{3.9.1}$$

As mentioned in Section 2.2, Rockendorf et al. (1993, 1995) suggested a simplified model for F', expressed as:

$$F' = \frac{\dfrac{1}{U_L}}{\dfrac{1}{U_L} + \dfrac{1}{U_{int}}} = \frac{U_{int}}{U_{int} + U_L} \tag{3.9.2}$$

where $1/U_{int}$ is the internal heat resistance between the fin (average) and the heat carrier fluid. $1/U_{int}$ can be divided into two heat resistances; one within the fin, $1/U_{fin}$, and one between the fin base and the heat carrier fluid, $1/U_{b\text{-}f}$:

$$1/U_{int} = 1/U_{b\text{-}f} + 1/U_{fin} \tag{3.9.3}$$

If the heat resistance in the contact area between the fin base and the pipe is neglected, $1/U_{b\text{-}f}$ can for a fin absorber of width W be written:

$$1/U_{b\text{-}f} = \frac{W}{F_p h_i \pi d_i} \tag{3.9.4}$$

where d_i is the pipe inner diameter and h_i is the heat transfer coefficient between the pipe inner wall and the heat carrier. F_p is the fin efficiency for the pipe wall, which can be calculated from:

$$F_p = \frac{\tanh(m_p L_p)}{m_p L_p} \tag{3.9.5}$$

$$m_p = \left(\frac{h_i d_i}{d_m k_p \delta_p}\right)^{0.5} \tag{3.9.6}$$

where $d_m = (d_i+d_o)/2$ and $L_p = \pi d_m/2$ for a pipe welded on the fin. d_o is the outer diameter of the pipe. k_p and δ_p are the heat conductivity and thickness of the pipe wall. For a fin absorber with an integral pipe, the same formula for F_p can be used, but with $L_p = \pi d_m/4$. The calculated F_p should then also be replaced by $(2wF_p+b)/W$ in eqn 3.9.4. If the pipe is not circular, the periphery of the pipe could be used instead of πd.

For a given U_L and known fin properties, $1/U_{fin}$ can be calculated from the following equations:

$$1/U_{fin} = \frac{1-F_a}{F_a U_L} \tag{3.9.7}$$

$$F_a = \frac{2wF+b}{W} = \left(1-\frac{b}{W}\right)F + \frac{b}{W} \tag{3.9.8}$$

$$F = \frac{\tanh(mw)}{mw} \tag{3.9.9}$$

$$m = \left(\frac{U_L}{k\delta}\right)^{0.5} \tag{3.9.10}$$

where b is the width of the absorber part in direct metal contact with the pipe, w is the width of a fin wing ($2w+b=W$), k is the heat conductivity of the fin and δ is the fin thickness. A diagram of U_{int} vs U_L, calculated in this way for an absorber with W = 0.150 m, b = 0.010 m, $k\delta$ = 0.1 W/K and $F_p h_i d_i$ = 10 W/mK, is shown in Fig. 3.3.

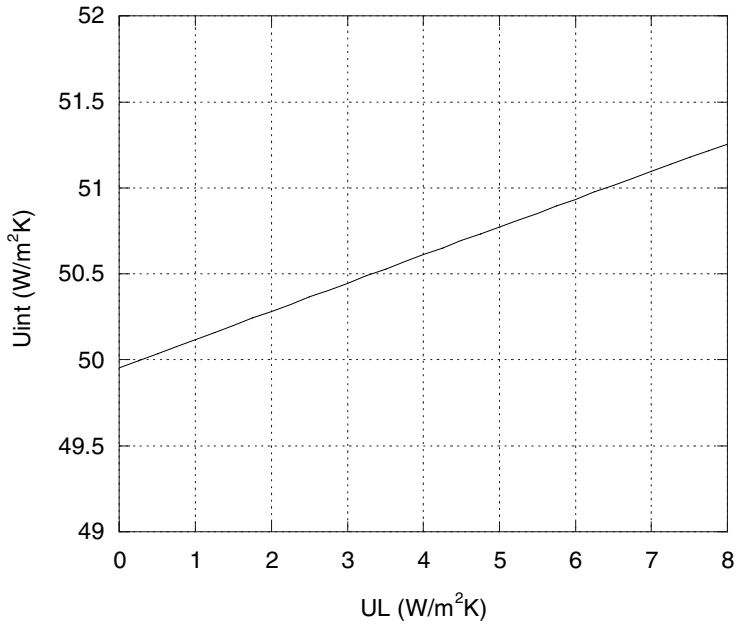

Fig. 3.3 *U_{int} vs U_L, calculated for an absorber with W = 0.150 m, b = 0.010 m, $k\delta$ = 0.1 W/K and $F_p h_i d_i$ = 10 W/mK.*

An alternative way to obtain $1/U_{fin}$ is to make a serial expansion of the expression for F in eqn 3.9.9:

$$F = \frac{\tanh(mw)}{mw} = 1 - (mw)^2/3 + 2(mw)^4/15 \ldots. \qquad (3.9.11)$$

By inserting the expression for F_a of eqn 3.9.8 into eqn 3.9.7 and replacing F by the expression in eqn 3.9.11, truncating after the second term in the nominator and after the first term in the denominator, the following expression is obtained:

$$1/U_{fin} = \frac{2w^3}{3k\delta W} = \frac{(W-b)^3}{12k\delta W} \qquad (3.9.12)$$

This is the limit value for $1/U_{fin}$ as U_L approaches zero. It gives only an approximate value of U_{fin} for real values of U_L, but the accuracy could be sufficient if U_L is not too large. For the absorber used in Fig. 3.3, it gives a relative error in U_{int} and $1\text{-}F'$ of about 1% for U_L = 3 W/m^{2}K and about 2% for U_L = 6 W/m^{2}K. It corresponds to absolute errors in F' for this absorber of about 0.0005 and 0.002, respectively. Using eqns 3.9.7-10 with $U_L = U_0$ gives values of $1/U_{fin}$ with even higher accuracy.

When calculating the temperatures and the energy gain of a collector it is more practical to use U_{int} than F'.

3.10 Calculation of temperatures and energy output

To obtain the temperatures of the layers, an equation system of the energy balance equations for all the layers is solved. The equation system can be written in the form:

$$\boldsymbol{A}\,\boldsymbol{T} = \boldsymbol{B} \tag{3.10.1}$$

where $\boldsymbol{A}$ is a square matrix of size n, while $\boldsymbol{T}$ and $\boldsymbol{B}$ are vectors of size n.

The solution of this equation system is:

$$\boldsymbol{T} = \boldsymbol{A}^{-1}\,\boldsymbol{B} \tag{3.10.2}$$

$\boldsymbol{A}$, $\boldsymbol{T}$ and $\boldsymbol{B}$ can be written:

$$\boldsymbol{A} = \begin{pmatrix} \sum_{j=0}^{n+1} h_{1,j} & -h_{1,2} & -h_{1,3} & \ldots\ldots & -h_{1,n} \\ -h_{2,1} & \sum_{j=0}^{n+1} h_{2,j} & -h_{2,3} & \ldots\ldots & -h_{2,n} \\ -h_{3,1} & -h_{3,2} & \sum_{j=0}^{n+1} h_{3,j} & \ldots\ldots & -h_{3,n} \\ \ldots\ldots & \ldots\ldots & \ldots\ldots & \ldots\ldots & \ldots\ldots \\ -h_{n,1} & -h_{n,2} & -h_{n,3} & \ldots\ldots & \sum_{j=0}^{n+1} h_{n,j} \end{pmatrix} \tag{3.10.3}$$

$$\boldsymbol{T} = \begin{pmatrix} T_1 \\ T_2 \\ T_3 \\ .... \\ T_n \end{pmatrix} \tag{3.10.4}$$

$$\boldsymbol{B} = \begin{pmatrix} h_{1,0}T_0 + h_{1,n+1}T_{n+1} + q_{a,1} \\ h_{2,0}T_0 + h_{2,n+1}T_{n+1} + q_{a,2} \\ h_{3,0}T_0 + h_{3,n+1}T_{n+1} + q_{a,3} \\ ..... \\ h_{n,0}T_0 + h_{n,n+1}T_{n+1} + q_{a,n} \end{pmatrix} \tag{3.10.5}$$

where $h_{i,j} = h_{c,ij} + h_{rad,ij}$. T_0, T_1, T_n and T_{n+1} are the temperatures of the ambient air, the outer cover, the absorber and the heat carrier, respectively. For $i = j$, $h_{i,j} = 0$ and for $i \neq j$, $h_{j,i} = h_{i,j}$. For a collector with an IR-opaque cover (for instance a glass pane) and a fin absorber, the heat transfer coefficient between layer i and the ambient, $h_{i,0}$, is zero for all i but i=1 and i=n. $h_{n,0}$ equals the back and edge losses from the absorber, U_b. Only the absorber will then have a direct heat exchange with the heat carrier fluid. Therefore $h_{n,n+1} = U_{int}$, but otherwise for $i \neq n$, $h_{i,n+1} = 0$.

$q_{a,i}$ is the sum of the absorbed part of the solar irradiance, G, and the (negative) absorbed part of the net sky (long-wave) irradiance, q_{net}, in layer i, where $q_{net} = F_{sky}\sigma(T_{sky}^4 - T_a^4)$. F_{sky} is the view factor from the collector to the sky and T_{sky} is the effective sky temperature (which can be obtained from measured long-wave sky irradiation, $q_{sky} = \sigma T_{sky}^4$). Expressed as a formula, $q_{a,i}$ can be calculated from:

$$q_{a,i} = f_{0,i}\, q_{net} + A_i G \tag{3.10.6}$$

where A_i is the weighted average total solar absorptance of layer i, calculated according to formulas given in Section 3.5 or 3.8. $f_{0,i}$ is the radiation heat exchange factor between the ambient and the layer i, calculated from equations given in Section 3.3 or 3.6.

The energy output can then be calculated from

$$q = h_{n,n+1}(T_n - T_{n+1}) \tag{3.10.7}$$

3.11 Computer program calculations

CoDePro (Koo and Beckman, 1999) is a computer program which calculates collector parameters for a flat plate collector. It is based on EES, a program which solves non-linear equation systems (Klein and Alvarado, 2002). The program uses the "net-radiation method" (see Section 3.3) for calculating the heat radiation exchange between the layers. The radiosity equations are solved in an equation system together with all the other equations. All calculations are performed with non-spectral optical data. The program calculates the parameters η_0, a_1 and a_2 (see Section 2.2) and also the parameter of the incidence angle dependence, b_0. The parameters are determined through linear regression analyses of the efficiency at different inlet temperatures and at different angles of incidence (up to 60°).

A computer program for calculating values of g and U_L for a glazing with flat films or a honeycomb, called "G-WERT", was made by Platzer (1988b). The honeycomb part is based on calculation procedures by Platzer (1992a), partly described in Section 3.6.

The calculation procedures described in Sections 3.3-3.9 are suitable for computer programming. Since all the equations for the absorbed irradiances and the heat transfer coefficients between the different layers are explicit, the calculations can easily be made both spectral and angular dissolved.

A program has been made for calculating the collector efficiency and different collector specific parameters for a glazing with parallel films between the absorber and the cover. The program was used in Section 2.2 for calculating different collector parameters and in Chapter 4 for comparing calculated and measured parameters.

Another program for a glazing with a honeycomb structure between the absorber and the cover has also been developed. The program calculates the incidence angle dependent g- and temperature dependent U_L-values of a collector with a honeycomb glazing. The program was used in Chapter 4 for comparing calculated and measured parameters.

The programs can be used for calculating collector specific parameters and predicting the performance of a collector, but also for studying how different changes in collector materials and properties will affect the energy output of the collector. Such a study was made by Hellström et al. (2000), in which the solar energy simulation program Minsun (Chant and Håkansson, 1985) was also used for the analysis.

3.12 Conclusions

- A complete set of algorithms for calculating the energy output for a flat plate collector with flat films or honeycombs between the cover and the absorber is presented.
- An explicit algorithm, based on ray tracing analysis, for calculating the radiation heat exchange factors between the different sheets (which can be semitransparent in the IR) is given. This method is more straightforward and easier to use than the implicit so-called net-radiation or radiosity method. The method is suitable for computer programming and the calculations can easily be made spectral and angular resolved.
- For a collector with a honeycomb between the cover and the absorber, a finite difference solution, in which the honeycomb is divided into a number of layers, is used. Algorithms for calculating the radiation heat exchange factors between the different layers are presented. The method is more straightforward and easier to comprehend than an approximate analytical method and does not make the geometrical approximation presumed by an alternative numerical method. Formulas are also given for calculating the absorbed solar energy in each layer depending on the solar position.
- The algorithms can be used in a computer program for determining the energy output, the efficiency and collector characteristic parameters. Such a program can, for instance, together with a system simulation program, be used for analysing the impact of design or material changes in the collector.

4 Comparison of calculation results with measurements

4.1 Introduction

Measurements of transparent insulation materials (TIMs) were performed with three instruments at the Älvkarleby Laboratory, which can be used for measuring heat conductivity, total heat loss coefficients directional-hemispheric solar transmittance. They are described below.

A guarded hot plate apparatus is used for measurements of heat conductivity. The instrument consists of two parallel plates at different temperatures; one hot and one cold plate. The 8 mm thick aluminium hot plate is divided into two parts; one central plate from which the applied electrical heat is measured and one (square) "ring", which works as a heat guard. Both parts are heated by electrical heating foils attached to their back sides. Between the central plate and the guard ring there is a 3 mm air gap. By measuring the heat from the central plate only, influences of heat losses at the edges are avoided and the heat flow is mainly one-dimensional. At the back of the hot plate there is a 50 mm XPS sheet between two 12 mm gypsum boards and outside them there is an 8 mm aluminium guard plate (at the same temperature as the hot plate). The 37 mm aluminium cold plate is cooled by a flow of water through internal channels. The distance between the plates can be altered by moving the cold plate. All sides are covered by 50 mm PUR sheets. The flow of cooling water is regulated to a constant inlet temperature. A regulation system was used for keeping the heat guards at the same, constant temperature as the hot plate. All temperatures are measured with thermocouples. The guarded hot box can be tilted to any angle. Measurements are taken at steady state. The heat conductivity is obtained from:

$$k = Lq_e / (T_h - T_c) \qquad (4.1.1)$$

where L is the thickness of the layer, q_e is the electrical power per central hot plate area and $T_h - T_c$ is the temperature difference between the hot and the cold plate.

The instrument was calibrated with a 70 mm EPS sheet. The measured heat conductivity for different mean temperatures, with a constant temperature difference of 10°C, was compared with data from the manufacturer. The two values were equal at 30°C, but the temperature derivative was somewhat larger for the instrument. At 45°C the measured value was 2 % larger than the given data. The guarded hot plate apparatus was previously described by Hellström et al. (1990a).

An unguarded hot box, which can be seen as a small flat plate collector model, is used for measurements of U_L of glazings with different kinds of transparent insulation. The hot box consists of a 3 mm thick aluminium "absorber" plate 0.7 m × 0.7 m in a glazed, 45° tilted box, with a thick EPS insulation at its back and edges. The absorber plate is heated electrically by a heating foil attached to its back side. It can be replaced for the purpose of altering the emittance. Three plates with the emittance of 0.065, 0.23 and 0.84 are available. The cover is a 4 mm glass or acrylic sheet. The distance between the cover and the absorber is normally 0.14 m, but could be altered. The temperatures at nine evenly distributed locations on the absorber are measured with thermocouples and an average value gives T_p. Temperatures are also measured with thermocouples on the cover and in the ambient air.

The back and edge heat losses were determined from measurements of a 70 mm EPS sheet of known heat conductivity as "glazing", to U_b = 0.50 + 0.00125(T_p - T_a), where T_p is the plate temperature and T_a is the ambient temperature. The measured back and edge heat losses are however, strictly speaking, only valid for this material as "glazing". If, for instance, the measurement is performed without transparent insulation (with a cover only), the edge losses will be slightly larger than if a polymer film or a honeycomb is mounted in the air gap. This is because a TIM in the air gap insulates the edge area close to the cover, where the edge insulation otherwise is thin. CFD calculations could be a way to analyse this in more detail. Edge losses are part of the heat losses also for a solar collector, but they are more important for this instrument because of the small glazing area.

The total heat loss coefficient is obtained as:

$$U_L = q_e / (T_p - T_a) \qquad (4.1.2)$$

where q_e is the electrical heating power per absorber area. The heat loss coefficient for the glazing can be obtained from $U_t = U_L - U_b$. This value is, however, only valid for the laboratory environment conditions and has to be recalculated for outdoor conditions.

An integrating sphere, 0.95 metre in diameter, with the inside walls covered by $BaSO_2$ particles suspended in a laquer, was used for measurements of directional-hemispherical solar transmittance. The diameter of the opening hole can be changed between 0.10 and 0.36 m. It can be used for measurements up to about 60° incidence angle. The instrument has a collimator (1 m long and 0.1 m in diameter), a light chopper and a pyroelectrical detector. The latter is mounted in the sphere wall and shielded from direct irradiation. A lock-in amplifier gives a measured voltage, which is proportional to the intensity in the sphere. The transmittance is obtained as the ratio between measurements with and without sample. The value has to be corrected for the influence of the back side reflectance of the sample. A discharge lamp gives a spectrum similar to the solar spectrum. A metal halogen lamp is an alternative radiation source. It has a spectrum with a slight shift towards the IR, but is more stable than the discharge lamp. The integrating sphere was previously described by Hellström et al. (1990a).

The measurements presented in this chapter were part of a research project on transparent insulation for solar collectors. Some of the results of the project were reported by Hellström et al. (1990-1992).

4.2 Measurements of heat conductivity of a honeycomb structure

The heat conductivity of a polycarbonate honeycomb was measured with an instrument described in Section 4.1. The measurements were compared with calculated values, which were obtained from the calculation procedure given in Chapter 3. The (apparent) heat conductivity is obtained with eqn 4.1.1 from the measured total heat transfer, which consists of coupled radiation and conduction (as described in Chapter 3).

Two thicknesses of the PC honeycomb, 50 and 100 mm, were measured for two different values of the hot plate emittance. The honeycomb consists of strips, four cells wide, which are glued together. The outer walls of the strips are thicker than the inner walls, which are about 55 μm thick. On average the cell size is around 3.9×4.5 mm. The calculations were performed for IR properties of the inner walls, which were obtained from spectrophotometer measurements. The spectrally integrated values of the film IR emittance and reflectance for the normal incidence were 0.46 and 0.08, respectively (for the temperature 318 K).

Painted and unpainted aluminium foils, attached to the boundary plates, were used to obtain different values of emittance of the ambient surfaces. The hemispherical emittances of the foils were measured with a calorimetric instrument at Uppsala University. The resulting heat conductivity for different mean temperatures and two different values of the hot plate emittance, ε_h = 0.772 and ε_h = 0.033, are given in Fig. 4.1 and 4.2, respectively. The cold plate emittance, ε_c, was in both cases 0.840. The temperature differences between the surfaces in the measurements were in all cases 10°C. The corresponding calculated conductivities are also shown in the diagrams.

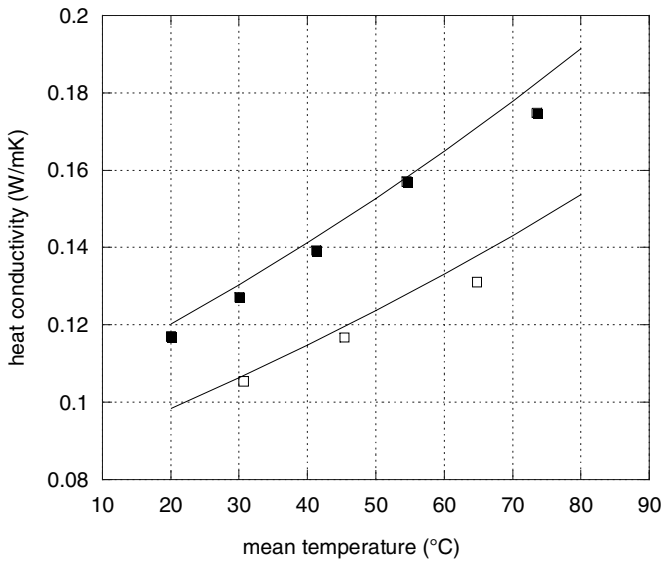

Fig. 4.1 *(Apparent) heat conductivity for a PC honeycomb with ε_h = 0.772 and ε_c = 0.840 as a function of the mean temperature of the hot and the cold plates. Lines = calculations. Marks = measurements: Unfilled = thickness 50 mm. Filled = thickness 100 mm.*

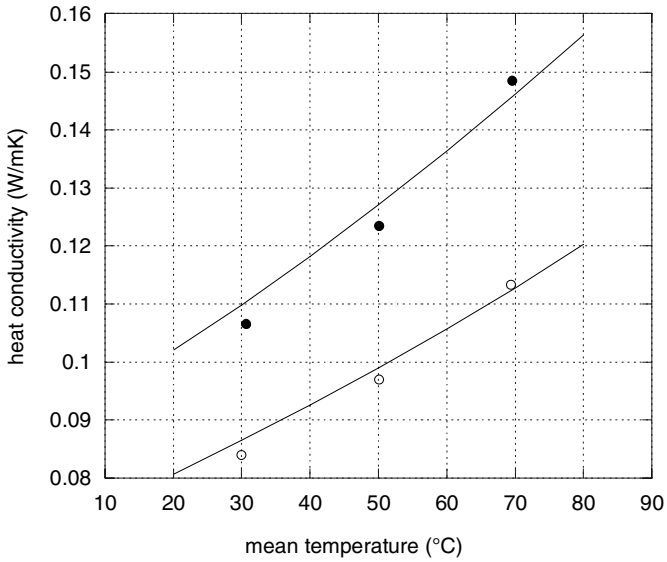

Fig. 4.2 *(Apparent) heat conductivity for a PC honeycomb with $\varepsilon_h = 0.033$ and $\varepsilon_c = 0.840$ as a function of the mean temperature of the hot and the cold plates. Lines = calculations. Marks = measurements: Unfilled = thickness 50 mm. Filled = thickness 100 mm.*

The measured and calculated values agree reasonably well, although, in most cases, the measured values are slightly lower. The temperature distribution across the honeycomb is also obtained from the calculations. The calculated relative temperature distribution for the 50 mm polycarbonate honeycomb, for the same surface emittances as in Fig. 4.1 and 4.2, is given in Fig. 4.3.

It can be seen from Fig. 4.3 that the heat conductivity is larger (since the temperature derivative is smaller) in the central part of the honeycomb (a so called bulk property, see Platzer 1992b) than at the edges. This means that a thicker honeycomb will have a higher average heat conductivity, which is also shown in Fig. 4.1 and 4.2. Making a honeycomb twice as thick gives then a heat transfer coefficient, $h = k/L$, which is more than half as large.

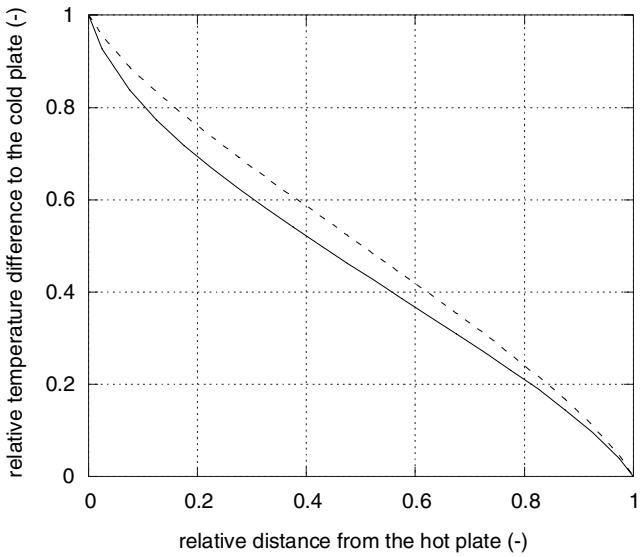

Fig. 4.3 *Relative temperature difference between the hot and the cold ambient surfaces as a function of relative distance between the surfaces for two different hot plate emittances. Upper (dotted) line: ε_h = 0.772. Lower line: ε_h = 0.033. For both: ε_c= 0.840.*

4.3 Measurements of heat loss coefficients for a glazing with an absorber parallel film

Measurements of the heat loss coefficient for the total glazing were performed in an unguarded hot box, described in Section 2.1. A 25 μm FEP film was mounted in the middle of the gap between the absorber and the cover, giving two air gaps of 70 mm. Calculations for the same geometry were also performed with the procedure described in Chapter 3, using a gap convection correlation by Yiqin and Hollands (1991) and a surface convection correlation (for the convective heat transfer between the cover and the ambient) by Al-Arabi and Sakr (1988). The film emittance and IR reflectance at normal incidence, which were used in the calculations, were measured with a spectrophotometer. The integrated values (for the temperature 318 K) were 0.39 and 0.055, respectively. The resulting values of U_L (= U_t + U_b) from both measurements and calculations as a function of the temperature difference between the absorber plate and the ambient are shown in Fig. 4.4 for the different absorber emittances,

ε_p. A good agreement between the measurements and calculations was obtained for most values of T_p - T_a, although the correlation used for calculating the convective heat transfer is only approximate.

Existing measurements on films with different IR emittance/reflectance values were also used for a comparison with calculations. The measurements were performed with the same hot box as for the 25 µm FEP film, but with a shorter distance, 0.10 m, between the cover and the absorber. The films were made of polyethylene (PE), acrylic plastic (PMMA) and teflon (FEP). The measured, spectrally integrated IR emittance/reflectances at normal incidence for the films were 0.15/0.07, 0.95/0.05 and 0.28/0.06, respectively. Fig. 4.5 shows the measured U_L for T_p - T_a = 50°C for the hot box as a function of the absorber emittance. In Fig. 4.6 the corresponding calculated values are shown. Fig. 4.5 and 4.6 also illustrate the fact that the impact of the film emittance on the U_L vaue of glazing is large only if the absorber emittance is high. A reasonably good agreement between measured and calculated values was obtained also in this case.

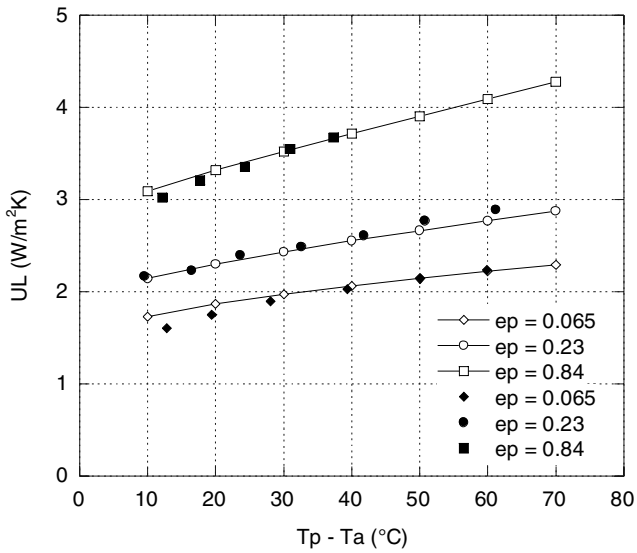

Fig. 4.4 *U_L for the hot box with a 25 µm FEP film between the cover and the absorber vs the absorber-ambient temperature difference, for different absorber emittances, ε_p. Filled marks: measurements. Unfilled: calculations. U_b = (0.5+0.00125(T_p-T_a)) W/m²K is included.*

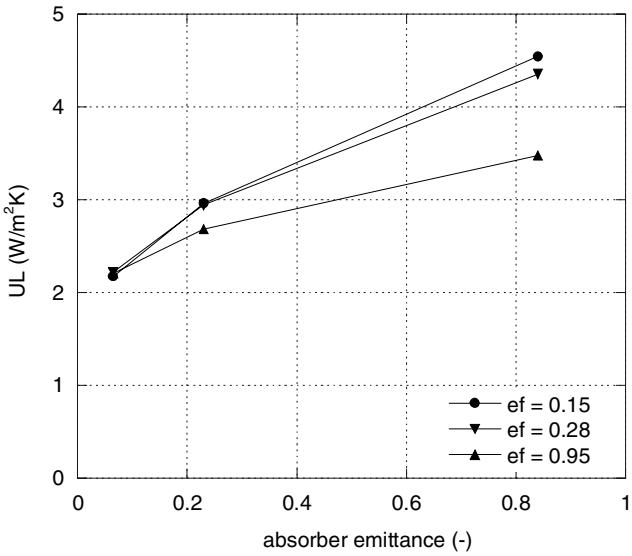

Fig. 4.5 *Measured U_L of the hot box with a polymer film of different emittances, ε_f, between the cover and the absorber vs absorber emittance. $T_p - T_a = 50°C$. $U_b = 0.5625$ W/m^{2}K is included.*

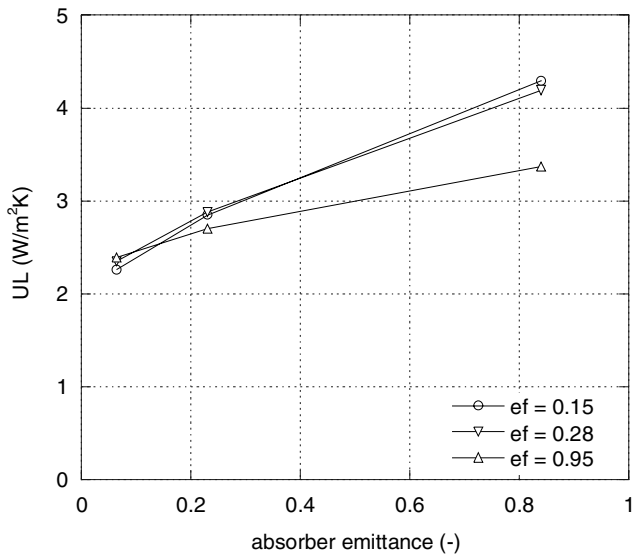

Fig. 4.6 *Calculated U_L of the hot box with a polymer film of different emittances, ε_f, between the cover and the absorber vs absorber emittance. $T_p - T_a = 50°C$. $U_b = 0.5625$ W/m^{2}K is included.*

4.4 Measurements of heat loss coefficients for a glazing with a honeycomb

Measurements of the heat loss coefficient for the total glazing were performed with a 50 mm polycarbonate honeycomb (described in Section 4.2) attached to the cover by strings of silicone rubber. The air gap to the absorber was then 90 mm. Calculations for the same glazing were performed with the procedure described in Chapter 3, using a gap convection correlation by Hollands et al. (1976) and a surface convection correlation by Al-Arabi and Sakr (1988). The gap convection correlation is derived for isothermal and smooth boundary surfaces, but in this case the honeycomb boundary surface is not plane. However, due to lack of alternatives (as discussed in Section 3.7), this correlation was used for the calculations.

The measured and calculated U_L as a function of the temperature difference between the absorber plate and the ambient, for the absorber emittance 0.065, are plotted in Fig. 4.7. It is seen that the measured values are slightly smaller than the calculated values for small values of T_p - T_a. The difference decreases as T_p - T_a increases. For temperature differences higher than 20°C, the deviations are smaller than 0.05 W/m^{2}K.

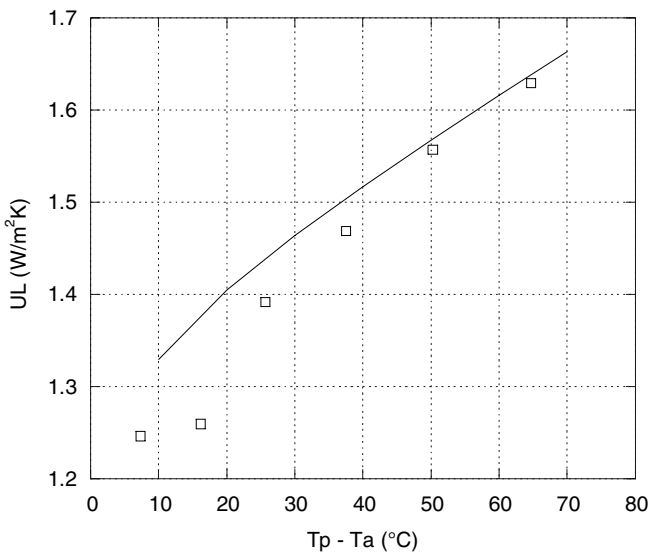

Fig. 4.7 U_L *of the hot box for a glazing with a 50 mm PC honeycomb vs* T_p-T_a. *Absorber emittance = 0.065. Marks: measurements. Line : calculations.* $U_b = (0.5+0.00125(T_p-T_a))$ W/m^{2}K *is included.*

Two other honeycombs with the same thickness as the PC honeycomb but with a wider cell size were also measured and compared with calculations. The 50 mm honeycombs have square cells of size 8 × 8 mm, made from 25 mm polymer films. The distance between the cover and the absorber was in this case only 70 mm. This means that the air gap to the absorber was 20 mm. The back and edge losses were, however, assumed to be unchanged. The integrated emittances for the two honeycomb wall films at normal incidence were 0.12 and 0.50. The absorber emittance was 0.065. The results of the measurements and the calculations are shown in Fig. 4.8.

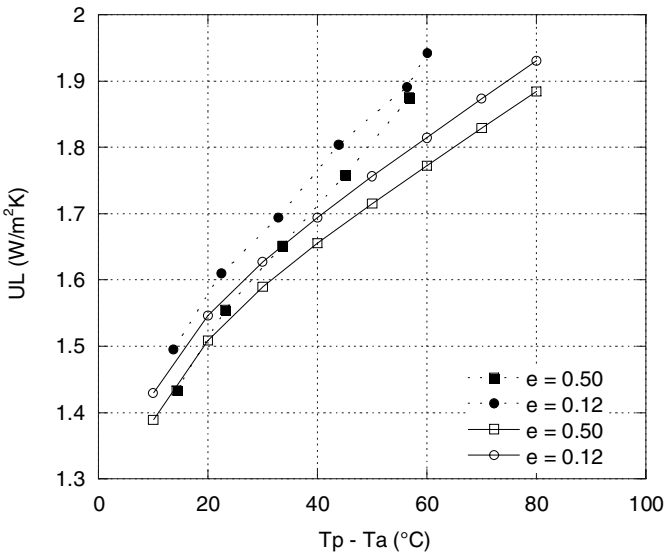

Fig. 4.8 *Values of U_L of the hot box with a 50 × 8 × 8 mm honeycomb of different honeycomb film emittances vs T_p - T_a for the absorber emittance 0.065. Unfilled marks: calculations. Filled marks: measurements. U_b = (0.5+0.00125(T_p-T_a)) W/m²K is included.*

In contrast to the PC honeycomb, the measured U_L for the two honeycombs are slightly higher than the calculated values. The difference increases with increasing T_p - T_a. This could be a result of a slight onset of convection within the honeycomb cells at higher temperature differences. Similar results have been reported by Hollands et al (1992b) for a 40 mm FEP honeycomb with the square cell size 9.5 mm and a 9 mm air gap.

On the other hand, most of the other measurements in the hot box (compare with Fig. 4.4 and Fig. 4.7) also have shown a tendency towards a larger temperature derivative for the measured than for the calculated

U_L. Also the fact that the measurements were made with a smaller distance between the absorber and the cover, which could result in larger edge losses, indicate that such a conclusion should not be drawn.

4.5 Measurements of heat loss coefficients for a glazing without transparent insulation

Measurements were also performed without transparent insulation in the glazing (with a cover only). They were performed in the unguarded hot box, described in Section 2.1, with an air gap of 140 mm. The calculations were performed using a gap convection correlation by Buchberg at al. (1976) and a surface convection correlation by Al-Arabi and Sakr (1988). The results for the different absorber emittances, ε_p, are shown in Fig. 4.9. The measured values were in general 0.1-0.2 W/m^{2}K higher than corresponding calculated values. One reason for this could be that the edge heat losses are somewhat larger, since the edges in this case are not insulated by transparent insulation. This is discussed further in Section 2.1. The used approximate convection correlations have in this case also a larger impact on the calculated heat loss coefficient. Yet, the agreement between the calculated and measured values is reasonably good.

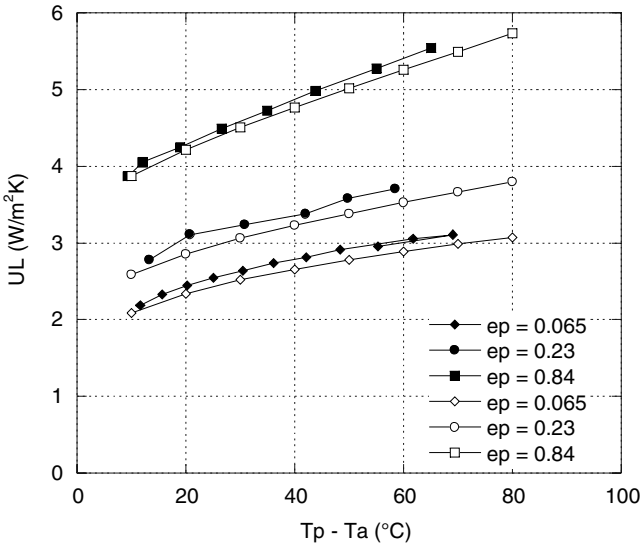

Fig. 4.9 *U_L for the hot box with a cover only vs T_p - T_a for different absorber emittances, ε_p. Filled marks: measurements. Unfilled marks: calculations. U_b = (0.5+0.00125(T_p-T_a)) W/m^{2}K is included.*

4.6 Measurements of incidence angle dependent solar transmittance

Incidence angle dependent hemispherical solar transmittance measurements were performed in an integrating sphere, described in Section 4.1. The result of the measurements for a 50 mm polycarbonate (PC) honeycomb, described in Section 4.2, is shown in Fig. 4.10. Two parameters needed for calculating the transmittance of the honeycomb according to Section 3.8 are the wall absorptance, α = 1- (τ + ρ), and the fraction of the incident light impinging on the honeycomb edges, f_w.

The PC honeycomb consists of strips, four cells wide, which are glued together. The outer walls of the strips are thicker than the inner walls. This, together with other non-ideal properties like corrugation and irregularities, makes it hard to determine the size of f_w. Also a can be hard to determine accurately, since (τ + ρ) gives a value close to one and the value of α is (normally) only a fraction of a per cent. Effective values of the two parameters could however be determined from the transmittance measurements, as shown below.

For the two-dimensional case (with the incident light parallel to one of the wall directions), a somewhat simplified formula for the transmittance through the honeycomb, τ_{hc}, can be written (compare Section 3.8):

$$\tau_{hc} = (1 - f_w)(1 - \alpha)^{A \tan(\theta)} = (1 - f_w)\exp(A \tan(\theta) \cdot \ln(1 - \alpha)) \quad (4.6.1)$$

where α is the absorptance, A is the aspect ratio, θ is the incidence angle and f_w is the fraction of the incident light impinging on the honeycomb edges.

Symons (1982) and Platzer (1992c) suggested that the structure of eqn 4.6.1 would be used in a model, where two parameters, τ_0 and a are obtained from measured data:

$$\tau_{hc} = \tau_0 \exp(-a \tan(\theta)) \quad (4.6.2)$$

Platzer (1992c) also showed from measurements of the same honeycomb with different thicknesses that the two parameters are functions of the thickness and that they can both be modelled as linear functions.

The parameters τ_0 and a can be used to calculate effective values of f_w and α from the equations 4.6.1 and 4.6.2. These effective values could then be used in the calculation procedure of Section 3.8. The calculations can not, however, be made angular resolved or spectral, since the parameters and thereby the effective values are (integrated) average values.

In Fig. 4.10, the parameters τ_0 and a of eqn 4.6.2 were obtained by fitting the equation to the measured data for the PC honeycomb. The fit is shown in the figure. The parameter values $\tau_0 = 0.947$ and $a = 0.0577$ were obtained.

Also a 50 mm polypropylene (PP) honeycomb of the (square) cell size 8 mm was measured. This honeycomb was also treated in Section 4.4. The transmittance measurements and the fit of eqn 4.6.2 are given in Fig. 4.11. The values of the fitted equation agreed somewhat better with the measured values for this honeycomb. The obtained parameters were $\tau_0 = 0.970$ and $a = 0.0542$.

Finally, the measured angle dependent solar transmittance for a 25 μm FEP film is given in Fig. 4.12. For comparison, the dotted line gives the calculated solar transmittance, obtained from the Fresnel relations (see Section 3.2) for a film with a transmittance at normal incidence of 0.96 and a zero absorptance. This corresponds to a material with a refractive index of around 1.33, which is the approximate value for a FEP film.

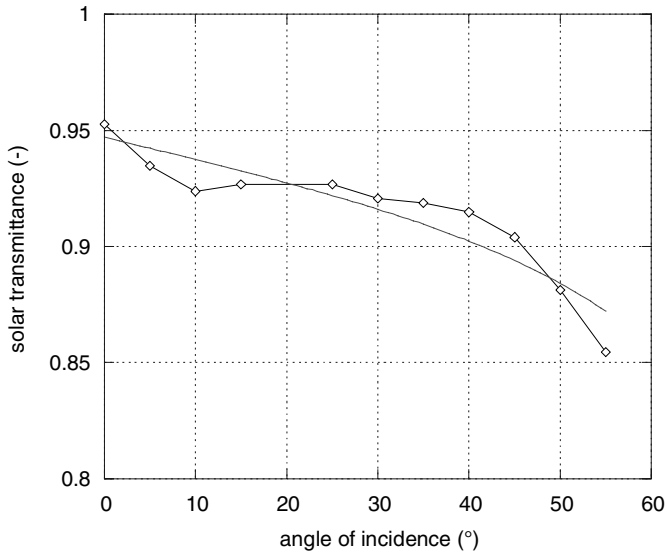

Fig. 4.10 *Measured directional-hemispherical solar transmittance for a 50 mm PC honeycomb with cell size 3.9 mm × 4.5 mm. A fit of eqn 4.6.2 is included, giving t_0 = 0.947 and a = 0.0577.*

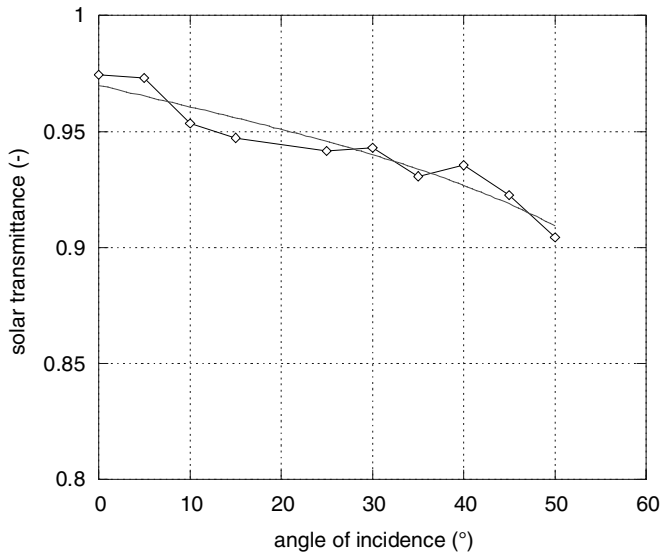

Fig. 4.11 *Measured directional-hemispherical solar transmittance for a 50 mm PP honeycomb with a square cell size of 8 mm. A fit of eqn 4.6.2 is included, giving τ_0 = 0.970 and a = 0.0542.*

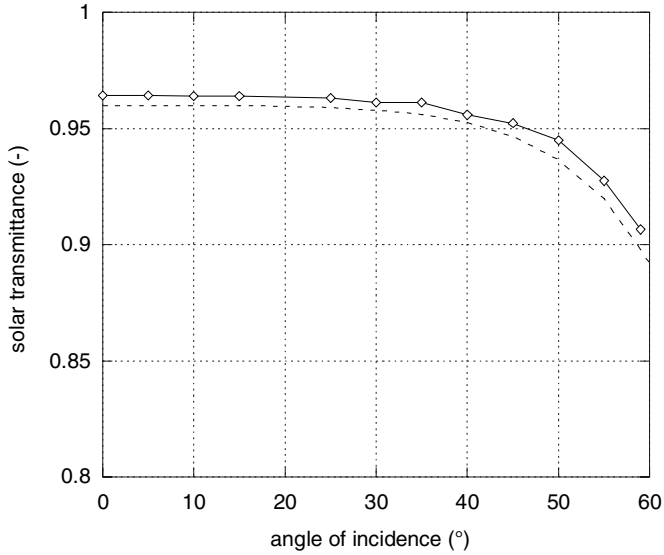

Fig. 4.12 *Measured directional-hemispherical solar transmittance for a 25 µm FEP film. The dotted line gives the angle dependent transmittance from the Fresnel relations, calculated from a transmittance at normal incidence of 0.96 and zero absorptance.*

4.7 Conclusions

- Measurements of heat conductivity and total heat loss coefficients of glazings, performed for different transparent insulation materials, are presented and compared with calculations. The results show, in most cases, good agreement. This indicates that the heat loss calculation procedures of Chapter 3 gives results of reasonable accuracy.
- Measurements of incidence angle dependent hemispherical solar transmittance, performed for two different honeycombs and a FEP film, are also presented. The values could not be directly compared with calculated values since two of the parameters needed for the calculation procedure could not be directly obtained, due to the non-ideal shape of the real honeycombs. Instead the two parameters are obtained by fitting a theoretical equation for the honeycomb transmittance to measured data. The measured angle dependent solar transmittance of the FEP film was close to that calculated.

5 Derivation of efficiency factors for uneven irradiation on a fin absorber

5.1 Introduction

The equation for thermal energy output, q, for a flat plate solar collector, expressed as a function of the mean heat carrier temperature of the collector, T_f, can be written:

$$q = F'(S - U_L(T_f - T_a)) = F'S - F'U_L(T_f - T_a) \qquad (5.1.1)$$

where S is the absorbed irradiance and F' is the collector efficiency factor (Duffie and Beckman, 1991). As the name indicates, F' is proportional to the collector efficiency. Division of q by the irradiance, G, gives the collector efficiency.

The even (uniform) irradiation on the absorber in a flat plate collector results in an F' which is the same for both the absorbed irradiance, S, and the heat losses, $U_L(T_f - T_a)$. However, for a concentrating collector with uneven (non-uniform) irradiation on a fin absorber, the two F' are not the same. The different F' for the absorbed uneven irradiance, S_c, is here denoted F'_c.

It would not be appropriate to call F'_c a collector efficiency factor, since it is only proportional to the zero-loss ($T_f - T_a = 0$) efficiency. "Zero-loss" or "optical" efficiency factor would therefore be a more appropriate term and the latter is used in this paper. By analogy, the fin efficiency for uneven irradiation is denoted F_c, instead of F, which is the fin efficiency for even irradiation and heat losses.

Hottel and Whillier (1958) and Bliss (1959) derived formulas for calculating F' (and F_R) for a flat plate collector with a fin absorber. This was later recapitulated by Duffie and Beckman (1991). Using a finite differ-

ence method, Clemes and Brunger (1988) derived a set of equations for calculating the absorber temperature distribution, the collector efficiency factor and the fin efficiency for a non-uniformly irradiated solar fin. Cases of absorbed irradiances concentrated near the fin tip and the fin base were calculated and compared with a uniform irradiance.

In this chapter analytical expressions are derived for calculating F_c and F'_c for uneven irradiation on a fin absorber of constant thickness. In addition, formulas for calculating the temperature distribution across the absorber are derived. The derivations are based on the assumption of a temperature independent, constant U_L-value across the absorber fin. It is also shown how the resulting F'_c of the absorber can be used to calculate a corresponding heat removal factor for a collector with uneven irradiation, $F_{R,c}$.

The content of this chapter is almost identical to a published article by the author (Hellström, 2004). One difference is that two of the equations (5.3.1-2) here are given an alternative, simplified expression (shown within the brackets). The article was based on a reported research project (Hellström 2001), where the same type of analysis was made also for a solar cell/collector hybrid absorber.

The formulas in the chapter could for instance be used in energy output simulations of a concentrating collector. Adsten et al. (2001-04) used the results to calculate a weighted annual average of F'_c for the MaReCo, a truncated, asymmetric CPC collector (Karlsson and Wilson, 2000), by weighting the distribution of F'_c across the absorber against the annual solar irradiation distribution on the absorber. The latter was calculated from the measured concentration distribution on the absorber as a function of the projected solar altitude angle and the annual solar irradiation in each segment of projected angle.

5.2 Some definitions

The optical efficiency factor of the absorber, F'_c, depends on the distribution of absorbed solar irradiation across the absorber. It is shown in Section 5.5 that F'_c for absorbed irradiation at a certain distance from the edge of the absorber is independent of absorbed irradiation at other locations. It can therefore be expressed as $F'_c(x)$, where x is the distance from the edge of the absorber. Rewriting eqn 5.1.1 for uneven irradiation on an absorber of width W then gives:

$$q = \frac{1}{W}\int_0^W F'_c(x)S_c(x)dx - F'U_L(T_f - T_a) \qquad (5.2.1)$$

To distinguish the absorber average from the local optical efficiency factor, $F_c(x)$, the former will be denoted $F'_{c,a}$. It can be calculated from:

$$F'_{c,a} = \frac{\int_0^W F'_c(x)S_c(x)dx}{\int_0^W S_c(x)dx} \qquad (5.2.2)$$

It is also convenient to denote the average absorbed irradiance on the absorber $S_{c,a}$, to distinguish it from the locally absorbed irradiance, $S_c(x)$:

$$S_{c,a} = \frac{1}{W}\int_0^W S_c(x)dx \qquad (5.2.3)$$

For real calculations, the integrals of eqns 5.2.1, 5.2.2 and 5.2.3 are replaced by finite difference sums. Eqns 5.2.2 and 5.2.3 can be used with eqn 5.2.1 to obtain:

$$q = F'_{c,a}S_{c,a} - F'U_L(T_f - T_a) \qquad (5.2.4)$$

Schematic drawings of two types of fin absorbers are shown in Fig. 5.1; one where the pipe is welded to the fin and one where the pipe is integral. In this analysis the former type is used, where it is assumed that the bottom surface of the fin is well insulated and that interaction with the surroundings (absorption and heat losses) takes place only at the top surface of the fin. The results are, however, approximately valid for both types of fin absorbers. On the area where the fin base and the pipe wall are in direct metal-to-metal contact (width b), the temperature is assumed to be uniform (T_b). The fin efficiency, F, of a fin wing must be calculated with the effective wing width $w = (W-b)/2$. The heat loss coefficient, U_L, is assumed to be temperature independent and the same for all locations, x, on the absorber fin.

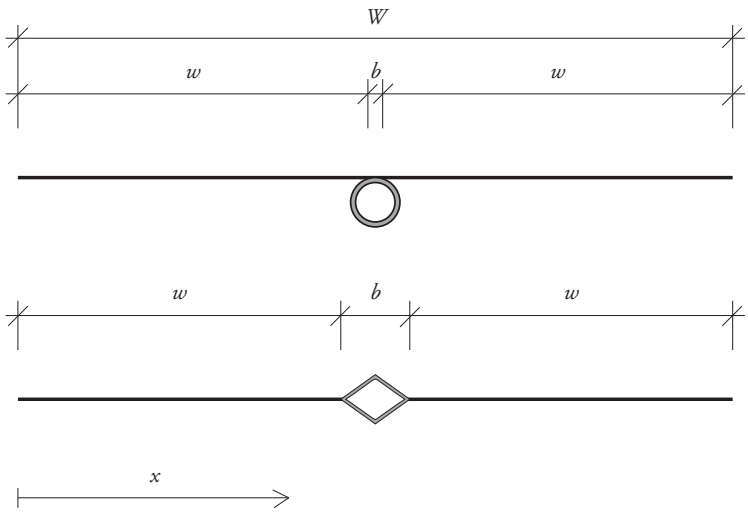

Fig. 5.1 *Schematic drawings of two types of fin absorbers, one with a welded pipe (upper) and one with an integral pipe (lower).*

5.3 Formulas of fin efficiency and optical efficiency factor

The local fin efficiency of a fin absorber with irradiation absorbed at an arbitrary distance $x \leq w$ from the edge of the fin, can be written:

$$F_c(x) = \frac{\cosh(m(w-x)) - \tanh(m(w-x))\sinh(m(w-x))}{1+\tanh(mx)\tanh(m(w-x))}$$

$$\left(= \frac{1}{\cosh(m(w-x)) + \tanh(mx)\sinh(m(w-x))}\right) \qquad (5.3.1)$$

where $m = (U_L/(k\delta))^{0.5}$, k is the fin material conductivity and δ is the fin thickness. Eqn 5.3.1 is derived in Section 5.5.

For the area in contact with the pipe, $w \leq x \leq w+b$, the local fin efficiency, $F_c(x) = 1$. For $w+b \leq x \leq 2w+b$, $F_c(x)$ can be calculated using eqn 5.3.1 by substituting x for $2w+b-x$ ($= W-x$) in the right-hand side of the equation. If the irradiation is concentrated at the edge of the fin (at $x = 0$), the local fin efficiency is:

$$F_c(0) = \cosh(mw) - \tanh(mw)\sinh(mw)\ (= \frac{1}{\cosh(mw)}) \qquad (5.3.2)$$

An energy flow balance for the fin base (instead of the heat carrier as in eqn 5.2.1) gives the following equation for the utilized energy flow, q:

$$q = \frac{1}{W}\int_0^W F_c(x)S_c(x)dx - \frac{2wF+b}{W}U_L(T_b - T_a)$$

$$= \frac{1}{W}\int_0^W F_c(x)S_c(x)dx - F_aU_L(T_b - T_a) \qquad (5.3.3)$$

where F_a is the absorber average fin efficiency for even irradiation and heat losses:

$$F_a = \frac{2wF+b}{W} = (1-\frac{b}{W})F + \frac{b}{W} \qquad (5.3.4)$$

and F is the ordinary fin efficiency of the fin wings for even irradiation and heat losses:

$$F = \frac{\tanh(mw)}{mw} \qquad (5.3.5)$$

If the heat resistance between the fin base and the pipe and through the pipe wall is neglected, the temperature difference between the fin base, T_b, and the heat carrier, T_f, can be expressed:

$$T_b - T_f = \frac{qW}{h_i\pi d_i} \qquad (5.3.6)$$

where h_i is the heat transfer coefficient between the pipe inner wall and the heat carrier fluid.

Replacing T_b in eqn 5.3.3 by the expression for T_b in eqn 5.3.6 and simplifying leads to

$$q = \frac{\frac{1}{W}\int_0^W F_c(x)S_c(x)dx - F_aU_L(T_f - T_a)}{1+\frac{F_aU_LW}{h_i\pi d_i}} \qquad (5.3.7)$$

For real calculations, the integral of eqn 5.3.7 is replaced by a finite difference sum. Comparing eqn 5.3.7 with eqn 5.2.1 gives

$$F' = \frac{F_a}{1+\frac{F_a U_L W}{h_i \pi d_i}} = \frac{\frac{1}{U_L}}{\frac{1}{F_a U_L}+\frac{W}{h_i \pi d_i}} \tag{5.3.8}$$

and

$$F'_c(x) = \frac{F_c(x)}{1+\frac{F_a U_L W}{h_i \pi d_i}} \tag{5.3.9}$$

Eqns 5.3.8 and 5.3.9 then lead to eqn 5.3.10:

$$F'_c(x) = \frac{F'}{F_a} F_c(x) \tag{5.3.10}$$

Eqn 5.3.10 shows that the local optical efficiency factor, $F'_c(x)$, can be calculated from the local fin efficiency, $F_c(x)$, multiplied by the ratio between the collector efficiency factor, F', and the absorber average fin efficiency for even irradiation, F_a. Eqn 5.3.10 is also valid if the assumption of neglecting the heat resistance between the fin base and the pipe wall is changed. F' would then have to be calculated with an equation different from eqn 5.3.8.

Provided that the irradiance distribution, $G_c(x)$, and thereby the distribution of $S_c(x) = \alpha \cdot G_c(x)$ across the absorber is known (from measurements or ray tracing), the absorber average optical efficiency factor, $F'_{c,a}$, can be calculated from eqn 5.2.2 (with the integrals replaced by finite difference sums).

$F'_c(x)$ for an absorber with W = 0.15 m, b = 0.01 m, $k\delta$ = 0.1 W/K, $h_i d_i$ = 10 W/mK and U_L = 10 W/m^{2}K calculated with the equations above, is shown in Fig. 5.2. The level of F' is shown for comparison. For even irradiance, $S_c(x) = S$, the average optical efficiency factor, $F'_{c,a}$, equals F'. Eqn 5.2.2 then gives:

$$F' = \frac{1}{W}\int_0^W F'_c(x)\,dx \tag{5.3.11}$$

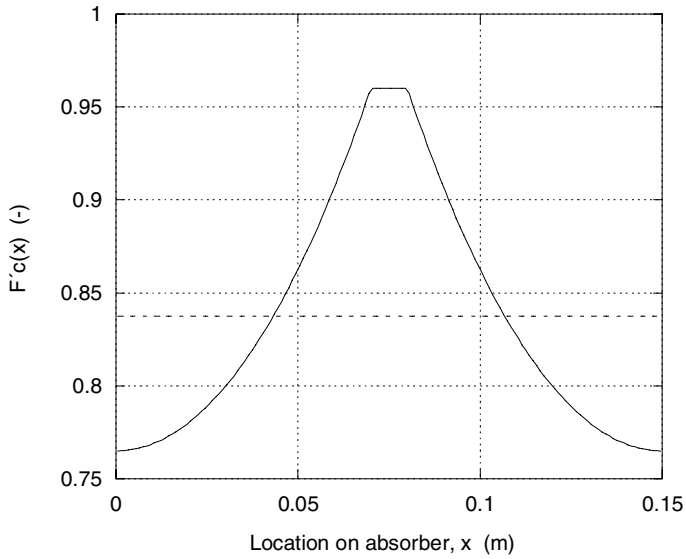

Fig. 5.2 *$F'_c(x)$ versus location of the absorbed irradiation, x, (distance from the edge), for an absorber with* W *= 0.15 m, b = 0.01 m, kδ = 0.1 W/K, $h_i d_i$ = 10 W/mK and U_L = 10 W/m^{2}K. The level of F′ (dotted line) is shown for comparison.*

If the energy output equation is expressed as a function of the inlet temperature, T_i, instead of the mean temperature as in eqn 5.2.4, the corresponding equation can be written:

$$q = F_{R,c}S_{c,a} - F_R U_L(T_i - T_a) \tag{5.3.12}$$

where $F_{R,c}$ can be calculated from

$$F_{R,c} = \frac{F_R}{F'} F'_{c,a} \tag{5.3.13}$$

A formula for calculating F_R/F' is given by Duffie and Beckman (1991). Eqn 5.3.13 is not derived here, but can easily be deduced from the derivation of F_R, as given by Duffie and Beckman (1991).

5.4 Formulas of absorber temperature distribution

The absorbed irradiation, $S_c(x')\Delta x'$, at the distance $x' \leq w$ from the edge of the absorber fin contributes to a temperature rise on the absorber compared with the fin base temperature, $T(x) - T_b$, which is different for each distance from the edge of the fin, $x \leq w$. For the steady state this local temperature rise on the absorber, $\Delta T_s(x, x')$, can be expressed as

$$\Delta T_s(x,x') = \frac{mS_c(x')\Delta x'}{U_L} \cdot \frac{\tanh(m(w-x'))\cosh(m(x-x')^{\#}) - \sinh(m(x-x')^{\#})}{1+\tanh(mx')\tanh(m(w-x'))} \cdot \frac{\cosh(m(x'-(x'-x)^{\#}))}{\cosh(mx')} \quad (5.4.1)$$

where $X^{\#} = (X + \text{abs}(X))/2$. If $X \geq 0$, $X^{\#} = X$, otherwise $X^{\#} = 0$. Eqn 5.4.1 is derived in Section 5.5.

For $x' \geq w+b$ and $x \geq w+b$, $\Delta T_s(x, x')$ can be calculated using eqn 5.4.1 by substituting x' for $2w+b-x'$ and x for $2w+b-x$ in the right-hand side of the equation. For all other combinations of x' and x, the temperature rise is zero.

The absorbed irradiation also causes a rise in T_b and thereby indirectly a change in the absorber temperature. The local temperature change, $\Delta T_L(x)$, caused by the level of $T_b - T_a$ is:

$$\Delta T_L(x) = -(T_b - T_a)\left(1 - \frac{\cosh(mx)}{\cosh(mw)}\right) \quad (5.4.2)$$

Eqn 5.4.2 is valid for $x \leq w$. For $w \leq x \leq w+b$, the temperature change is zero and for $x \geq w+b$, eqn 5.4.2 can be used by substituting x for $2w+b-x$ in the right-hand part of the equation. Eqn 5.4.2 is derived in Section 5.5.

If the irradiance distribution, $G_c(x') = S_c(x')/\alpha$, across the absorber is known (from measurements or ray tracing), the total temperature rise distribution, $T(x) - T_b$, can be calculated by first taking the sum of $\Delta T_s(x, x')$ for all x' and then adding $\Delta T_L(x)$:

$$T(x) - T_b = \sum_{x'} \Delta T_s(x,x') + \Delta T_L(x) \quad (5.4.3)$$

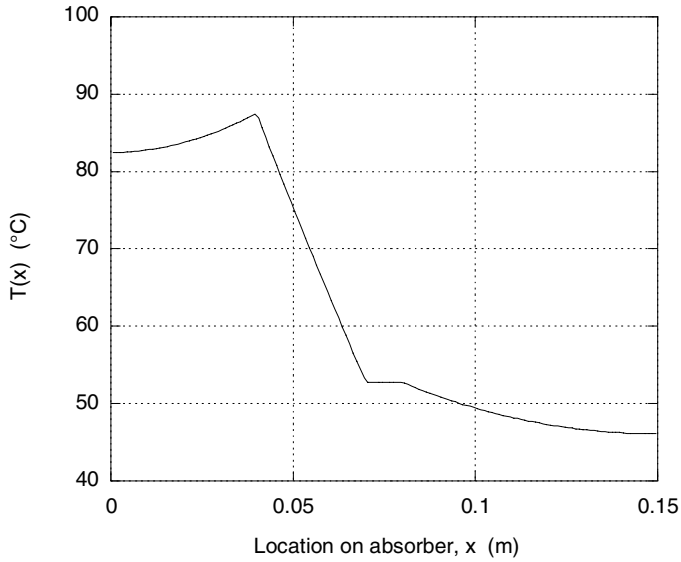

Fig. 5.3. *T(x) versus location,* x, *on the absorber fin with W = 0.15 m, b = 0.01 m, $k\delta$ = 0.1 W/K, $h_i d_i$ = 10 W/mK, U_L = 10 W/m^{2}K, T_f = 50°C and T_a = 20 °C. All absorbed irradiation, 150 W/m, is assumed to be concentrated at x = 0.04 m.*

The fin base temperature, T_b, can be calculated from a known heat carrier temperature, T_f, using eqn 5.3.6 with eqn 5.3.7 (or eqn 5.2.1), if the integral in eqn 5.3.7 (or eqn 5.2.1) is replaced by a finite difference sum. The temperature distribution across the absorber can thereby be calculated.

The temperature distribution, $T(x)$, on an absorber with W = 0.15 m, b = 0.01 m, $k\delta$ = 0.1 W/K, $h_i d_i$ = 10 W/mK and U_L = 10 W/m^{2}K, calculated with the equations above, is shown in Fig. 5.3. All the absorbed irradiation, $S_c(x')\Delta x'$ = 150 W/m, is assumed to be concentrated at a line at x' = 0.04 m. T_a and T_f are assumed to be 20°C and 50°C, respectively. The result can also be seen as the contribution to $T(x)$ - T_a from $S_c(x')\Delta x'$ and $U_L(T_f - T_a)$.

5.5 Derivation of formulas

Eqns 5.4.1 and 5.4.2, used for calculating $T(x) - T_b$, and eqn 5.3.1, for calculating $F_c(x)$, are derived in this chapter.

The case when all the concentrated irradiation is absorbed at the edge of the fin ($x' = 0$) is treated first. Only one absorber wing (of width w) is used for the analysis. x is the distance from the edge, $0 \le x \le w$. Also an absorbed even irradiance, S, is included in the analysis. Both the heat loss coefficient (U_L) and the heat conductivity (k) of the fin material are assumed to be independent of the temperature variations across the fin. The main difference of this analysis, compared with a derivation without concentrated irradiation, as given for instance by Duffie and Beckman (1991), is a difference in the boundary conditions.

The heat balance for a small area on the fin approaching zero can be written:

$$\frac{d^2\psi}{dx^2} - m^2\psi = 0 \tag{5.5.1}$$

where $\Psi = T(x) - T_a - S/U_L$ and $m = (U_L/(k\delta))^{0.5}$. The general solution to eqn 5.5.1 is:

$$\Psi = C_1\sinh(mx) + C_2\cosh(mx) \tag{5.5.2}$$

The boundary conditions when the concentrated irradiation is absorbed at $x' = 0$ are:

$$\left.\frac{d\psi}{dx}\right|_{x=0} = -\frac{S_c(0)\Delta x'}{k\delta} \tag{5.5.3}$$

$$\psi|_{x=w} = T_b - T_a - S/U_L \tag{5.5.4}$$

where $S_c(0)\Delta x'$ is the absorbed irradiation per absorber length at $x' = 0$. Differentiating eqn 5.5.2 and comparing with eqn 5.5.3 gives

$$C_1 = -S_c(0)\Delta x' m/U_L \tag{5.5.5}$$

Using eqn 5.5.5 and eqn 5.5.4 with eqn 5.5.2 gives

$$C_2 = \tanh(mw)\, S_c(0)\Delta x' m/U_L + (T_b - T_a - S/U_L)/\cosh(mw) \tag{5.5.6}$$

Inserting the expressions for C_1 and C_2 into eqn 5.5.2 leads to:

$$T(x) - T_b = \left(\frac{S}{U_L} - (T_b - T_a)\right)\left(1 - \frac{\cosh(mx)}{\cosh(mw)}\right) + \frac{mS_c(0)\Delta x'}{U_L}(\tanh(mw)\cosh(mx) - \sinh(mx)) \quad (5.5.7)$$

From eqn 5.5.7 it is obvious that the absorbed irradiation at $x = 0$ results in a contribution to $T(x) - T_b$ which is independent of the contributions from S and $T_b - T_a$. The temperature rise is a linear combination of the different sources. This is a consequence of the fact that the contribution to $T(x) - T_b$ from each source is a function of temperature independent variables. The contribution to $T(x) - T_b$ from each source is therefore unaffected by the other sources.

The utilized energy rate per length of the fin wing is:

$$q' = -k\delta \left.\frac{dT}{dx}\right|_{x=w} = -\frac{U_L}{m^2}\left.\frac{dT}{dx}\right|_{x=w} \quad (5.5.8)$$

By differentiating eqn 5.5.7 and inserting the derivative for $x = w$ into eqn 5.5.8, the expression for q' is:

$$q' = w(S - U_L(T_b - T_a))\frac{\tanh(mw)}{mw} + S_c(0)\Delta x'(\cosh(mw) - \tanh(mw)\sinh(mw)) \quad (5.5.9)$$

Using the concept of fin efficiency, q' can also be written

$$q' = F(S - U_L(T_b - T_a))w + F_c(0)S_c(0)\Delta x' \quad (5.5.10)$$

Identifying $F_c(0)$ from eqns 5.5.9 and 5.5.10, leads to:

$$F_c(0) = \cosh(mw) - \tanh(mw)\sinh(mw) \quad (5.5.11)$$

Eqn 5.5.11 is the same as eqn 5.3.2**.**

For the case when the concentrated irradiation is focused on a line at a distance x' from the edge, the absorbed energy will be conducted into two paths, one towards the edge, $q'_e(x')$, where $0 \le x < x'$, and one towards the pipe, $q'_p(x')$, where $x' < x \le w$.

The energy flow towards the edge is a heat loss determined by the difference between the absorber temperature at the focal line and at the fin base, $T(x') - T_b$. (T_b is here the reference temperature, since heat

losses due to $T_b > T_a$ are treated separately, as shown in eqn 5.5.9). Using the fin efficiency, F_e, for the part of the fin where $x \leq x'$, the heat loss per length of the absorber can be written:

$$q'_e(x') = F_e UL(T(x')-T_b)x' = \frac{\tanh(mx')}{mx'} U_L(T(x')-T_b)x' \qquad (5.5.12)$$

The energy flow towards the pipe can be determined by the same type of analysis as for the previous case (irradiation absorbed at the edge), except that the effective width is $w - x'$ instead of w, the location is $(x - x')$ instead of x and the energy flow at x' is $S_c(x')\Delta x' - q'_e(x')$ instead of $S_c(x')\Delta x'$. Since the absorbed even irradiance, S, and the heat losses, $U_L(T_b - T_a)$, are unaffected by the change of focal line, they will be set to zero for this analysis. Eqn 5.5.7 for $x' \leq x \leq w$ will then be:

$$T(x) - T_b = \frac{m(S_c(x')\Delta x' - q'_e(x'))}{U_L}$$
$$\cdot \tanh(m(w - x'))\cosh(m(x - x')) - \sinh(m(x - x'))) \qquad (5.5.13)$$

Inserting the expression for $q'_e(x')$ in eqn 5.5.12 into eqn 5.5.13 with $x = x'$ and simplifying, results in

$$T(x') - T_b = \frac{mS_c(x')\Delta x'}{U_L} \cdot \frac{\tanh(m(w - x'))}{1 + \tanh(mx')\tanh(m(w - x'))} \qquad (5.5.14)$$

Eqns 5.5.14 and 5.5.12 can then be used together with eqn 5.5.13 to obtain:

$$T(x) - T_b = \frac{mS_c(x')\Delta x'}{U_L}$$
$$\cdot \frac{\tanh(m(w - x'))\cosh(m(x - x')) - \sinh(m(x - x'))}{1 + \tanh(mx')\tanh(m(w - x'))} \qquad (5.5.15)$$

Eqn 5.5.15 is the same as eqn 5.4.1 for $x' \leq x \leq w$.

For $0 \leq x \leq x'$, the heat loss part of eqn 5.5.7 is used with x′ instead of w as the effective width, $T(x')$ instead of T_b as the "fin base" temperature and T_b instead of T_a as the reference temperature. (The temperature change due to $T_b > T_a$ is added separately, as shown in eqn 5.5.7):

$$T(x) - T(x') = -(T(x') - T_b)(1 - \frac{\cosh(mx)}{\cosh(mx')}) \qquad (5.5.16)$$

Adding $T(x') - T_b$ to both sides of eqn 5.5.16 and inserting the expression for $T(x') - T_b$ from eqn 5.5.14 then gives:

$$T(x) - T_b = \frac{mS_c(x')\Delta x'}{U_L} \cdot \frac{\tanh(m(w-x'))}{1+\tanh(mx')\tanh(m(w-x'))} \cdot \frac{\cosh(mx)}{\cosh(mx')} \tag{5.5.17}$$

Eqn 5.5.17 is the same as eqn 5.4.1 for $0 \le x \le x'$. Eqn 5.5.15 and eqn 5.5.17 are together equivalent to eqn 5.4.1.

The contribution to $T(x) - T_b$ from $T_b - T_a$ is given by the heat loss part of eqn 5.5.7:

$$T(x) - T_b = -(T_b - T_a)\left(1 - \frac{\cosh(mx)}{\cosh(mw)}\right) \tag{5.5.18}$$

Eqn 5.5.18 is the same as eqn 5.4.2.

The contributions to $T(x) - T_b$, as given by eqns 5.5.15, 5.5.17 and 5.5.18, are all functions of temperature independent variables. They are therefore independent of each other and can be added (superposed). For the same reason contributions to $T(x) - T_b$ from absorbed irradiation at different x' can also be added. This is done in eqn 5.4.3.

An expression for the utilized energy rate per length of the fin wing is given by eqn 5.5.8. By differentiating eqn 5.5.15 and inserting the derivative for $x = w$ into eqn 5.5.8, the expression for q' will be:

$$q' = S_c(x')\Delta x' \cdot \frac{\cosh(m(w-x')) - \tanh(m(w-x'))\sinh(m(w-x'))}{1+\tanh(mx')\tanh(m(w-x'))} \tag{5.5.19}$$

Using the fin efficiency concept, the energy rate can be expressed:

$$q' = F_c(x')S_c(x')\Delta x' \tag{5.5.20}$$

Identifying the local fin efficiency from eqns 5.5.19 and 5.5.20, gives

$$F_c(x') = \frac{\cosh(m(w-x')) - \tanh(m(w-x'))\sinh(m(w-x'))}{1+\tanh(mx')\tanh(m(w-x'))} \tag{5.5.21}$$

Eqn 5.5.21 is the same as eqn 5.3.1.

Since $T(x) - T_b$ in eqn 5.5.15 is independent of other irradiation sources, so is $F_c(x')$ in eqn 5.5.21, as it is derived from eqn 5.5.15. This is then true also for $F'_c(x')$, since it is obtained from $F_c(x')$ (see eqn 5.3.10).

5.6 Conclusions

- For a concentrating collector with an uneven (non-uniform) irradiation on the absorber, the efficiency factor for the gain term, here called the optical efficiency factor, F'_c, is different from F' and a function of the irradiation distribution on the absorber. Formulas for calculating F'_c for a fin absorber with constant fin thickness are derived. The local fin efficiency, $F_c(x)$, can be calculated with the derived equation and used for calculating the local optical efficiency factor, $F'_c(x)$. The average optical efficiency factor, $F'_{c,a}$, can be calculated from the intensity distribution on the absorber. $F'_{c,a}$ could also be used for calculating a heat removal factor for uneven irradiation, $F_{R,c}$.
- Formulas for calculating the temperature distribution across the absorber for the case of uneven irradiation are also derived. The local temperature on the absorber, $T(x)$, can be calculated from the derived equations. All derivations are made with the approximate assumption of a temperature independent, constant U_L-value across the absorber fin.

6 Measurements of the collector efficiency factor

6.1 Introduction

The collector efficiency factor, F', is an important characteristic of a solar absorber in a flat plate collector. It can be defined from its use in the energy output equation for flat plate collectors as given by Duffie and Beckman (1991):

$$q = F'((\tau\alpha)G - U_L(T_f - T_a)) = F'(\tau\alpha)G - F'U_L(T_f - T_a) \qquad (6.1.1)$$

where $(\tau\alpha)$ is the effective transmittance-absorptance product, G is the irradiance, U_L is the heat loss coefficient from the absorber plate to the ambient and $T_f - T_a$ is the temperature difference between the heat carrier fluid and the ambient.

F' in eqn 6.1.1 can be written as $F' = U_{sys}/U_L$, where U_{sys} is the total heat loss coefficient (counted per absorber area) from the heat carrier fluid to the ambient. F' is often defined in the literature (see e.g. Duffie and Beckman 1991) as the ratio of the actual energy output to what the energy output would be if the absorber plate temperature, T_p, were equal to T_f. This definition is however only consistent with eqn 6.1.1 if U_L is independent of $T_p - T_a$, which is usually not the case.

F' for a fin absorber can be calculated if the flow conditions and the properties and dimensions of the absorber materials are known. Formulas for calculating F' for a fin absorber of constant fin thickness were derived by Hottel and Whillier (1958) and Bliss (1959), and recapitulated later by Duffie and Beckman (1991). Correlations for pipe flow heat transfer coefficients at different flow conditions are also needed for the calculation of F'.

Measurements of F' are useful if accurate calculations are not possible, for instance if the pipe flow does not match the conditions assumed in the flow heat transfer correlations or if the contact area heat resistance between the fin base and the pipe is unknown. Accurate measurements

can also be regarded as more objective than calculations and therefore more trustworthy, since they do not rely on approximate flow correlations or assumptions about the absorber construction.

Measurements of F' for an absorber strip were performed by Frey et al. (1995). A fin absorber in a box (0.25 m wide, 1.2 m long) was irradiated by a solar simulator. The irradiance, G, was measured with a pyranometer and the energy output, q, was monitored. The measurements were performed for $T_f - T_a = 0$. Spectral measurements of the absorptance were made and weighted against the spectral intensity distribution of the solar simulator to achieve an integrated value. F' was then obtained as the ratio of the energy output to the absorbed irradiance: $F' = q/(\alpha G)$. Measurements of F' for different heat carrier flow rates for commercial absorbers were reported. The values of U_L, for which the F' values were measured, were however not determined.

A different approach to measure F' was taken by Rockendorf et al. (1993, 1995). An internal heat transfer coefficient (U_{int}) was defined as $U_{int} = q/(T_p - T_f)$, where T_p is the average absorber plate temperature. From this, F' can be calculated as: $F' = U_{int}/(U_L + U_{int})$. Rockendorf et al. (1995) presented three different methods to measure U_{int} (and thereby indirectly F'), called the "integral", the "local" and the "absorber strip" methods. The integral method was also earlier shown by Rockendorf et al. (1993). All three methods are described briefly below.

In the "integral" method, a collector is tested according to two different standards, one where all the collector parameters are obtained from measurements with solar irradiation and one where the heat losses are measured separately without irradiation. In both cases, the resulting collector parameters are η_0, a_1 and a_2, used in the equation: $\eta = \eta_0 - a_1(T_f - T_a)/G - a_2(T_f - T_a)^2/G$. U_{int}, from which F' can be calculated, is then a function of the difference in the parameter a_1 obtained from the two test methods. The method requires very accurate measurements and stable conditions. The uncertainty in F' was estimated by the authors to be around ± 0.015. The obtained F' (corresponding to F'_0 in Ch. 2.2) is an average value for the collector absorber, valid for $U_L = a_1/F'$, where a_1 is obtained from the measurements without irradiation.

In the "local" method, the fin temperature is measured at a calculated relative distance from the edge of the fin wing, which for a standard collector is around 0.579. This temperature is approximately equal to the average fin temperature, T_p, for a fin of constant thickness. The measurements could be performed during an ordinary collector test, where q, T_i and T_o (inlet and outlet temperatures) are monitored and T_f is obtained from T_i and T_o. U_{int} and F' could thereby be calculated with U_{int}

$= q/(T_p - T_f)$ and $F' = U_{int}/(U_L + U_{int})$. By measuring at different locations in the flow direction, an average value for the collector could be obtained.

The "absorber strip" method uses an absorber strip placed in a well insulated box. The outer parts of the fin wings are electrically heated and the strip is cooled by the heat carrier flow in the pipe. The fluid temperature is kept below the ambient to give $T_p \approx T_a$ in order to minimize the heat losses from the absorber plate. By using the fin base temperature, T_b, it is possible to split the internal heat resistance, $1/U_{int}$, into two parts; one within the fin, $1/U_{fin}$, where $U_{fin} = q/(T_p - T_b)$, and one between the fin base and the heat carrier fluid, $1/U_{b\text{-}f}$, where $U_{b\text{-}f} = q/(T_b - T_f)$. U_{fin} and $U_{b\text{-}f}$ can be determined by measuring q, T_b, T_f and T_p, where T_p is either measured at a calculated distance from the edge of the absorber or calculated from the measured edge temperature. U_{int} can then be calculated, and thereby also F' for any value of U_L.

In this chapter an indirect method to measure F' for a single fin absorber strip is investigated. F' is obtained from temperature measurements in an experimental set-up without irradiation using the relation: $F' = (T_p - T_a)/(T_f - T_a)$. A specially designed thermocouple technique provides accurate temperature measurements across one of the absorber fin wings, from which the average absorber plate temperature, T_p, is calculated. T_f is obtained from measurements of the inlet and the outlet temperatures of the absorber strip. The value of U_L, for which the measured F' is valid, is measured with a specially designed heat flow meter.

This chapter is based on results from a reported research project (Hellström and Håkansson, 2003). H. Håkansson was responsible in the project for the measurement technique.

6.2 Some theoretical concepts

Some of the theoretical background is already given in Sections 2.2 and 3.9, but the basic concepts will be given here as well.

If the irradiance, G, is zero in eqn 6.1.1, the energy output equation will be:

$$q = -F'U_L(T_f - T_a) = -F_aU_L(T_b - T_a) = -U_L(T_p - T_a) \qquad (6.2.1)$$

where F_a is the total fin efficiency for the absorber plate, T_b is the fin base temperature and T_p is the average temperature on the absorber plate. F' and F_a can (for $G = 0$) then be expressed:

$$F' = \frac{T_p - T_a}{T_f - T_a} = \frac{F_a(T_b - T_a)}{T_f - T_a} \tag{6.2.2}$$

$$F_a = \frac{T_p - T_a}{T_b - T_a} \tag{6.2.3}$$

For a fin wing with a constant thickness δ and width w, the fin efficiency, F, can be calculated from

$$F = \frac{\tanh(mw)}{mw} \tag{6.2.4}$$

where $m = (U_L/(k\delta))^{0.5}$. For the part of the absorber where the fin is in direct metal-to-metal contact with the pipe, the temperature is assumed to be constant, T_b. The fin efficiency for this part (of width b) equals one. The average fin efficiency, F_a, for the absorber (of width $W = 2w+b$) can then be calculated from

$$F_a = \frac{2wF + b}{W} = (1 - \frac{b}{W})F + \frac{b}{W} \tag{6.2.5}$$

If the heat resistance between the fin base and the pipe and through the pipe wall is neglected, the collector efficiency factor can be calculated from (see for instance Duffie and Beckman, 1991):

$$F' = \frac{\frac{1}{U_L}}{\frac{1}{F_a U_L} + \frac{W}{h_i \pi d_i}} \tag{6.2.6}$$

To make an approximate correction for the heat resistance in the pipe wall for an absorber with a welded pipe, a fin efficiency for the pipe wall, F_p, is introduced. It can be estimated from:

$$F_p = \frac{\tanh(mL)}{mL} \tag{6.2.7}$$

where $L_p = \pi d_m/2$ and $m_p = ((h_i d_i/d_m)/(k_p \delta_p))^{0.5} \cdot$ d_m is here the (arithmetic) mean of the outer and inner pipe diameter, $d_m = (d_i+d_o)/2 \cdot$ h_i is the heat transfer coefficient between the fluid and the pipe inner wall and $(k_p \delta_p)$ is the product of the heat conductivity and the thickness of the pipe wall. For a fin absorber with an integral pipe, the same formula can be used, but with $L_p = \pi d_m/4$. If the pipe is not circular, the periphery of the pipe could be used instead of πd in the formula. The integral type

absorber has an area of width b for which $F_p = 1$, which would make an average value of F_p more correct to use: $F_{p,a} = F_p(1\text{-}b/W) + b/W$. F' is then:

$$F' = \frac{\dfrac{1}{U_L}}{\dfrac{1}{F_a U_L} + \dfrac{W}{F_p h_i \pi d_i}} \tag{6.2.8}$$

By using the concept of U_{int}, as suggested by Rockendorf et al. (1993 and 1995), eqn 6.2.8 can be written:

$$F' = \frac{\dfrac{1}{U_L}}{\dfrac{1}{U_L} + \dfrac{1-F_a}{F_a U_L} + \dfrac{W}{F_p h_i \pi d_i}} = \frac{\dfrac{1}{U_L}}{\dfrac{1}{U_L} + \dfrac{1}{U_{int}}} \tag{6.2.9}$$

where

$$1/U_{int} = 1/U_{fin} + 1/U_{b\text{-}f} \tag{6.2.10}$$

$$1/U_{fin} = \frac{1-F_a}{F_a U_L} \tag{6.2.11}$$

$$1/U_{b\text{-}f} = \frac{W}{F_p h_i \pi d_i} \tag{6.2.12}$$

U_{fin}, and thereby also U_{int}, is a weak function of U_L, but can for large values of F_a with good accuracy be treated as a constant. $(1\text{-}F_a)$ is then approximately proportional to U_L. If $U_{b\text{-}f} >> U_{fin}$, also $(1\text{-}F')$ is approximately proportional to U_L.

6.3 Description of the experimental set-up

A cross-section of the experimental set-up is shown in Fig. 6.1. Three absorber strips with a length of 1 m were placed next to each other in an arrangement with parallel flow. The central strip was measured at mid-length (0.5 m), while the two adjacent strips functioned as heat guards, keeping the heat flow from the measured absorber strip approximately one-dimensional (in the upward and downward directions). 20 mm thick XPS plates were placed under the fin wings and below them were a 70

mm thick XPS plate on top of two 2 mm aluminium plates on a table. Overhangs of the aluminium plates on the table served as cooling fins, keeping the plate temperature uniform and close to the ambient.

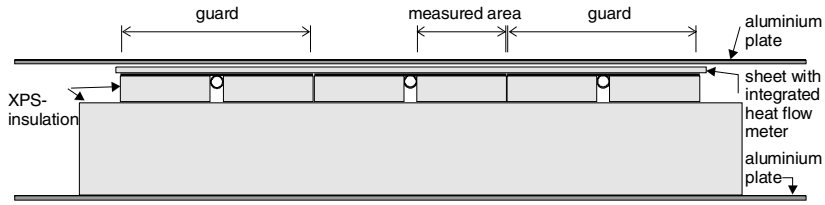

Fig. 6.1 *Cross-section of the measurement set-up*

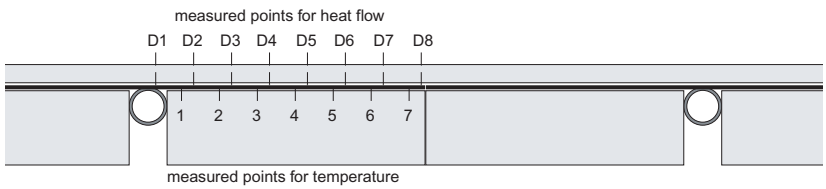

Fig. 6.2 *Cross-section of part of the measurement set-up, where the locations for the thermocouples are marked by arrows. Those marked "D" are for the heat flow measurement device.*

The temperature distribution across the fin was measured with thin thermocouples on the XPS plate below one of the fin wings of the measured absorber. Seven thermocouples with an internal distance of 10 mm, 4 mm from the edges, were attached to the XPS plate. Due to the thick insulation below the fin, the fin temperatures were obtained with high accuracy, even though the fin was not entirely flat and the contact with the thermocouples not perfect. The locations of the 7 thermocouples are shown in Fig. 6.2.

Gaps between the XPS plates provided space for the tubes, see Fig. 6.2. The temperatures of the heat carrier fluid at the inlet and the outlet were measured with pt100 sensors, which were 2.7 mm thick and mounted in copper tubes (8 mm inside diameter). A coil in the outlet tube mixed the fluid with the objective of reaching a uniform outlet temperature. The fluid temperature at the measured location, T_f, was estimated from the inlet (T_i) and the outlet (T_o) temperatures.

A heat flow meter was constructed to measure the front (top) heat losses. It consists of a 5 mm cellular plastic sheet (k = 0.35 W/m^{2}K) with hardened surface layers. Eight thermocouples on each side of the sheet are mounted in a row with a 10 mm distance between them. The thermocouples are connected in pairs to measure the temperature difference across the sheet. The locations of the thermocouples are shown in Fig. 6.2.

The heat flow meter was placed on top of the absorber. A heavy aluminium sheet was put on top, giving a uniform surface temperature and providing weight on the layers below, in order to even out non-plane layers. A fan on top of the aluminium sheet gave an even surface temperature close to the ambient. Thin cellular plastic sheets were placed between the layers, adjacent to the heat flow meter, in order to provide a smooth contact area. The heat flow meter was calibrated with a specially constructed, guarded heat source with a uniform heat flow.

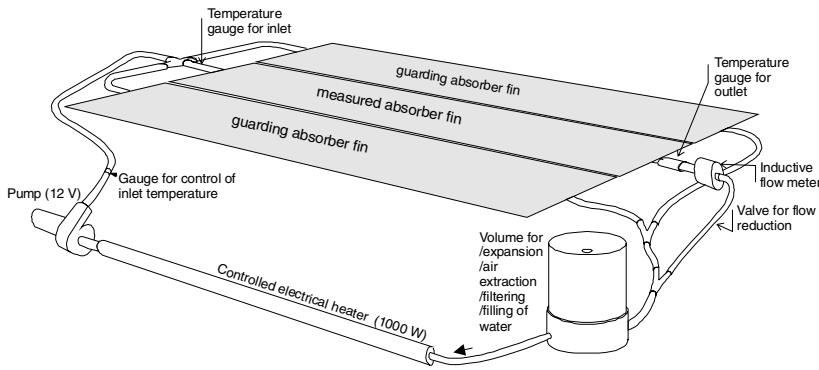

Fig. 6.3 Sketch of the test system.

A sketch of the test system is shown in Fig. 6.3. A pump circulates the heat carrier fluid in a closed loop. A specially constructed regulated electrical heater heats the fluid to a set inlet temperature. An inductive flow meter measures the volume flow rate through the measured absorber strip.

The thermocouples used were of type T (copper-constantan). Thin thermocouple wires (∅ 0.08 mm) were used close to the measurement points. This has three advantages: Thin wires do not conduct heat as well, which increases the accuracy of the measurements. They also use less space and thereby disturb the measurements less. Thin wires are more flexible and therefore easier to mount.

Another measurement arrangement that contributes to a high accuracy is the specially made unit on which the thermocouple reference junctions are placed. It consists of an aluminium block that evens out the temperature variations, and a thermistor, which measures the temperature of the aluminium block. The thermistor and its connection wires are glued to the aluminium block and encapsulated by an aluminium sheet, which is also glued to the block. The reference junctions are soldered on thin laminated circuit cards, which are glued to the aluminium block.

The thermocouples of the heat flow meter are arranged so that they measure only the temperature difference across it (without using a reference temperature). Also this contributes to a high accuracy.

6.4 Methodology

The measurement method uses the following steps:

1. Temperatures are measured across the fin, at the in-/outlet of the heat carrier fluid and in the surrounding air.
2. The measured fin temperatures are used for fitting the parameters m and T_b of the theoretical function:

$$T(x) - T_a = (T_b - T_a)\frac{\cosh(mx)}{\cosh(mw)} \qquad (6.4.1)$$

   where $m = (U_L/(k\delta))^{0.5}$ and $T(x)$ is the fin temperature at the distance x from the edge (see for instance Duffie and Beckman, 1991).

3. F, F_a and T_p are solved from eqns 6.2.4, 6.2.5 and 6.2.3, respectively.
4. T_f is calculated from $T_f - T_a = (T_i - T_a)\exp(x \cdot \ln((T_o - T_a)/(T_i - T_a)))$, where x is the relative distance from the inlet. x was around 0.5 in our experiment. This equation assumes that U_L is constant along the fin. The equation gives a value for the temperatures used which is very close to the arithmetic mean: $T_f = (1-x)T_i + xT_o$
5. F' is obtained from eqn 6.2.2.
6. The heat losses in the forward (upward) direction are measured with a heat flow meter. The back heat losses, (which are much smaller than those for the front), are estimated from the heat conductivity and thickness of the insulating material (XPS) and the

temperature difference across the sheets. By dividing the total heat losses by $(T_p - T_a)$, the value of U_L for the measurement is obtained.

7. U_{int}, U_{fin} and $U_{b\text{-}f}$ can then also be obtained from eqns 6.2.9-11.
8. The fluid flow rate is monitored during the measurements for determining the flow conditions.
9. To recalculate F' for a different value of U_L, recalculate m and repeat steps 3 and 5.

6.5 Measurements and results

The measurements were performed for two types of absorbers, A and B. The type A absorber has a copper pipe welded to a 147 mm wide and 0.25 mm thick copper fin, while the type B absorber consists of a 143 mm wide and 0.55 mm thick aluminium fin with an integral copper pipe. A schematic drawing of the two absorber types is given in Fig. 5.1.

Measurements were first performed with a solid electrical heater in the absorber tube instead of the heat carrier fluid, which resulted only in values of F_a. The heating power was regulated to obtain different values of $(T_p - T_a)$. Two different levels of U_L were obtained by adding a sheet of foam plastic insulation layer on top of the absorber. The measurements were performed with the type A absorber only. The results are presented in Table 6.1, where theoretically calculated values of F_a are given for comparison. Good agreement was obtained between the measured and calculated values of F_a for different values of $(T_p - T_a)$ and U_L. The maximum deviation was 0.001.

Table 6.1 Measured and theoretically calculated F_a for different values of $T_p - T_a$ and U_L.

Abs. type	k W/mK	W mm	δ mm	T_p-T_a °C	U_L W/m²K	F_a meas. –	F_a calc. –	F_a diff. –
A	390	147	0.25	31.36	3.45	0.944	0.944	0.000
				44.33	3.55	0.942	0.943	-0.001
				21.88	5.10	0.921	0.920	+0.001
				40.24	5.22	0.918	0.918	0.000

Measurements were then performed with water as the heat carrier fluid in order to obtain values of F'. Values of F_a were also part of the results. The measurements were conducted with both types of absorbers. The inner (original) diameter of the pipes was (approximately) 8.4 mm for A and 9.5 mm for B, while the cross-section area of the non-circular (rhomboid) integral pipe (B) was 60mm^2.

The value of U_L was larger for the A than for the B absorber in the measurements. The reason for this was that the integral B absorber, due to its geometry, required an extra layer of cellular plastic on top of the fin wings in order to get a flat surface as the base for the heat flow meter.

Results for heat carrier flow rates at around 20, 40 and 60 litres per hour are summarized in Table 6.2. Theoretically calculated vales of F_a and F' are shown for comparison.

Table 6.2 Measured and calculated values of F_a and F' for different heat carrier flow rates.

Abs. type	k	W	δ	flow rate	Re	$T_p - T_a$	U_L	meas. F_a	calc. F_a	meas. F'	calc. F'	diff. F'
	W/mK	mm	mm	l/h	-	°C	W/m^{2}K	-	-	-	-	-
A	390	147	0.25	18.69	1859	40.53	5.25	0.919	0.918	0.870	0.855	+0.0145
				40.54	4066	41.89	5.27	0.917	0.918	0.888	0.901	-0.013
				59.37	5849	41.65	5.27	0.917	0.918	0.896	0.905	-0.010
B	235	143	0.55	20.27	1794	43.99	3.50	0.969	0.968	0.931	0.925	+0.006
				37.70	3363	45.04	3.50	0.968	0.968	0.944	0.957	-0.014
				61.79	5521	45.12	3.51	0.968	0.968	0.948	0.962	-0.014

The measured values of F_a show also here good agreement with the calculated values. The measured values of F' for the two absorbers are not directly comparable since they are obtained for different values of U_L. Values of F' were therefore recalculated for U_L = 4 W/m^{2}K and the result of this is shown in Table 6.3, where some other derived parameters are also shown.

For laminar flow, Re < 2300, the measured values of F' for both the absorbers are slightly higher (0.006-0.012) than the calculated values. For flow in the transition region (not fully developed turbulence), 2300 < Re < 10000, the measured values are slightly lower (0.008-0.016) than those calculated. This means that the difference between F' for the two flow regions is smaller for the measured than for the calculated values. Similar resultats were obtained also by Hausner and Fechner (1998).

Table 6.3 Calculated and measured values of F' (recalculated for U_L = 4 W/m^{2}K), values of U_{int}, U_{fin}, $U_{b\text{-}f}$, F_p and h_i from measurements and calculated values of h_i.

Abs. type	flow rate l/h	U_{int} W/m^{2}K	U_{fin} W/m^{2}K	$U_{b\text{-}f}$ W/m^{2}K	F_p –	meas. h_i W/m^{2}K	calc. h_i W/m^{2}K	meas. F' –	calc. F' –	diff. F' –
A	18.69	35	60	85	0.906	520	396	0.897	0.886	+0.012
	40.54	41	58	145	0.842	957	1782	0.912	0.923	-0.011
	59.37	45	58	200	0.785	1417	2596	0.918	0.926	-0.008
B	20.27	47	110	82	0.964	409	355	0.922	0.915	+0.006
	37.70	58	107	128	0.945	651	1503	0.936	0.952	-0.016
	61.79	63	107	156	0.933	803	2542	0.941	0.956	-0.016

Also the values of U_{int}, U_{fin}, $U_{b\text{-}f}$, F_p and h_i, derived from the measurements, and theoretically calculated values of h_i are shown in Table 6.3. As expected, $U_{b\text{-}f}$ increases with the flow rate for the two absorbers, while U_{fin} is almost constant. Absorber B has a slightly lower $U_{b\text{-}f}$, but a higher U_{fin}, U_{int} and F' than A. The total difference in F' between the two absorbers is for the different flow rates 0.023-0.025 (for this value of U_L). The reason for this difference, in about equal parts, is that absorber A has a slightly wider fin wing (0.072 m compared with 0.0645 m) and a smaller $k\delta$ (0.0975 W/K compared with 0.1293 W/K). The difference is reduced due to a somewhat smaller heat resistance between the fluid and the pipe wall in absorber A.

For calculating the theoretical value of h_i for flow in the transition region (Re > 3000), a formula by Gnielinski (1976) was used. The hydraulic diameter was used in the calculation for the integral pipe absorber. Correlations by Kays (1955) and Kays and Crawford (1980) were used for calculating h_i for laminar flow and constant heat flux in the entry region. A correction was made for the non-circular geometry of the integral pipe absorber. The calculations were performed according to Incropera and DeWitt (2002).

Two typical examples of temperature measurements across the fin for the absorbers A and B with theoretical fits are given in Fig. 6.4 and 6.5, respectively. The fits resulted in the parameters T_b and m, from which the values of F, F_a and T_p were obtained.

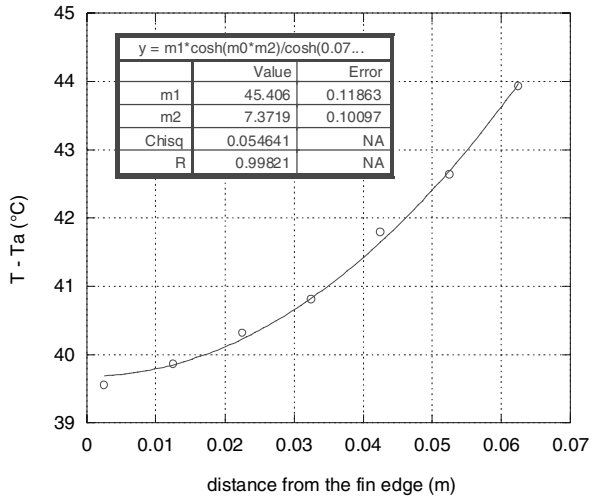

Fig. 6.4 *Measured local fin temperature difference to the ambient air for the type A absorber, with a fit to a theoretical function (eqn 6.4.1). The resulting parameters T_b - T_a and m are given in the figure (=m1 and m2). T_b - T_a is the temperature difference at the distance 0.072 m from the edge.*

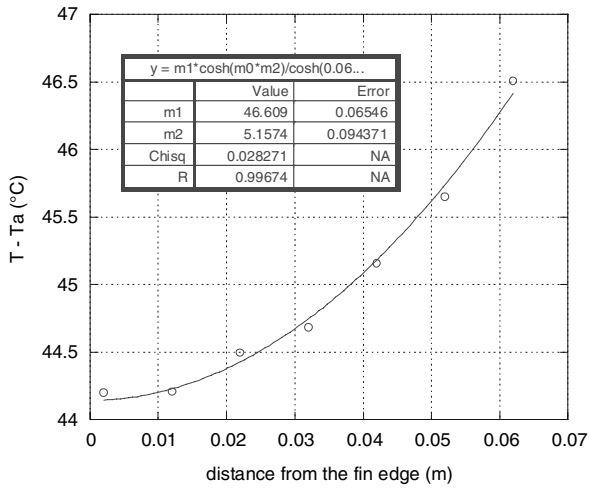

Fig. 6.5 *Measured local fin temperature difference to the ambient air for the type A absorber, with a fit to a theoretical function (eqn 6.4.1). The resulting parameters T_b - T_a and m are given in the figure (=m1 and m2). T_b - T_a is the temperature difference at the distance 0.0645 m from the edge.*

6.6 Error analysis

The accuracy of the resulting values of F_a and F' (as a function of U_L) is determined by the accuracy of the measurements of temperatures and U_L. The value of F_a for a certain U_L is obtained from the relation $(T_p - T_a)/(T_b - T_a)$, while the value of F' is obtained from the relation $(T_p - T_a)/(T_f - T_a)$.

The temperatures of the fin and the ambient were measured with thermocouples. The main errors for the thermocouple measurements with a logger in our experiment are:

A. Errors from the voltage measurements of the thermocouples
B. Error from the thermistor measurement of the reference temperature
C. Error due to deviations in Seebeck coefficient

Errors due to a heat leakage through the thermocouple wires, to or from the junctions, were largely eliminated by the use of very thin thermocouple wires close to the junctions. Errors that would occur from a temperature difference between the reference (the thermistor) and the cold junction were also strongly reduced by the use of an aluminium block as the reference, on which the thermistor was glued and encapsulated by a sheet of aluminium.

According to the manual of the logger used (Campbell CR10), the maximum errors from A and B are approximately 0.05°C and 0.20°C. The maximum error from C for $(T_p - T_a)$ is 0.25°C for a relative error of 0.5% (according to the manufacturer). If all these errors are added, the total error is approximately 0.55°C for $(T_p - T_a)$. However, since the temperatures in the relation $F_a = (T_p - T_a)/(T_b - T_a)$ are measured with thermocouples with the same reference, the error in F_a from B is eliminated. For similar reasons the errors from A and C are also strongly reduced. T_p and T_b are obtained from the same set of measured temperatures across the fin. They are measured with thermocouples that originate from the same wire (and thereby from the same batch).

The results of the measurement of $F_a = (T_p - T_a)/(T_b - T_a)$ for a certain U_L were in all cases very close (±0.001) to the theoretically calculated value, which corresponds to a maximum deviation in $(T_p - T_a)$ compared with $(T_b - T_a)$ of ±0.05°C. These small deviations are more likely to be an effect of the measurement performance than an effect of the instrumentation.

An error, ΔT_e, in T_f, T_p or T_a, gives an absolute error in F' of about $\Delta T_e F'^2/(T_p-T_a)$, $\Delta T_e F'/(T_p-T_a)$ and $\Delta T_e(1-F')F'/(T_p-T_a)$, respectively. If (as in our case) $F' \approx 0.89$ and $(T_p-T_a) \approx 42$°C, an error in the fluid and absorber plate temperature of 0.1°C, would give an absolute error in F' of approximately 0.002, while an error in the ambient temperature of the same magnitude would cause an error of only around 0.0002.

By using thermocouples also for the measurements of the fluid inlet and outlet temperatures, it would be possible to get measurements with a very low uncertainty also for $F' = (T_p - T_a)/(T_f - T_a)$. If thermocouples from the same batch are used, the relative deviation of the Seebeck coefficient is normally less then 0.1% according to a company that delivers the thermocouples, which would then also be the relative error in F'. This corresponds in our case to 0.05°C. An extra measurement error in $(T_f - T_a)$ of 0.1°C, due to T_f being determined from T_i and T_o, would give a total error in F' of ±0.003.

However, in this experiment, PT100 sensors were used for the fluid measurements. The uncertainty of these measurements is about ±0.2% corresponding to ±0.1°C. The uncertainty of the measurement of $(T_f - T_a)$ is then at maximum 0.65°C and of $(T_p - T_a)$ 0.35°C, giving a total uncertainty in F' of about ±0.02. This uncertainty can however be reduced, due to other performed measurements, which will be shown below.

The heat losses from the measured absorber fin could be calculated also from the difference between T_i and T_o. If the measured U_L of the absorber fin is approximated to be constant across the fin, the heat losses could also be calculated in this way. A calculation was made to find how much the measured temperature difference between the outlet and the inlet would have to change in order for the two calculations to agree. The result for the three flow rates, starting with the lowest, was -0.15, -0.10 and +0.10°C for the type A absorber and -0.30, -0.10 and +0.01°C for the type B absorber. These results indicate that there are some errors in the measurements of T_f. A reason for the errors could be that the copper tubes with the PT100 sensors, for practical reasons, were not well insulated. A second reason could be insufficient mixing of the fluid upstream from the inlet sensor.

T_f was calculated from T_i and T_o, which were measured with PT100 sensors. A thermocouple was also mounted on the pipe wall of the type A absorber. This pipe wall temperature could also be calculated from T_f and compared with the measured value. The difference was 0.08, 0.11 and 0.15°C for the three measurements. The maximum "extra" error for

T_f compared with thermocouple measurements can then be estimated to be ≤ 0.3°C. When an error of 0.05°C from the variations in the Seebeck coefficient is added, the absolute error for $F' = (T_p - T_a)/(T_f - T_a)$ is ±0.007.

An uncertainty in the measurements of U_L could also be expressed as an uncertainty in F', using the relation $F' = U_{int} / (U_L + U_{int})$. The maximum relative error from the measurement of U_L could be estimated to around 1%, which corresponds to 0.05 W/m^{2}K. An absolute error in U_L of ΔU_e gives an absolute error in F' of $F'\Delta U_e/(U_L + U_{int})$. An error in U_L of about 0.05 W/m^{2}K would then for U_L = 4 W/m^{2}K and U_{int} = 35 W/m^{2}K, give an error in F' of around 0.001. Adding this uncertainty to the one above gives a total uncertainty in F' of about ±0.008. If thermocouples were to be used for the measurement of T_f, this would give an estimated total uncertainty of ±0.004 in the measured F'.

6.7 Discussion

Although not a large effect, the value of F' is dependent on the distance from the inlet, since it depends on the heat transfer coefficient between the pipe inner wall and the fluid, which is a function of the distance from the inlet. The measured F' is then, strictly speaking, a local value. For a collector manufacturer, the collector average value of F' would probably be the most interesting value. However, for a manufacturer of absorber strips, the absorber could be used in different types of collectors and it could then be of more use to have a value of F' for a certain position on the strip. In this test, F' was measured 0.5 m from the inlet. It might be possible to find and choose a different distance, which would give a more representative value of F'.

6.8 Conclusions

- A method for accurately measuring the collector efficiency factor, F' and the absorber average fin efficiency, F_a, is presented and tested. The method uses accurate temperature measurements, without irradiation, across the absorber plate, in the heat carrier fluid and in the ambient air. The heat loss coefficient, U_L, for which the measured F' and F_a are valid, is measured with a (specially constructed) heat flow meter.

- Two absorbers of different types, A and B, were tested. The measured values of F_a show only small deviations (± 0.001) from the theoretically calculated values. For laminar flow (Re < 2300), the measured values of F' for both the absorbers were slightly higher (0.006 - 0.012) than the calculated values, while in the transition region (2300 < Re < 10000), the measured values were slightly lower (0.008 - 0.016) than the calculated values.
- The error limits of the measured F' were for the test estimated to ± 0.008, but are with an improved measurement technique estimated to be ± 0.004.

7 Conclusions

The conclusions are also given at the end of each chapter (2-6).

- If the temperature dependence of the collector efficiency factor is taken into account in the energy output equation for a flat plate collector, a dependence of the product of the irradiation and the temperature difference, ΔTG, is also obtained. This extra term, proportional to ΔTG, is usually not part of the energy output equation. If the term is not explicitly expressed in the equation, its value will instead be implicitly included in other terms of the equation. It is shown that for the theoretical equation $q = F'S - F'U_L\Delta T$, the extra term is about equally, included in the gain and the loss terms. For the equation often used in tests today, $q = \eta_0 - a\Delta T$, the extra term is mainly included in the loss term. For the equation $q = g_{sys} - U_{sys}\Delta T$, which uses the conventional definitions of g and U, the term is included in the gain term.

- The equation $q = g_{sys} - U_{sys}\Delta T$ is suggested as the basis for an alternative way to test solar collectors, using measurements without irradiation to determine the heat loss coefficients. The test method works stepwise, identifying at most two parameters from each set of measurement periods, which reduces errors due to cross-dependences between parameters. This could result in both good accuracy and good repeatability, although the model has an extra term compared with the CEN standard test models.

- A complete set of algorithms for calculating the energy output for a flat plate collector with flat films or honeycombs between the cover and the absorber is presented.

- An explicit algorithm, based on ray tracing analysis, for calculating the radiation heat exchange factors between the different sheets (which can be semitransparent in the IR) is given. This method is more straightforward and easier to use than the implicit so-called net-ra-

diation or radiosity method. The method is suitable for computer programming and the calculations can easily be made spectral and angular resolved.

- For a collector with a honeycomb between the cover and the absorber, a finite difference solution, in which the honeycomb is divided into a number of layers, is used. Algorithms for calculating the radiation heat exchange factors between the different layers are presented. The method is more straightforward and easier to comprehend an the approximate analytical method and does not make the geometrical approximation presumed by an alternative numerical method. Formulas are also given for calculating the absorbed solar energy in each layer depending on the solar position.

- The algorithms can be used in a computer program for determining the energy output, the efficiency and collector characteristic parameters. Such a program can, for instance, together with a system simulation program, be used for analysing the impact of design or material changes in the collector.

- Measurements of heat conductivity and total heat loss coefficients of glazings, performed for different transparent insulation materials, are presented and compared with calculations. The measurements are in most cases in good agreement with the calculations. This indicates that the heat loss calculation procedures can be used with reasonable accuracy.

- Measurements of incidence angle dependent hemispherical solar transmittance, performed for two different honeycombs and a FEP film, are also presented. The values could not be directly compared with calculated values since two of the parameters needed for the calculation procedure could not be directly obtained, due to the non-ideal shape of the real honeycombs. Instead the two parameters are obtained by fitting a theoretical equation for the honeycomb transmittance to measured data. The measured angle dependent solar transmittance of the FEP film was, close to that calculated.

- For a concentrating collector with an uneven (non-uniform) irradiation on the absorber, the efficiency factor for the gain term, here called the optical efficiency factor, F'_c, is different from F' and a function of the irradiation distribution on the absorber. Formulas for calculating F'_c for a fin absorber with constant fin thickness are derived. The local fin efficiency, $F_c(x)$, can be calculated with the derived equation

and used for calculating the local optical efficiency factor, $F'_c(x)$. The average optical efficiency factor, $F'_{c,a}$, can be calculated from the intensity distribution on the absorber. $F'_{c,a}$ could also be used for calculating a heat removal factor for uneven irradiation, $F_{R,c}$.

- Formulas for calculating the temperature distribution across the absorber for the case of uneven irradiation are also derived. The local temperature on the absorber, $T(x)$, can be calculated from the derived equations. All derivations are made with the approximate assumption of a temperature independent, constant U_L-value across the absorber fin.

- A method for accurately measuring the collector efficiency factor, F' and the absorber average fin efficiency, F_a, is presented and tested. The method uses accurate temperature measurements, without irradiation, across the absorber plate, in the heat carrier fluid and in the ambient air. The heat loss coefficient, U_L, for which the measured F' and F_a are valid, is measured with a (specially constructed) heat flow meter.

- Two absorbers of different types were tested. The measured values of F_a show only small deviations (± 0.001) from the theoretically calculated values. For laminar flow (Re < 2300), the measured values of F' for both the absorbers were slightly higher (0.006 - 0.012) than the calculated values, while in the transition region (2300 < Re < 10000), the measured values were slightly lower (0.008 - 0.016) than the calculated values.

- The error limits of the measured F' were for the test estimated to ± 0.008, but are with an improved measurement technique estimated to be ± 0.004.

Summary

A theoretical model for the energy output from a glazed, flat plate collector is derived by modelling F' as the sum of a constant and a temperature dependent part: $F' = F'_0 + F'_1(T_p - T_a)$. The resulting energy output equation contains only the constant part, F'_0. Compared with the CEN standard test models, the collector model has an extra term, which is proportional to ΔTG. The resulting formula for the energy output is similar to one given earlier by Rockendorf et al. (1993, 1995). An alternative way of testing a flat plate collector, based on this model, is suggested. Through a stepwise parameter identification process, using measurements without irradiation for the heat loss coefficients, errors due to cross-dependences between the parameters could be minimized. Both good accuracy and good repeatability could then be obtained, although the model has an extra term compared with the CEN standard test models.The differences between three collector models, of which one is used in a standard test method today (CEN 2001), one is a theoretical equation (Duffie and Beckman, 1991) and one is the basis for the proposed test procedure, are shown.

A complete set of algorithms for calculating the energy output for a flat plate collector with flat films or honeycombs between the cover and the absorber is presented. An algorithm, based on ray tracing analysis, for calculating the radiation heat exchange factors between the different sheets (which can be semitransparent in the IR) is given. For a collector with a honeycomb between the cover and the absorber, a finite difference solution, in which the honeycomb is divided into a number of layers, is presented. Algorithms for calculating the radiation heat exchange factors between the different layers are presented. Formulas are also given for calculating the absorbed solar energy in each layer depending on the position of the sun. The algorithms can be used in a computer program for determining the energy output, the efficiency and collector characteristic parameters. Such a program can, for instance, together with a system simulation program, be used for analysing the impact of changes of the design or materials in the collector.

Measurements of heat conductivity and total heat loss coefficients of glazings, performed for different transparent insulation materials, are presented. The measurements are compared with calculations and the results show, in most cases, good agreement. This shows that the presented heat loss calculation procedures can be trusted to give results of reasonable accuracy. Measurements of directional-hemispherical solar transmission, performed for three different honeycombs and a FEP film, are also presented. A comparison with calculated values was not possible in this case of the honeycomb. Two of the parameters needed for calculating the solar transmittance from the given procedure could not be determined accurately due to the non-ideal shape of the honeycombs. Instead, the two parameters can be obtained from the measurements by fitting a theoretical equation for the honeycomb transmittance to measured data. The measured angle dependent solar transmittance of the FEP film was, however, close to that calculated.

For a concentrating collector with an uneven (non-uniform) irradiation on the absorber, the efficiency factor for the gain term, here called the optical efficiency factor, F'_c, is different from F' and a function of the irradiation distribution on the absorber. Formulas for calculating F'_c for a fin absorber with constant fin thickness are here derived. The local fin efficiency, $F_c(x)$, can be calculated with a derived equation and used for calculating the local optical efficiency factor, $F'_c(x)$. The average optical efficiency factor, $F'_{c,a}$, can be calculated from the intensity distribution on the absorber. $F'_{c,a}$ could also be used for calculating a heat removal factor for uneven irradiation, $F_{R,c}$. Formulas for calculating the temperature distribution across the absorber for the case of uneven irradiation are also derived. The local temperature on the absorber, $T(x)$, can be calculated from the derived equations. All derivations are made with the approximate assumption of a temperature independent, constant U_L-value across the absorber fin.

A method for accurate measurements of the collector efficiency factor, F' and the absorber average fin efficiency, F_a, is presented and tested. The method uses accurate temperature measurements, without irradiation, across the absorber plate, in the heat carrier fluid and in the ambient air. The heat loss coefficient, U_L, for which the measured F' and F_a are valid, is measured with a heat flow meter. Two absorbers of different types were tested. The measured values of F_a show only small deviations ($\pm$ 0.001) from theoretically calculated values. For laminar flow, Re < 2300, the measured values of F' for both absorbers were 0.006 - 0.012 higher than the calculated values, while in the transition region, 2300 <

Re < 10000, the measured values were 0.008 - 0.016 lower. The maximum error of the measured F' is for the test estimated to ± 0.008, but with an improved measurement technique it is estimated to be ± 0.004.

Acknowledgements

I want to thank my tutors; dr Maria Wall for giving me the opportunity to finish this work and for her great support, and professor Björn Karlsson, with whom I have been working for a long time, for his sustained support and good companionship.

I also want to thank all the people at Energy and Building Design for their co-operation and friendship. Special thanks to dr Bengt Perers for reviewing the work, to Gunilla Kellgren for handling the administrative planning and to Hans Follin for doing the layout. Also thanks to dr Håkan Håkansson, who, with great skill, was responsible for the measurement technique in the research project on which Chapter 6 is based.

Finally, I want to thank the people with whom I have been working over the years at the Älvkarleby Laboratory, Uppsala University, SERC and elsewhere.

The thesis is based on work which was financially supported by the Swedish Energy Agency, FORMAS (the Swedish Research Council for Environment, Agricultural Sciences and Spatial Planning), Elforsk AB (the Swedish Electrical Utilities' R&D Company) and Vattenfall Utveckling AB.

References

Adsten, M., Hellström, B., & Karlsson, B. (2001). Measurement of radiation distribution on the absorber in an asymmetric CPC collector. *Proc. ISES Solar World Congress 2001*, Adelaide, Australia.

Adsten, M., Hellström, B., & Karlsson, B. (2002). Comparison of the optical efficiency of a wide and a narrow absorber fin in an asymmetrically truncated concentrating collector. *Proc. EuroSun 2002*, Bologna, Italy.

Adsten, M., Hellström, B., & Karlsson, B. (2004). Measurement of radiation distribution on the absorber in an asymmetric CPC collector. *Solar Energy 76* (1-3), 199-206.

Al-Arabi, M., & Sakr, B. (1998). Natural convection heat transfer from inclined isothermal plates. *Int. J. Heat Mass Transfer 31* (3), 559-566.

Bartelsen, B. Janssen, S., & Rockenndorf, G. (1993). Heat transfer by natural convection in the air gap of flat plate collectors. *Proc. ISES Solar World Congress 1993*, Budapest, Hungary.

Bliss, R.W. (1959). The derivation of several "plate efficiency factors" useful in the design of flat-plate solar heat collectors. *Solar Energy 3*, 55-64.

Buchberg, H., Catton, I., & Edwards, D.K. (1976). Natural convection in enclosed spaces – a review of application to solar energy. *J. Heat Transfer 98*, 182-188.

Cane, R.L.D., Hollands, K.G.T., Raithby, G.D., & Unny, T.E. (1977). Free convection heat transfer across inclined honeycomb panels. *J. Heat Transfer 99*, 86-91.

CEN (2001) European Standard EN 12975-2. *Thermal solar systems and components - Solar collectors - Part 2: Test methods*. European Committee for Standardization (CEN), Brussels.

Chant, V.G., & Håkansson, R. (1985). *The MINSUN simulation and optimisation program*. Application and users guide. A report for IEA, SH&C, Task VII.

Clemes, S.B., & Brunger, A.P. (1988). Thermal analysis of a non-uniformly irradiated solar fin. Proc. *SESCI Conference, Ottawa, Canada, 1988*.

Duffie, J. A., & Beckman, W. A. (1991). *Solar Engineering of Thermal Processes*, 2nd edn, John Wiley & Sons, New York.

Edwards, D.K., & Tobin, R.D. (1967). Effect of polarization on radiant heat transfer through long passages. *J. Heat Transfer 89*, 132-138.

Edwards, D.K., Arnold, J.N., & Catton, I. (1976). End-clearence effects on rectangular-honeycomb solar collectors. *Solar Energy 18*, 253-257.

Edwards, D.K. (1977). Solar absorption by each element in an absorber-coverglass array. *Solar Energy 19*, 401-402.

Edwards, D.K., & Rhee, S.J. (1984). Nongray-radiative and convective-conductive thermal coupling in Teflon-glazed, selective-black, flat-plate solar collectors. *J. Solar Energy Engineering 106*, 206-211.

Fischer, S., Heidemann, W., Müller-Steinhagen, H., Perers, B., Bergquist, P., & Hellström, B. (2004). Collector test method under quasi-dynamic conditions according to the European standard EN 12975-2. *Solar Energy 76* (1-3), 117-123.

Frey, R., Frei, U., & Brunold, S. (1995). *Bestimmung des Kollektor-Wirkungsgradfaktors F' an flüssigkeitsführenden Solarabsorbern*, Internal Report, SPF, Rapperswil, Switzerland. (available at www.solarenergy.ch: Forschung-Kollektoren).

Gnielinski, V. (1976). *Int. Chem. Eng. Vol. 16*, pp. 359.

Harrison, S.J., Rogers, B.A., Soltau, H., & Wood, B.D. (1993). *The characterization and testing of solar collector thermal performance*. A report of IEA, SH&C, Task III: Performance testing of solar collectors.

Hausner, R., & Fechner, H. (1998). Influence of the flow condition (laminar / turbulent) in the fluid tube on the collector efficiency factor of a fin absorber. *Proc. EuroSun 1998*, Portoroz, Slovenia.

Helgesson, A., Karlsson, B., & Nostell, P. (2000). Angular dependent optical properties from outdoor measurements of solar glazings. (Proc. EuroSun 00, Copenhagen, Denmark). *Solar Energy 69* (1-6), 93-102.

Hellström, B. (1988a). *Inverkan av konvektion på temperaturfördelning och värmeförluster i solfångare*. (Influence of convection on temperature distribution and heat losses in solar collectors). Diploma work at the Department of Heating and Ventilation, Royal Institute of Technology. Internal Report U(L) 1988/34, Vattenfall, Älvkarleby, Sweden. (In Swedish).

Hellström, B., Karlsson, R., & Karlsson, B. (1988b). Convection dependent distribution of temperatures and heat losses in a flat plate collector model. *Proc. North Sun '88, Borlänge*, Sweden. 359-362.

Hellström, B., Bergkvist, M., Ribbing, C-G., & Karlsson, B. (1990a). Solar transmittance and lambda values of transparent insulation. *Proc. Building Physics in the Nordic Countries, Trondheim*, Norway.

Hellström, B., Karlsson, B., & Svensson, L. (1990b). Performance of collectors with flat films or honeycombs. *Proc. North Sun '90, Reading*, England.

Hellström, B., & Karlsson, B. (1991a). Evaluation of a honeycomb glazing for high temperature solar collectors. *Proc. 4:th International Workshop on Transparent Insulation Technology, Birmingham*, England.

Hellström, B., & Karlsson, B. (1991b). Optimization of a honeycomb glazing. *Nordic Solar Energy R & D Meeting, Borlänge*, Sweden.

Hellström, B., Perers, B., & Karlsson, B. (1992). Comperative performance of TIM in collectors. *Proc. 5:th International Workshop on Transparent Insulation Technology, Freiburg*, Germany.

Hellström, B. (1998a). *Comparative evaluation of two solar collector test methods*. Internal Report UR 98:9, Vattenfall Utveckling AB, Älvkarleby, Sweden.

Hellström, B., & Perers, B. (1998b). Comparison of two standard collector test methods. *Proc. EuroSun 1998*, Portoroz, Slovenia.

Hellström, B., Adsten, M., Nostell, P., Wäckelgård, E., & Karlsson, B. (2000). The impact of optical and thermal properties on the performance of flat plate solar collectors. *Proc. EuroSun 2000*, Copenhagen, Denmark.

Hellström, B. (2001). P*arameter impact on temperature distribution and collector efficiency of a solar cell/collector hybrid in a CPC geometry*. Internal Report U01:22, Vattenfall Utveckling AB, Älvkarleby, Sweden.

Hellström, B., & Håkansson, H. (2003). *Mätning av verkningsgradsfaktorn, F´*. (Measurements of the collector efficiency factor, *F´*). Final report of a research project. Internal Report EBD-R--04/4, ISBN 91-85147-03-6, EBD, LTH, Lund University. (In Swedish).

Hellström, B. (2004). Derivation of efficiency factors for uneven irradiation on a fin absorber. *Solar Energy 77* (3), 261-267.

Hollands, K.G.T., Unny, T.E., Raithby, G.D., & Konicek, L. (1976). Free convective heat transfer across inclined air layers. *J. Heat Transfer 98*, 189-193.

Hollands, K.G.T., Marshall, K.N., & Wedel, R.K. (1978). An approximate equation for predicting the solar transmittance of transparent honeycombs. *Solar Energy 21* (3), 231-236.

Hollands, K.G.T., & Wright, J.L. (1983). Heat loss coefficients and effective Ä± products for flat-plate collectors with diathermanous covers. *Solar Energy 30*, 211-216.

Hollands, K.G.T., Raithby, G.D., Russel, G.D., & Wilkinsson, R.G. (1984). Coupled radiative and conductive heat transfer across honeycomb panels and through single cells. *Int. J. Heat Mass Transfer 27* (11), 2119-2131.

Hollands, K.G.T., & Iynkaran, K. (1985). Proposal for a compound-honeycomb collector. *Solar Energy 34* (4-5), 309-316.

Hollands, K.G.T., Ford, C., Iynkaran, K., & Brundrett, E. (1987). Manufacture, solar transmission, and heat transfer characteristics of a compound-honeycomb. *Proc. ISES Solar World Congress 1987*, Hamburg, Germany.

Hollands, K.G.T., & Iynkaran, K. (1992a). Analytical model for the thermal conductance of compound honeycomb transparent insulation, with experimental validation. *Proc. North Sun Conference 1992*, Trondheim, Norway, 339-344.

Hollands, K.G.T., Iynkaran, K., Ford, C., & Platzer, W.J. (1992b). Manufacture, solar transmission, and heat transfer characteristics of large-celled honeycomb transparent insulation. *Solar Energy 49* (5), 381-385.

Hottel, H. C., & Whillier, A. (1958). Evaluation of flat-plate solar-collector performance. *Trans. Conference on the Use of Solar Energy 2*, 74-104, University of Arizona Press.

Inaba, H. (1984). Experimental study of natural convection in an inclined air layer. Int. J. *Heat Mass Transfer 27* (8), 1127-1139.

Incropera, F.D., & DeWitt, D.P. (2002). *Fundamentals of heat and mass transfer, 5th edn*, pp. 485-500. John Wiley & Sons, New York.

Karlsson, B., & Wilson, G. (2000). MaReCo design for horizontal vertical or tilted installation. *Proc. EuroSun 2000 Solar Congress*, Copenhagen, Denmark.

Kays, W.M. (1955). *Trans. ASME, Vol. 77*, pp. 1265.

Kays, W.M., & Crawford, M.E. (1980). *Convective heat and mass transfer*, McGraw-Hill, New York.

Klein, S.A., & Alvarado, F.L. (2002). *EES: Engineering Equation Solver (Ver. 6.647),* a software distributed by F-Chart Software, Madison, Wisconsin (www.fchart.com).

Koo, J.-M., & Beckman, W.A. (1999). *CoDePro: Flat-plate Solar Collector Design Program (Ver. 0725)*, a software (freely) distributed by the Solar Energy Laboratory, University of Wisconsin - Madison (sel.me.wisc.edu).

Källblad, K. (1998). *Thermal models of buildings*, Doctoral dissertation at the Department of Building Science, LTH, Lund University, Report TABK--98/1015.

Marcus, S.L. (1983). An approximate method for calculating the heat flux through a solar collector honeycomb. *Solar Energy 20* (2), 127-131.

Perers, B. (1995). *Optical modelling of solar collectors and booster reflectors under non stationary conditions. Application for collector testing, system simulation and evaluation*. Doctoral thesis, Uppsala University, ISBN 91-554-3496-7.

Platzer, W.J. (1988a). *Solare Transmission und Wärmetransportmechanismen bei transparenten Wärmedämmaterialien*, Doctoral dissertation, Albert-Ludwigs-Universität, Freiburg, Germany.

Platzer, W.J. (1988b). *G-WERT*, a software by Werner J. Platzer, Fraunhofer Institute for Solar Energy Systems (ISE), Freiburg, Germany.

Platzer, W.J. (1992a). Calculation procedure for collectors with a honeycomb cover of rectangular cross section. *Solar Energy 48* (6), 381-393.

Platzer, W.J. (1992b). Total heat transport data for plastic honeycomb-type structures. *Solar Energy 49* (5), 351-358.

Platzer, W.J. (1992c). Directional-hemispherical solar transmittance data for plastic honeycomb-type structures. *Solar Energy 49* (5), 359-369.

Rockendorf, G., Schreitmüller, K.R., & Wetzel, W. (1993). The difference of collector test results between the heat loss measurement and the methods with radiation. *Proc. ISES Solar World Congress 1993*, Budapest, Hungary, Vol. 5, 323-328.

Rockendorf, G., Bartelsen, B., & Witt, A. (1995). Methods to determine the internal heat transfer coefficient between absorber and fluid of solar collectors. *Proc. ISES Solar World Congress 1995*, Harare, Zimbabwe.

Schinkel, W.M.M., & Hoogendoorn, C.J. (1983). Natural convection in collector cavities with an isoflux absorber plate. *J. Solar Energy Engineering 105*, 19-22.

Suehrcke, H., Däldehög, D. Harris, J.A., & Lowe, R.W. (2004). Heat transfer across corrugated sheets and honeycomb transparent insulation. *Solar Energy (76)*, 351-358.

Siegel, R., & Howell, J. R. (2002). *Thermal radiation heat transfer. 4:th ed.*, Taylor & Frances, New York - London.

Sparrow, E.M., & Cess, R.D. (1966). *Radiation heat transfer*. Brooks/Cole Publishing Company, Belmont, California.

Symons, J.G. (1982). The solar transmittance of someconvection suppression devices for solar energy applications: An experimental study. *J. Solar Energy Engineering 104*, 251-256.

Tien, C.L., & Yuen, W.W. (1975). Radiation characteristics of honeycomb solar collectors. *Int. J. Heat Mass Transfer 18*, 1409-1413.

Yiqin, Y., Hollands, K.G.T., & Brunger, A.P. (1991). Measured top heat loss coefficients for flat plate collectors with inner Teflon covers. *Proc. ISES Solar World Congress 1991*, Denver, Colorado. Vol. 2:1, 1200-1205.

LUND UNIVERSITY
Lund Institute of Technology

ISSN 1671-8136
ISBN 91-85147-06-0